High Speed Separations of Complex Mixtures using nano-Liquid Chromatography Coupled with micro Free Flow Electrophoresis

A DISSERTATION SUBMITTED TO THE FACULTY OF THE UNIVERSITY OF MINNESOTA BY

Matt Geiger

IN PARTIAL FULFILLMENT OF THE REQUIREMENTS FOR THE DEGREE OF DOCTOR OF PHILOSOPHY

Michael T. Bowser, Advisor

March 2016

Acknowledgements

When I first entered college I never would have thought I would pursue a graduate degree in chemistry. Without the support and encouragement from many teachers, professors, family, and friends, I would not be where I am today.

I would like to thank Tim Anderson, my high school biology teacher, for helping me develop my science fair projects. He always made science exciting and fun in the classroom, and I attribute a large part of my curiosity for the sciences to him.

I would also like to thank Peter Myhrwold, my high school chemistry and physics teacher, for so many memorable classes. Your dedication to your students and excitement for teaching brought chemistry to life for me and were able to instill the passion for chemistry that I have today.

I would like to thank my undergraduate advisor, Dr. Bret Johnson, for suggesting I apply to graduate school. Without your encouragement and belief in me I never would have thought to pursue a graduate degree.

I would also like to thank Dr. Timothy Trygstad, my undergraduate organic chemistry professor. Working with him on my first chemistry research project turned lab work into something I was excited to do every day.

I would like to thank my graduate advisor, Mike Bowser. Joining his research group was the best decision I could have made entering my first year of graduate school. His constant guidance and understanding throughout many research highs and lows allowed me to develop many of the skills I have today.

I would like to thank all of the Bowser group members I've worked with over the past several years, especially Amy Stading, Alex Johnson, Rachel Harstad, Sarah Anciaux, Megan Weisenberger, and Nic Frost. Thank you for all of the discussions over the years and to those who assisted in fabrication of many microfluidic devices.

I would also like to thank my other University of Minnesota professors, especially Pete Carr. His class was one of my favorites and was certainly one of the most difficult. I would not have the appreciation and passion for separations that I do today without him.

I would like to thank the Nanofabrication Center and Mechanical Engineering machine shop staff, especially Terry Brough, for all of their help during fabrication.

I would like to thank my parents, Pat and Carol, for your constant support. Thanks for always encouraging me and letting me know that trying my best was all that mattered.

Finally, I would like to thank my wife, Joan. She came into my life at the perfect moment and has helped love and support me through the final stages of my graduate career. I love you.

Dedicated to my parents, Pat and Carol Geiger, my wife, Joan Geiger, and for my grandfather, Leo Geiger

Abstract

Micro free flow electrophoresis (μFFE) is a separation technique which can be used for unique applications due to its continuous nature. Separations are performed in space, as opposed to time, as laminar flow drives analytes down the separation chamber and are separated laterally by an electric field. This continuous nature makes it an attractive option to be used as a second dimension in multidimensional separations. The major focus of this work will be the development of a 2D separation platform coupling a commercial nano-liquid chromatography (nLC) instrument with an all glass μFFE device followed by investigating factors which could affect the efficiency of the technique. A new μFFE device was designed and fabricated for coupling with nLC. High peak capacity separations of tryptic peptides of BSA demonstrated the power of the technique. Broadening in temporal and spatial dimensions were investigated since peak capacity is calculated using analyte peak width. The observation that the adsorption of analytes only affects broadening in the temporal dimension is critical for maximizing peak capacity. Finally, the effect of using fluorescent labels in 2D nLC × μFFE separations will be demonstrated. The impact of label choice can be seen in the peak capacity and orthogonality of separations of amino acids and peptides.

Table of Contents

List of Tables

List of Figures

List of Abbreviations

1D	One-Dimensional
2D	Two-Dimensional
2D LC	Two-Dimensional Liquid Chromatography
2D PAGE	Two-Dimensional Polyacrylamide Gel Electrophoresis
µFFE	Micro Free Flow Electrophoresis
µFFIEF	Micro Free Flow Isoelectric Focusing
µFFZE	Micro Free Flow Zone Electrophoresis
µTAS	Micro Total Analysis System
ACN	Acetonitrile
aSi	Amorphous Silicon
BSA	Bovine Serum Albumin
CAD	Computer Aided Desgin
CCD	Charge Coupled Device
CE	Capillary Electrophoresis
CMC	Critical Micelle Concentration
CZE	Capillary Zone Electrophoresis
DMSO	Dimethyl Sulfoxide
DNA	Deoxyribonucleic Acid
EOF	Electroosmotic Flow
FFE	Free Flow Electrophoresis
FFF	Field Flow Fractionation
FFIEF	Free Flow Isoelectric Focusing
FFITP	Free Flow Isotachophoresis
FFZE	Free Flow Zone Electrophoresis
GC	Gas Chromatography
HEPES	4-(2-Hydroxyethyl)-1-Piperazineethanesulfonic Acid
HF	Hydrofluoric Acid
HPLC	High Performance Liquid Chromatography
IEF	Isoelectric Focusing
ITP	Isotachophoresis

LIF	Laser Induced Fluorescence
MEKC	Micellar Electrokinetic Chromatography
MES	Morpholine-4-ethanesulfonic acid
MS	Mass Spectrometry
MudPIT	Multidimensional Protein Identification Technology
nLC	nano Liquid Chromatography
NMR	Nuclear Magnetic Resonance
PEO	Poly(ethylene oxide)
pI	Isoelectric Point
PTFE	Polytetrafluoroethylene
RIE	Reactive Ion Etching
RNA	Ribonucleic Acid
SCX	Strong Cation Exchange
SDS	Sodium Dodecyl Sulfate
SELEX	Systematic Evolution of Ligands by Exponential Enrichment
SERS	Surface Enhanced Raman Scattering
TEPA	Tetraethylenepentamine
TFA	Trifluoroacetic acid
TLC	Thin Layer Chromatography
UV	Ultraviolet
PCR	Polymerase Chain Reaction
PDMS	Poly(dimethylsiloxane)
PECVD	Plasma Enhanced Chemical Vapor Deposition
PMMA	Poly(methyl methacrylate)
RP	Reversed Phase
ZDV	Zero Dead Volume
ZE	Zone Electrophoresis

Chapter 1

Introduction

1.1 Separations of Complex Mixtures

Over the last several decades significant advancements have been made in diagnostics, therapy, microbiology, and biochemistry. A major driving force in these advancements is due to the increased research in the fields of genomics, proteomics, and metabolomics. Pairing a well resolved separation with a sensitive detection strategy is able to provide both the selectivity and limits of detection required to analyze a biological sample. However, the high complexity of these samples puts a strain on the capabilities of current separation methods. Specifically, the traditional one-dimensional (1D) separation platforms routinely used are simply overwhelmed by the number of components in these mixtures. The following section describes the importance of the omics fields and the complexity of the samples, in addition to the current limitations of separation methods.

1.1.1 Omics Fields

The study of systems biology can provide key insights into the pathways and mechanisms in which living things function. The collective characterization and quantification of the molecular interactions that result in the structure, function, or dynamics of an organism is referred to as omics. Many of these fields have emerged such as genomics, lipidomics, proteomics, metabolomics, and even foodomics, referring to the studies of genes, lipids, proteins, metabolites, and food and nutrition, respectively. The common challenge facing researchers in these fields is the complex, coordinated regulation of many hundreds of proteins and genes. The human genome, for example, contains ~30,000 genes.[1]

These genes, however, encode thousands of proteins. An individual human cell can contain anywhere from 20,000 to 50,000 proteins. The need for powerful separation techniques is amplified by the dynamic range of these proteins, ranging from 10^2-10^8 copies.[1] Often times these samples are subjected to shotgun analysis, where the proteins are further broken down into peptides, increasing the complexity even more.[2] In metabolomics low molecular weight (<1,500 Da) compounds resulting from the metabolism of cells and tissues are analyzed. Human urine has been estimated to contain ~800 metabolites, while 4,600 have been identified in human blood.[3-5] Though not as complex as the genome or proteome, 1D separation methods are very quickly overwhelmed as will be described in the next section.

1.1.2 Traditional 1D Separation Methods

Any of the biological samples mentioned clearly require some form of separation prior to further analysis. Nucleic acids, such as DNA and RNA, which control the expression of genes, act on a slower time scale than protein interactions. Quantitative PCR and microarrays have become established methods to determine the genomic status of a system, but the need for high-throughput methods for proteins remains high. Growth in the field of proteomics has been limited by the lack of fast, reproducible, and high separation efficiency techniques. Compared to DNA, proteins are more complex, being made up of more “building blocks”, harder to separate, have a high variability of physical properties and functions, and are more difficult to detect.[6]

Peak capacity is the number of fully resolved peaks which can fit into a separation. Current 1D separation methods often fall short of the number of compounds in biological samples. (Figure 1.1)

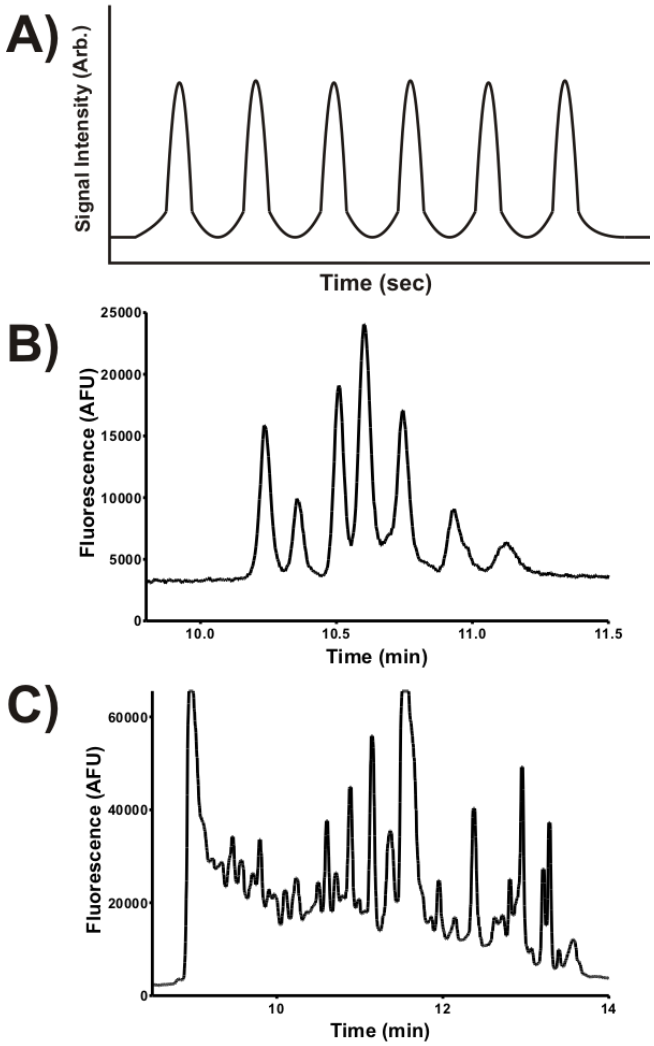

Figure 1.1: Peak capacity in 1D separations A) Ideal separation where all peaks are fully resolved at the baseline B) 1D separation where the peak capacity is sufficient to fully separate most of the peaks, though some are not fully resolved C) 1D separation of a complex sample. The number of peaks overwhelms the separation space and none of the peaks are fully resolved.

1D liquid chromatography (LC) methods typically produce peak capacities of around 500 in 30-60 minutes for peptides, while only 200-300 for non-peptide mixtures.[2] Capillary zone electrophoresis (CZE), which often provides high separation efficiencies up to one million theoretical plates per meter[7], also only produces peak capacities in the 300-500 range for peptides in a one hour analysis time.[8] These methods simply cannot "fit" the number of components in a complex sample across their separation spaces. (Figure 1.1c) Peak capacities greater than even 5,000 would be needed to even begin resolving these mixtures, which are not achievable in reasonable analysis times (<3 hours).

1.1.3 2D PAGE in Proteomics

Slab gel electrophoresis has been a useful tool in separating biological samples over the last several decades and is one of the most common techniques used. However, it is severely limited by slow analysis times, limited quantitation methods, and high degree of labor. In a 1D format only a few analytes can be identified, often with the use of antibody staining.[9] By switching to a multidimensional platform, many more compounds can be analyzed.

Two-dimensional polyacrylamide gel electrophoresis (2D PAGE) is often regarded as the gold standard in proteomic separations. First introduced by O'Farrell[10], 2D PAGE is a powerful separation technique because it separates analytes based on multiple properties. (Figure 1.2) First, compounds are separated by isoelectric point (pI) using isoelectric focusing (IEF). They are then separated according to their molecular weights by rotating the gel 90˚ and running sodium dodecyl sulfate polyacrylamide gel electrophoresis (SDS-

PAGE).[1] 2D PAGE is able to resolve up to 10,000 proteins, with ~2,000 being routine, allowing for its use in the study of genetic variations, cellular differentiation, diagnostics, and cancer research.

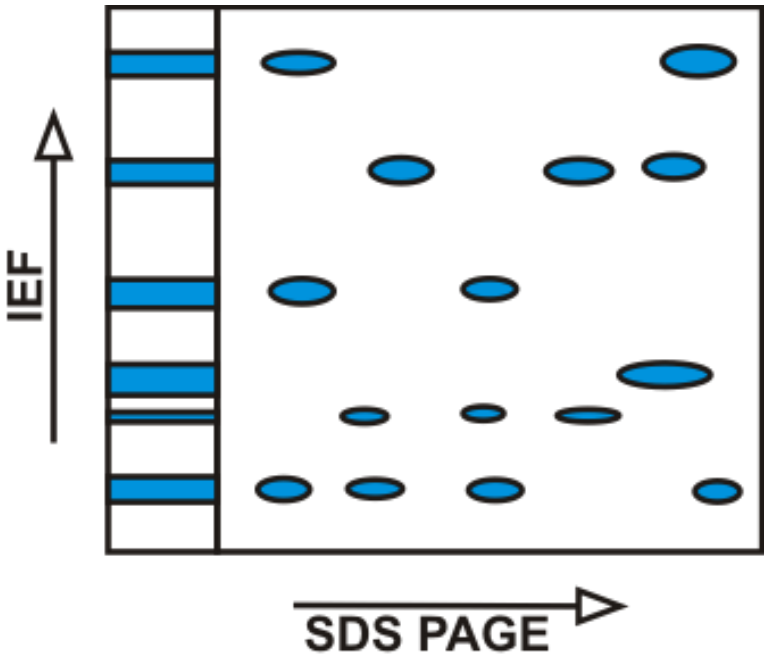

Figure 1.2: Two-dimensional polyacrylamide gel electrophoresis (2D PAGE) Analytes are first separated by pI using isoelectric focusing in the first dimension and then separated by molecular weight using PAGE in the second dimension.

Despite its high resolving power, 2D PAGE is limited by a low dynamic range (3-4 orders of magnitude), difficulty in analyzing proteins which are very alkaline or hydrophobic, and long analysis times (>24 hours) in addition to low reproducibility.[1]

1.2 Two-Dimensional Separations

The ability to combine multiple techniques to separate a sample by several properties can dramatically improve the quality of a separation compared to a 1D technique alone. As seen with 2D PAGE, very large numbers of constituents can be separated when pairing techniques. Both separations occurring in 2D PAGE are examples of separations in space, where components are allowed to migrate over a physical separation space for a fixed amount of time.[11] Due to the drawbacks of 2D PAGE, much research has been placed in coupling other 1D techniques, such as LC, CZE, and gas chromatography (GC). These differ from 2D PAGE in that they are all separations in time, meaning there is a fixed migration distance (ex. column length) and sample components elute at different times based on retention.[11] These column based platforms can either be on-line or off-line. Off-line methods collect fractions from the first dimension and analyze them separately with the second dimension. Though this method allows for sample manipulation and independent optimization of both dimensions, the tradeoff is significant increases in analysis times.

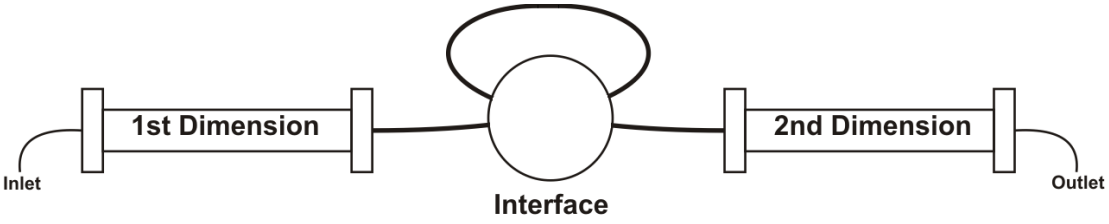

Figure 1.3: Diagram of an on-line 2D separation. The first dimension is sampled through an interface and injections are done onto a second separation. In the case of a comprehensive separation the second dimension must be run and fully re-equilibrated in the time it takes the injection volume to elute from the first dimension.

On-line methods use an interface to directly couple the first and second dimensions. (Figure 1.3) This coupling often results in much faster separations, however optimization is not as straightforward.

1.2.1 Comprehensive On-line 2D Methods

To fully understand the components of a complex mixture, the entirety of the first separation should be subjected to analysis by the second (i.e. be comprehensive). Erni and Frei first used comprehensive 2DLC to separate senna glycosides using size-exclusion chromatography (SEC) and RPLC.[12] Peak capacity was limited, however, due to only seven fractions being taken from the first dimension. For protein analysis Bushey and Jorgenson were able to achieve a peak capacity of 130 for a 6 hour comprehensive separation.[13] Since then, many combinations of 1D methods have been used to increase peak capacity and the rate of peak capacity production including LC×LC[13-15], GC×GC[16-18], LC×GC[19, 20], LC×CE[15, 21, 22], and CE×CE.[23-25]

One of the more powerful uses of LCxLC has been multidimensional protein identification technology (MudPIT). In MudPIT, a microcapillary is packed with both strong cation exchange (SCX) and reversed phase (RP) materials.[26-30] Peak capacities up to 3,200 have been reported, though long analysis times of up to 10 hours were needed.[15] The peak capacity of LCxCE systems has been shown to be as high as 20,000 in 5 hours.[31] Using microchip CE as a second dimension to HPLC, Yang *et al.* were able to achieve a peak capacity of 1,000 in around 1 hour.[22] Using a microfluidic device for MEKCxCE, Ramsey *et al.* were able to produce a peak capacity of 4,200 in ~15 minutes.[32] Using high

temperatures and short second dimension columns, peak capacities of 1,200 were obtained in 20 minutes using SCX for the first dimension and RPLC for the second.[33, 34] These hyphenated techniques are quickly approaching peak capacities high enough to handle complex samples. However, adequate sampling of the first dimension and orthogonality between the methods must also be taken into consideration.

1.2.2 Peak Capacity

Peak capacity was originally defined by Giddings as the maximum number of peaks that can be separated on a given column[35] (i.e. the number of equally spaced analyte peaks which could fit across the separation window). (Figure 1.1a) Typically, peaks are assumed to be equally spaced in the separation window. In the case of gradient elution RPLC, the separation window is defined by the gradient start time and the end of the gradient run. Karger *et al.*[36] introduced the multiplicative nature of 2D peak capacities, and this idea was later elaborated on by Guiochon[37] and Giddings[35] as:

$$n_{c,2D} = {}^{1}n_c \, {}^{2}n_c \qquad (1.1)$$

where the peak capacity of a 2D separation ($n_{c,2D}$) approaches the product of the peak capacities from the first (${}^{1}n_c$) and second (${}^{2}n_c$) dimensions. Since it's much faster to generate a peak capacity of *n* twice, rather than n^2 once, 2D separations appear to have a distinct advantage over their 1D counterparts.[10] For example, if a peak capacity of 100 were desired for a given separation, a peak capacity of only 10 in each dimension of a 2D separation would be needed.

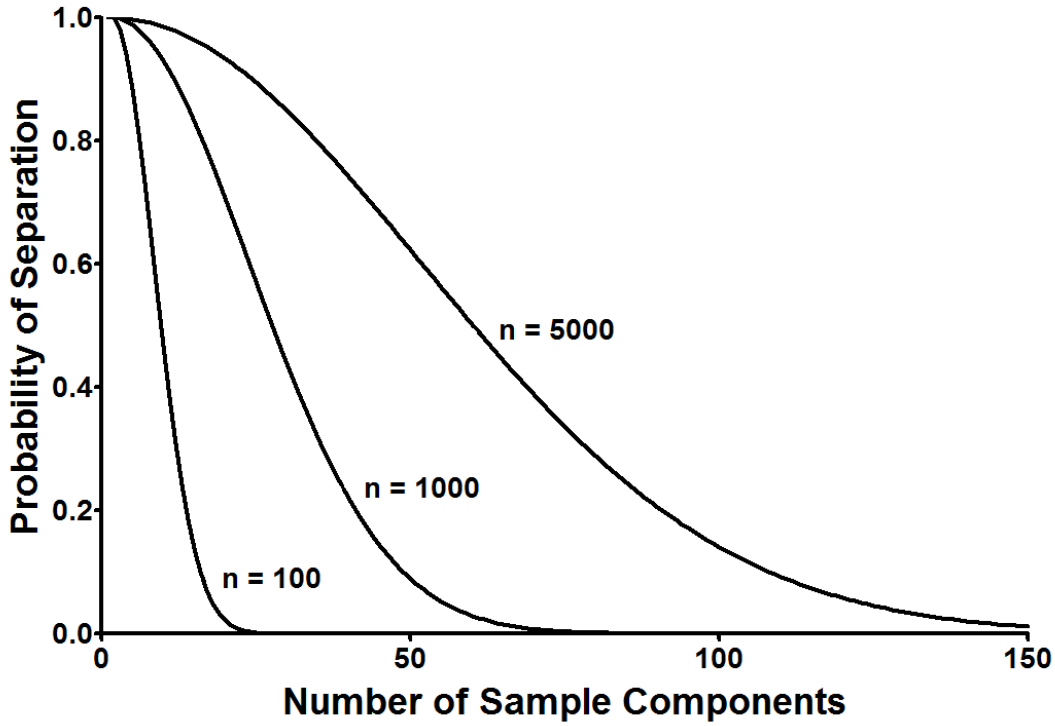

Figure 1.4: Probability of separating a mixture of sample components (*m*) for peak capacities (*n*) of 100, 1000, and 5000 (eq. 1.2 from reference 38)

Before going into the experimental application of this increased peak capacity, the relationship between peak capacity and actual chromatographic peaks should be addressed. Martin *et al.* used peak overlap analysis to describe the probability that all sample components will be resolved for a given peak capacity, *n*, and a given number of sample components, *m*.[38]

$$P_{m,n}(m) = (1 - \frac{m-n}{n-1})^2 \qquad (1.2)$$

The dramatic decrease in probability of separation can be seen as the samples become even slightly more complex. (Figure 1.4) A peak capacity of 100 can only separate a 10 component mixture 50% of the time. Once the sample has greater than 15 components, the probability drops below 10%. Even with peak

capacities of 1,000 or 5,000, sample mixtures containing more than 100 compounds are almost impossible to fully resolve without increasing the peak capacity.

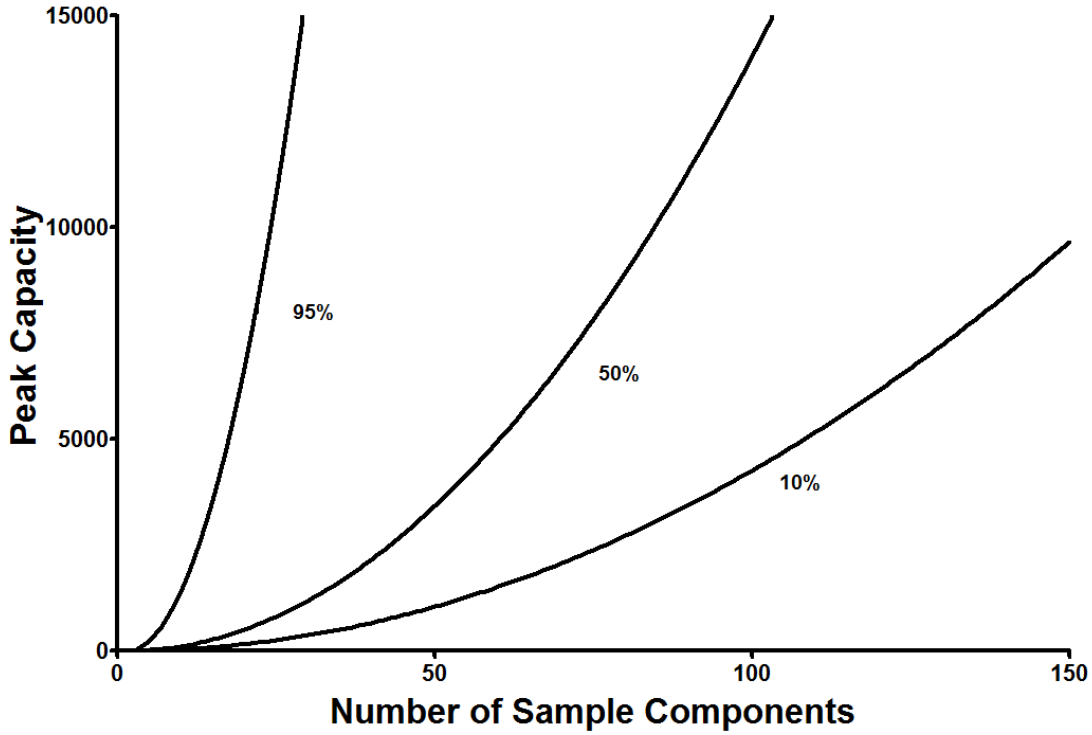

Figure 1.5: Peak capacity required to separate a sample of a set number of components (*m*) with probabilities of 10%, 50%, and 95% chance of complete separation (eq. 1.3)

$$n_{min} = 1 + \frac{(m-1)}{(1-P_x^{\frac{1}{m-2}})} \qquad (1.3)$$

The peak capacity required (n_{min}) to fully separate an *m* component mixture with P_x probability is given by equation 1.3. As the number of components increases from 10 to 100 the required peak capacity increases from 65 to 13,500 at the 50% probability level. (Figure 1.5) Even if a 10% probability would be tolerable, a 1,000 component mixture would require a peak capacity of

over 400,000! Both models in Figures 1.4 and 1.5 assume randomly distributed peak positions and uniform peak widths. With optimization, better separations than these models predict can be achieved, however they stress the importance on maximizing peak capacity.

Another advantage to high peak capacities can be seen in Figure 1.5 for the 95% probability curve. For relatively small samples (m < 20) the peak capacity required is around 5,500. Though this peak capacity is not readily achievable using a 1D separation, 2D techniques are quickly approaching this level. It becomes clear that high peak capacity separations have an advantage over their 1D counterpart. An exceptional 1D separation with a peak capacity of 500 could only separate a mixture of 5 or 6 compounds with 95% probability. Though optimization could be done to better the separation, the peak capacities generated in multidimensional separations would allow for separation without optimization.

1.2.3 Under Sampling

As mentioned in Section 1.2.1, on-line 2D separation methods collect fractions as they elute off of the first dimension and then are directly injected onto the second dimension. In order to achieve the peak capacity described in eq. 1.1, no resolution generated in the first dimension must be lost in the second dimension. This loss is often caused by the under sampling of the first dimension or remixing at the interface between dimensions. The sampling rate of a first dimension peak is defined as the number of fractions which are taken across the peak width. Murphy *et al.* originally proposed a sampling rate of 3-4 times across

the 8σ peak width.[39] Often, in 2DLC, the second dimension separation is unable to sample this quickly for shorter first dimension analysis times, resulting in deleterious losses in peak capacity simply by not sampling fast enough. Davis, Stoll, and Carr developed a metric, β, to account for under sampling and how the ideal peak capacity is reduced. The amount of reduction, or fraction of ${}^{1}n_c$ retained, is defined as $1/\beta$ (eq. 1.4).[40]

$$ {}^{1}n_c' = \frac{{}^{1}n_c}{\beta} \qquad (1.4) $$

$$ \beta = \sqrt{1 + \alpha \times \left(\frac{t_s}{{}^{1}\omega}\right)} \qquad (1.5) $$

The degree to which a peak is under sampled is proportional to the ratio of the second dimension cycle time, t_s, and the 4σ width of a first dimension peak, ${}^{1}\omega$. The under sampling coefficient, α, was determined to be 3.35 for separations of random multi-component systems (random retention times and peak heights in both dimensions).[41] The value of α was determined for a resolution of 1 between adjacent peaks. Even faster first dimension sampling rates would be required if higher resolution is needed to separate two or more components.

Figure 1.6 demonstrates the loss of peak capacity due to the under sampling of the first dimension. If a first dimension separation generating 100,000 theoretical plates in 60 minutes is chosen, it is estimated 62% of the peak capacity is lost, even if the second dimension cycle time is only 1 minute. On an LC time scale, this rate is pushing the limits of speed at which a gradient

can be run and the column re-equilibrated. The fastest LC x LC cycle times reported are between 12-21 seconds.[14, 33, 34] For the same 60 minute separation,

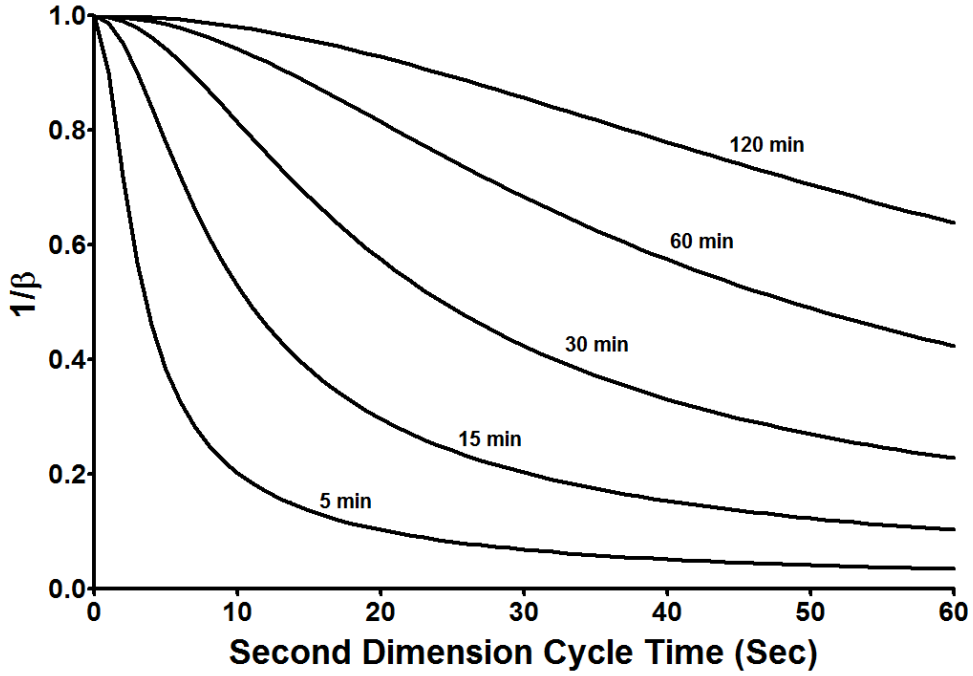

Figure 1.6: Fraction of peak capacity retained in the first dimension (1/β) vs. second dimension cycle time (t_s) for first dimension separation times of 5, 15, 30, 60, and 120 minutes assuming a first dimension efficiency of 100,000 theoretical plates.

these rates would still result in ~20% of the peak capacity lost due to under sampling. Going to a shorter first dimension separation of 15 minutes would result in 70% of the peak capacity being lost. The need to adequately sample the first dimension is often why 2D separations have long analysis times. It's important to emphasis also that any reductions in second dimension cycle time generally result in a reduced second dimension peak capacity. The result becomes an optimum sampling time for each set of first dimension separation conditions. [42, 43]

1.2.4 Orthogonality

In addition to correcting for the under sampling of the first dimension, the separation mechanisms must be orthogonal, or uncorrelated. The original use of orthogonality comes from 2D thin layer chromatography (TLC) or 2D PAGE, where the separations in the first and second dimensions are performed 90˚ to each other.[35]

Orthogonality represents how efficiently the separation space is utilized. There are two factors, proposed by Giddings, which determine the orthogonality of a 2D separation. The first is the separation dimensionality, which refers to the number of separation mechanisms used in the system (ex. the number of columns coupled together in 2DLC or 2DGC). The other is the dimensionality of the sample. Giddings proposed a sample can be characterized by the number of independent variables needed to identify the components of the sample (ex. size, charge, electrophoretic mobility, hydrophobicity, etc.).[44] If the sample were to not have enough complexity, the addition of more separation dimensions would offer minimal gains in peak capacity. For a separation using two-dimensions, for example, the sample must have a dimensionality of 2 or more to observe any degree of orthogonality.

There have been many methods for determining the orthogonality of both separation modes and samples including correlation coefficients[45, 46], fractal dimensionality[47], geometric approaches such as fan area[48], counting peaks[49], and modified forms of box counting.[50-52] Rutan *et al.* have demonstrated the use of metrics based on ecological home range calculations for determining the

fraction coverage (f) of peaks in a 2D separation space.[53] In particular, they found the minimum convex hull method to have advantages over previously mentioned methods.

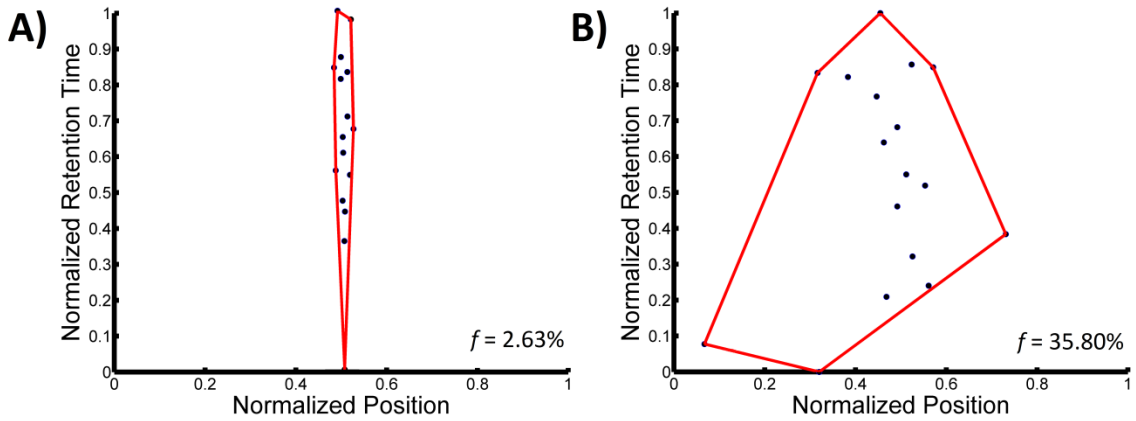

Figure 1.7: Minimum convex hull plots for 2D separations A) A separation where the separation modes are not orthogonal. No additional gains in resolution occur between the first and second dimensions B) A separation where the modes are fairly orthogonal and the peaks are spread out over a larger fraction of the separation space.

The minimum convex hull defines the usable, or accessible, separation space by drawing the smallest convex polygon (i.e. all interior angles are less than or equal to 180˚) around the outermost peaks of the separation. This approach is simple, lacks adjustable parameters, and can be calculated using a standard function in Matlab. Figure 1.7 demonstrates the use of the minimum convex hull for both separations of low (Figure 1.7a) and high (Figure 1.7b) degrees of orthogonality. Accounting for f modifies equation eq. 1.1 into eq. 1.6 to give the effective 2D peak capacity of a separation. Under sampling manifests itself in the first dimension peak width measured in the 2D separation space.

$$n_{c,2D} = {}^{1}n_c \, {}^{2}n_c \times \frac{1}{\beta} \times f \qquad (1.6)$$

However, often times f is not reported or taken into account when calculating $n_{c,2D}$ therefore both corrected and uncorrected values will be given when making comparisons in later sections.

1.3 Micro Free Flow Electrophoresis (μFFE)

Free flow electrophoresis (FFE) has been used over the last five decades primarily for the isolation and fractionation of cells, organelles, and protein mixtures.[54] With the increased interest in the omics fields, the applications of FFE as an analytical tool have been explored. As with many of the major analytical separation techniques such as LC, CE, or field flow fractionation (FFF) the miniaturization of FFE to a microfluidic format has resulted in increased performance and applications.

1.3.1 Free Flow Electrophoresis (FFE)

Free Flow electrophoresis was first introduced by Barrolier *et al.* in 1958[55]and Hannig in 1961.[56] In FFE, analytes are continuously driven by pressure flow through a separation chamber. An electric field is applied perpendicular to this flow and analytes are deflected into distinct streams based on their electrophoretic mobilities, as shown in Figure 1.8.[54]

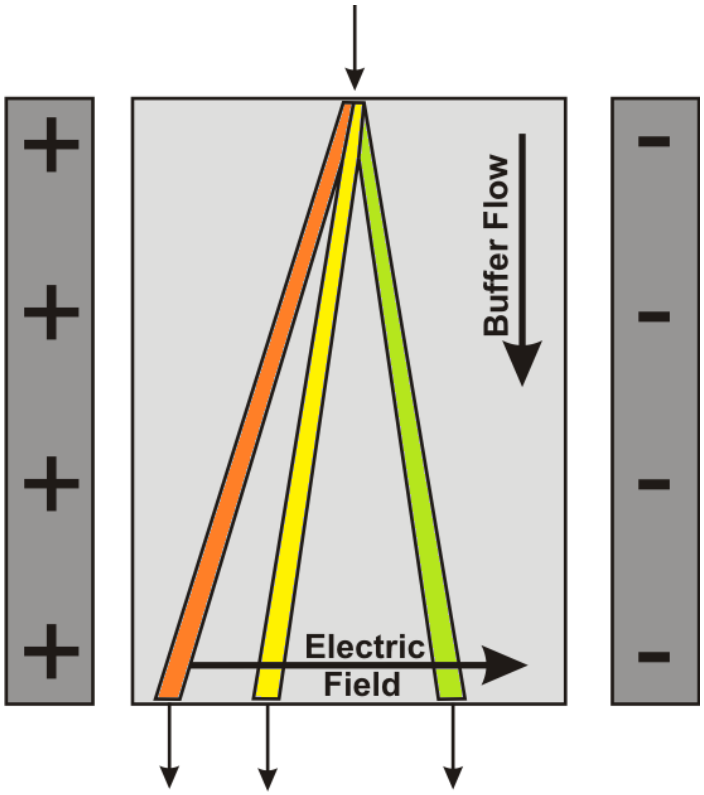

Figure 1.8: Operating principle of free flow electrophoresis (FFE). Sample is introduced to the top of a planar separation channel and driven by buffer flow. An electric field is applied perpendicular to the flow and analytes separate into bands based on their mobility. Fractions can then be collected at the end of the separation chamber.

Because the separation occurs in a different direction than the bulk flow, sample injection, separation, and collection take place continuously, unlike discrete injections used in traditional CE. The continuous nature of FFE has made it a common tool in protein and DNA purifications using separation modes such as free flow zone electrophoresis (FFZE)[57], free flow isoelectric focusing (FFIEF)[58, 59], and free flow isotachophoresis (FFITP).[60-62]

The dimensions and volumes used in FFE devices result in a relatively high cross-sectional area and low surface-area-to-volume ratio, leading to poor

heat dissipation. Joule heating is often observed as field strengths begin to go above 100 V/cm.[54, 63] The miniaturization of devices yields higher surface-area-to-volume ratios, decreased residence times, less sample and reagent requirements, and increased sensitivity.[64, 65] These advantages make FFE a prime technique to integrate into a microfluidic platform in order to eliminate Joule heating within the separation channel and find applications in micro-preparative separations.

1.3.2 Development and Fabrication of µFFE devices

Raymond *et al.* were the first to miniaturize FFE in 1994[66] using micro machined channels in silicon and further developed the technique in 1996.[67] They were able to show that the smaller separation volumes dissipated heat more rapidly, effectively removing Joule heating as a major source of band broadening. The main drawback to the use of silicon for the device, however, was the low field strengths (<50 V/cm) that could be applied due to the formation of electrolysis bubbles. These bubbles enter the separation channel and can distort the flow profile. Additionally, silicon has a breakdown voltage between 100-200V, limiting the maximum field strength even if bubbles weren't present.[66] Since then µFFE devices have been fabricated in polydimethylsiloxane[68-71], poly(methyl methacrylate) (PMMA)[72], biaxially-oriented polyethylene terephthalate (Mylar™)[73], and glass[74-80]. These materials allow for higher voltages to be applied compared to silicon, in addition to having lower material cost.

The generation of electrolysis bubbles still remains a limitation to the strength of the electric field which is applied. Preparative FFE devices use ion-exchange membranes to isolate the electrodes from the separation. These membranes are difficult to implement in a microfluidic format due to the small feature sizes, often 100 µm or less. Methods for either isolating or reducing electrolysis bubbles in µFFE devices have included channel arrays[66], multiple channel depth[81], suppression via redox couples[82], buffer additives[71, 83, 84], partitioning bars[69], glass bridges[76], ion permeable salt-bridges[79], functionalized gels[70], and hydrogel membranes.[78] A combination of multiple channel depth and buffer additives has been used in this work and has shown stream stability up to 2 hours for fluorescent dye separations[83] and applied field strengths up to 586V/cm.[81]

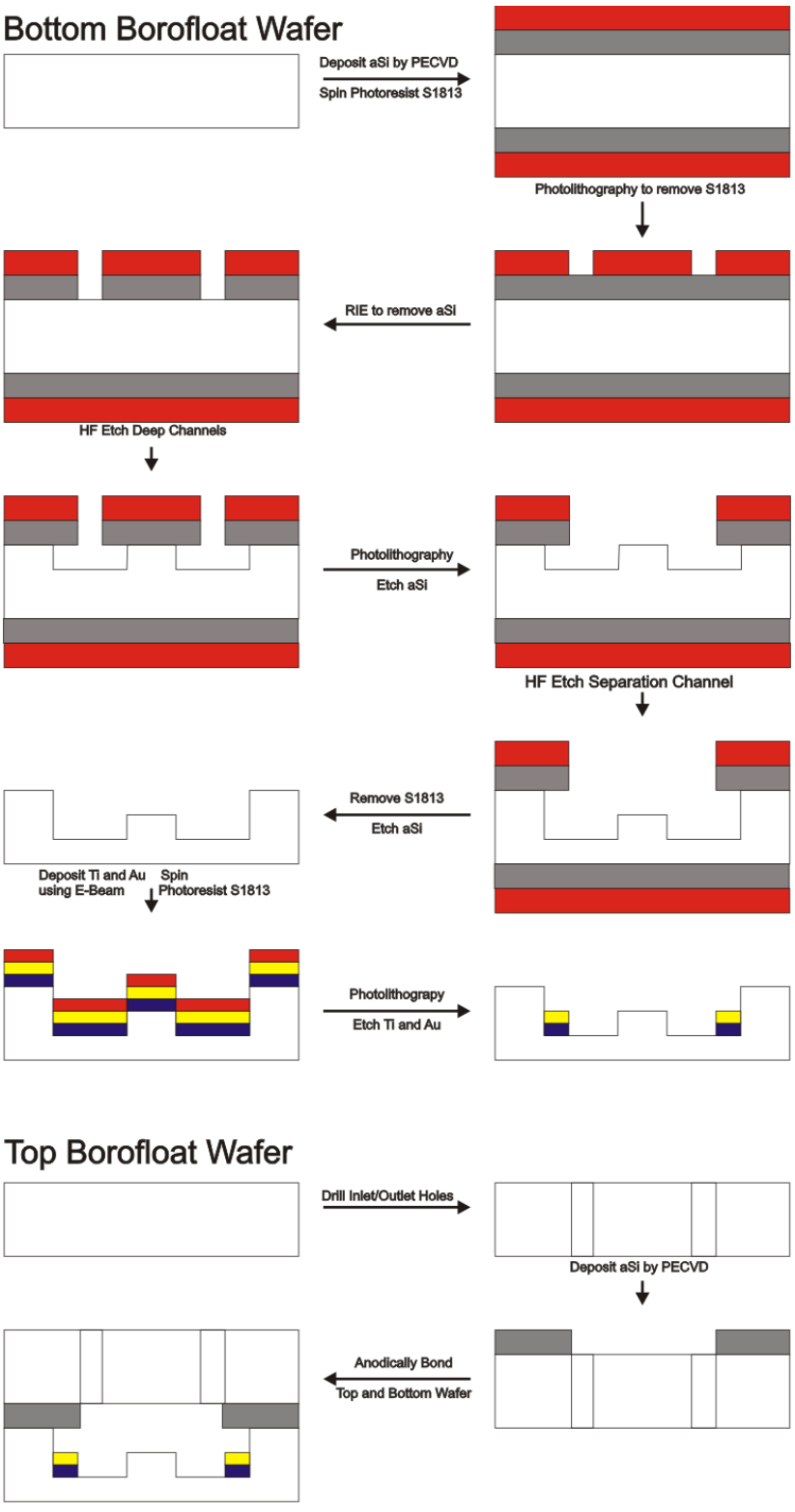

Figure 1.9: Fabrication scheme developed for glass µFFE devices. Borofloat® glass (white), amorphous silicon (gray), S1813 photoresist (red), titanium (blue), and gold (yellow).

Device fabrication in glass follows the process described in Figure 1.9. A borosilicate glass wafer is first protected by depositing a layer of amorphous silicon (aSi) using plasma enhanced chemical vapor deposition (PECVD). Standard photolithography and wet etching procedures are used to define and etch features into the glass. Photolithography and wet etching can be repeated to define features with multiple depths. The remaining aSi is then removed using reactive ion etching (RIE). Electrodes are patterned onto the devices by first depositing a layer of Ti and Au by electron beam evaporation and then using photolithography and wet etching to remove the unwanted metal. Access holes for fluidic and electrode connections are then drilled into a second wafer. This wafer may or may not already have features etched depending on the design of the device. The wafers are then anodically bonded together by depositing a thin layer of aSi to one wafer and applying a high voltage under vacuum and high heat. A completed device can be seen in Figure 1.10. More detailed descriptions of this process can be found in later experimental sections and group publications.[75, 81, 83, 85]

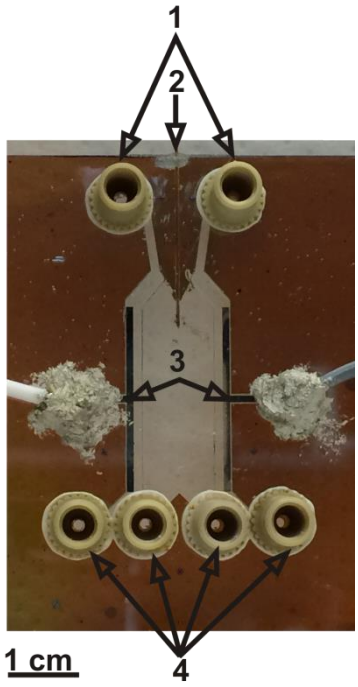

Figure 1.10: Completed µFFE device (1) buffer inlets (2) sample inlet capillary (3) electrodes (4) buffer outlets.

Detection schemes for microfluidic devices have utilized optical methods (fluorescence[78, 83, 85], UV[86], IR spectroscopy[87, 88], surface enhanced Raman scattering (SERS))[89, 90], electrical methods (conductivity[91], charge field effect[92], impedance[93], changes in potential[94], cyclic voltammetry[95]), NMR spectroscopy[96], and mass spectrometry.[80, 97] Detection of analytes in microfluidic devices is limited by the small volumes and short path lengths stemming from their small feature sizes. On-chip detection in µFFE offers a unique challenge because sensing across the entire separation channel, rather than a fixed point, is required. Schemes utilizing either a scanning point-source detector[66, 67, 72] or continuously imaging a broader area using a microscope[75, 78, 79, 81, 83, 85] have been employed, though the use of point detectors requires accurate and precise control of the spatial movement of the device. To improve limits of detection,

laser-induced fluorescence (LIF) is commonly used. In the work presented, a 488 nm laser is expanded into a line and directed across the separation channel of the µFFE device. A charge-coupled device (CCD) camera is positioned on top of an optical microscope above the µFFE chip. The CCD camera then converts the light intensity passing through filter cubes into a measurable signal. Further impacts of the use of LIF will be discussed in Chapter 4.

1.3.3 Modes of Operation and Applications

Much like its preparative counterpart, µFFE can be run in a variety of electrophoretic modes. Interchanging between µFFZE[66, 67, 75, 85], µFFIEF[71, 78, 98], and µFFITP[99] merely requires a change in buffer composition, such as the addition of ampholytes in the case of IEF. To date, separations of fluorescent dyes[71, 75], amino acids[66, 69, 71], peptides[85], proteins[67, 72, 76, 98, 100, 101], organelles[70, 77, 102], and whole cells[70] have been reported.

Most of these applications, however, have been proof-of-concept experiments to compare and improve chip design in addition to improvements in resolution. The design improvements and methods of improving stream stability have generated a few practical applications of µFFE. Kostal *et al.* were able to use µFFE for continuous separations of mitochondria from rat myoblasts in less than 30 seconds. Compared to preparative FFE, the micro devices used ~100-fold less sample, ~10-fold less buffer, and required a 15-fold lower electric field. In comparison to CE, µFFE was shown to have shorter analysis times and use less separation voltage. Additionally µFFE offers the potential to collect and

further characterize organelles, making it an attractive tool for micro total analysis systems (μTAS).[102]

Fonslow and Bowser developed the use of gradient μFFE to rapidly optimize buffer conditions for the separation of primary amines. A gradient of hydroxypropyl-β-cyclodextrin was applied over a 5 minute window allowing for 60 sets of buffer compositions to be tested. In comparison, to test even 15 sets of conditions using CE required 4 hours.[103] Gradient μFFE was also used by Turgeon *et al.* to investigate the equilibria of DNA aptamers with their protein targets. The continuous nature of μFFE allowed for 300 discrete concentrations of protein to be observed in 5 minutes, significantly faster than affinity CE assays. Another advantage of the μFFE system was the ability to see transitions of stoichiometries over a distribution of protein target concentration, revealing additional information about the dynamics of the complex.[104] μFFE was also used to isolate DNA aptamers for human immunoglobulin E. The continuous nature was again shown to be an advantage of traditional CE, allowing for a 300-fold improvement in library size screened. Four rounds of selection were able to be performed in only four days, with only one round being required to generate aptamers with low nM dissociation constants.[105] Using inkjet-printed sensors, Herzog *et al.* were able to fabricate a μFFIEF device which could be used for rapid pI determination. The applicability to use this method as part of a μTAS device was shown by obtaining protein pI's in less than 10 seconds.[98]

1.4 µFFE as a Second Dimension

To date, FFE in both preparative and microfluidic scale devices have only been used as pre-fractionation tools in off-line multidimensional separations. Moritz *et al.* used a FFIEF device to separate proteins into 96 fractions, each then subjected to a 6 minute RPLC gradient. Though a total peak capacity was calculated to be 6,720, the near 10 hour separation only results in a peak capacity generation rate of ~12 peaks/min.[106] Another multidimensional scheme was done using FFIEF followed by SCX and microcapillary RPLC. The addition of FFIEF was shown to produce 5-fold more protein identifications and 6-fold more peptide identifications. Though low abundance proteins typically hard to detect with 2D PAGE were able to be identified, the total analysis time for the system was almost 4 days.[107] The reduced sample requirements of µFFE and the continuous separation ability suggest that it could be utilized more effectively as a second dimension.

The cycle time of the second dimension in on-line comprehensive 2D separations has already been shown to be crucial in preserving the efficiency of the first dimension separation. (Section 1.1.6) As shown in Figure 1.6, cycle times even as fast as 10-20 seconds are not sufficient once analysis times become less than 30 minutes. µFFE offers a unique advantage since the separation occurs in space rather than time. The µFFE device essentially then acts as a chemically selective detector sampling infinitely fast. The only limitation on the cycle time is the time required to detect an analyte. In this work, a CCD camera is used for detection. Common exposure times to detect low nanomolar

concentrations of fluorescent dyes range from 100-250 msec.[75, 81, 85, 103, 108] The utility of this sampling rate, and the advantage μFFE has over traditional LC as a second dimension, can be seen if we compare the two methods using a first dimension peak width which is very narrow. The peak width of a peptide from a BSA tryptic digest was reported to be 48 seconds.[22] Using this width for a first dimension peak, a second dimension LC gradient of 12 seconds would result in 4 samples taken per peak, and ~17% of the peak capacity from the first dimension would be lost due to under sampling (eq. 1.4 and 1.5). In comparison, a camera exposure time of 100 msec using μFFE as a second dimension would generate 480 samples across the same peak, resulting in less than 0.5% of the first dimension peak capacity being lost. A more significant example can be seen if the peak width from the second dimension was used. Microchip CE peaks for the BSA tryptic digest were shown to be 0.65 seconds.[22] In the case of LC, ~90% of the peak capacity would be lost negating almost all of the separation achieved in the original separation. Using μFFE would still retain over 80% of the original peak capacity. The ability of μFFE to rapidly sample peaks gives it a distinct advantage over other separation methods, especially when peaks become narrow, giving it a wider range of use.

1.4.1 μFFE Interface

In order to fully maintain the peak capacity, there must also be no mixing of the sample stream when connecting the first dimension to the microfluidic chip. If the sample stream were to encounter any significant dead volumes, the mixing of analytes could occur, resulting in a loss in resolution.

In 2D separations using multiple columns, complicated valve systems are needed which are precisely controlled to keep injections timed.[14, 16] Conversely, there are commercially available products are made to make fluidic connections to microfluidic devices. IDEX Nanoports™ used in this work are placed over access holes and allow for a variety of tubing and capillary sizes to be connected. However, a dead space is created equal to the size of the hole in the glass, leading to a dead volume.

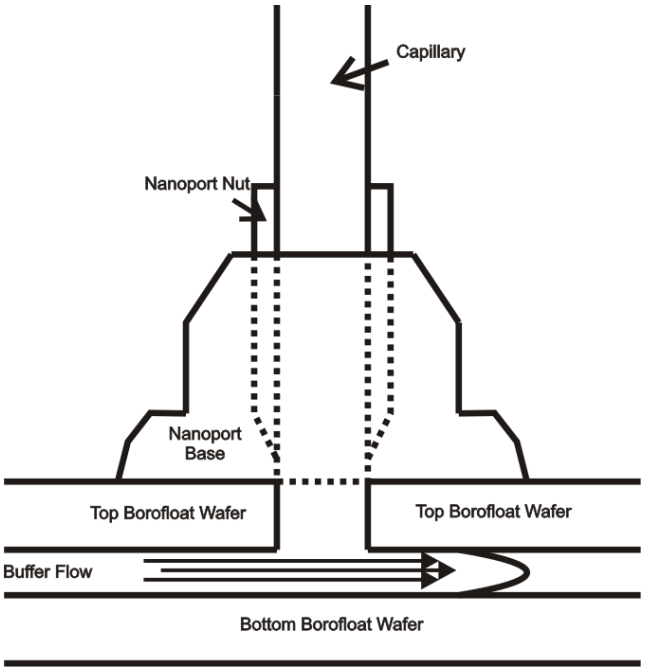

Figure 1.11: Diagram of a connection to a microfluidic device using a NanoPort™. A dead volume is created equal to the size of the hole put in the top substrate of the device.

This volume has minimal impact when a sample is being continuously injected for monitoring experiments; however this space is unsuitable for maintaining the resolution of a first dimension peak. Bings *et al.* made capillary connections to microfluidic devices by drilling into the edge of the device with a

flat bottomed drill bit. They were able to show ~98% of the theoretical plates of a peak were maintained through the interface.[109] However, due to the length of the channels and the need for precise alignment this method can not easily be implemented in µFFE. Fluidic connections have also been made using custom machined parts,[97] but the need for new, simple, strategies still remains. A new strategy for making a zero dead volume connection to a µFFE device will be discussed in Chapter 2.

1.4.2 Broadening in µFFE

The width of an analyte band in µFFE will limit the 2D peak capacity achievable since the separation space is fixed to the width of the device. The total variance of an analyte band (σ_{total}^2) is the sum of all of the factors that contribute to peak broadening:

$$\sigma_{total}^2 = \sigma_{inj}^2 + \sigma_D^2 + \sigma_{HD}^2 + \sigma_{EMD}^2 \qquad (1.7)$$

where σ_{inj}^2 is the broadening due to injection, σ_D^2 is the broadening due to diffusion, σ_{HD}^2 is the hydrodynamic broadening contribution, and σ_{EMD}^2 is the electromigration dispersion contribution.[108]

The variance due to injection width from eq 1.7 can be expressed by eq 1.8:

$$\sigma_{inj}^2 = \frac{w_{inj}^2}{12} \qquad (1.8)$$

where w_{inj}^2 is the width of the injected analyte stream.[108] The variance from this contribution is lowered as the width of the injection is reduced. The determining factor for the width of the sample band is dependent on hydrodynamic focusing. Hydrodynamic focusing will occur if the incoming stream is flowing at linear

velocities lower than the bulk flow velocity.[79] The ratio of linear flow rates between sample injection and buffer flow rate can be modified to narrow or widen a band.

Broadening due to diffusion can be expressed by eq 1.9:

$$\sigma_D^2 = 2Dt = \frac{2DL}{v} \qquad (1.9)$$

where *D* is the diffusion coefficient of the analyte, *t* is the analyte residence time between injection and detection, *L* is the length of the separation channel, and v is the flow velocity. From eq 1.9, it can be seen that a shorter residence time will minimize this contribution which can be achieved through higher flow rates.

Hydrodynamic broadening is due to the pressure-driven parabolic flow profile of the electrolyte buffer. (eq 1.10)

$$\sigma_{HD}^2 = \frac{h^2 d^2 v}{105DL} \qquad (1.10)$$

Broadening by this factor is related to the height of the separation channel (h), the migration distance (d), v, *D*, and *L*. This “cresent effect” has been described by Fonslow and Bowser and variance due to this source can be minimized by having small channel heights (common for microfluidic devices) and lower linear velocities to narrow the parabolic flow profile.[108]

Electromigration dispersion (σ_{EMD}^2) occurs when the buffer composition across the area where the electric field is applied is not constant, leading to areas of varying conductivities in the separation channel. This variation results in broadening because analytes will travel at different speeds through the different buffer compositions. In continuous μFFE separations, this source is not significant because the sample buffer conductivity can easily be matched to the

FFE electrolyte buffer. In 2D hyphenated systems, however, the mobile phase from the first dimension may not match conductivity with the electrolyte buffer, leading to potential broadening or focusing of peaks.[110, 111]

Substituting eq 1.8,1.9, and 1.10 into eq 1.7 gives the total variance of an analyte band (assuming no contribution from electromigration dispersion, as is typical for continuous µFFE separations):

$$\sigma_{total}^2 = \frac{w_{inj}^2}{12} + \frac{2DL}{v} + \frac{h^2 d^2 v}{105DL} \qquad (1.11)$$

A complex dependency between flow velocity and analyte migration distance (a function of applied voltage and flow velocity) on σ_{total}^2 can be observed. Fonslow *et al.* further rearranged eq 1.11 to give an optimum flow velocity of[108]:

$$v_{opt} = \frac{\sqrt{210}DL}{hd} \qquad (1.12)$$

Having this in-depth understanding of broadening mechanisms is critical for maximizing peak capacity in the µFFE dimension.

1.4.3 Orthogonality and Separation Modes

µFFE also can be very versatile as a second dimension due to the variety of electrophoretic separation modes it can operate under. As mentioned in section 1.3.2, µFFE can be employed using zone electrophoresis, micellar electrokinetic chromatography (MEKC), IEF, and ITP. In zone electrophoresis, components are separated into bands based on their net electrophoretic mobilities. MEKC incorporates a surfactant above its critical micelle concentration (CMC) to act as a pseudo-stationary phase. This phase allows for the separation of neutral species, which are normally difficult to separate by zone electrophoresis. IEF utilizes a pH gradient to separate analytes based on their

individual pI's. By applying an electric field across this gradient, molecules migrate until they are electrically neutral. In μFFE, a gradient is generally established by using pre-sorted ampholytes in the separation buffer.[78] ITP is another focusing technique which introduces a sample between a leading and trailing electrolyte. Analytes focus into zones in order to match conductivities of the leading and trailing buffers.[99] The number of modes available can provide orthogonal separation mechanisms to a range of first dimension techniques such as LC or CE.

1.5 Scope of Thesis

The increasingly complex samples seen in biomedical and environmental research have overwhelmed the ability of traditional one-dimensional separations to effectively analyze them. Even recently developed comprehensive on-line methods do not have sufficient peak capacity. Oftentimes the theoretically attainable peak capacity is not achieved due to under sampling of the first dimension or lack of orthogonality between separation modes. Chapter 2 will describe the development of a novel 2D separation platform coupling nano-liquid chromatography (nLC) with µFFE. A zero dead volume interface will be presented and shown to provide a suitable connection to the microfluidic chip. High peak capacities generated will show the potential of this technique. With the utility of the nLC × µFFE platform demonstrated, Chapter 3 will take a closer look at the differences in broadening between the temporal and spatial dimensions. The impact of surface adsorption will be explored to better understand how to maximize peak capacity in each dimension. Chapter 4 will explore the use of fluorescent labels in µFFE. The use of LIF requires the sample to be either natively fluorescent, or be labeled with a fluorogenic reagent. The impacts on sample dimensionality and overall orthogonality will be assessed. Lastly, Chapter 5 will detail the work accomplished up to this point, and provide a range of future applications for this technology.

Chapter 2

Coupling nano-Liquid Chromatography with Micro Free Flow Electrophoresis for Separations of Peptides

Geiger, M., Frost, N.W., and Bowser, M.T. *Anal. Chem.*, **2014**, *86 (10)*, 5136-5142

2.1 Summary

The throughput capabilities of two-dimensional (2D) separations is largely impacted by peak capacity lost due to the under sampling of first dimension peaks by the second dimension. The continuous nature of micro free flow electrophoresis (μFFE) offers a unique solution to the under sampling challenge. In this work nano-liquid chromatography (nLC) is coupled directly to a μFFE device to be used as the second dimension. Since μFFE is a continuous technique where separation occurs perpendicular to the flow, no complicated injection was necessary to interface the two techniques. The flow rates of nLC (50 – 500 nL/min) are also within the range of current μFFE devices (100 – 500 nl/min) eliminating the need for any flow modulation. A side-on interface was designed and fabricated into an all glass microfluidic device to minimize the dead volume in the nLC × μFFE interface, eliminating the potential for re-mixing, which can introduce band broadening. A Chromeo™ P503 labelled tryptic digest of BSA was used as a complex mixture to assess the performance of the system. Total 2D peak capacities as high as 2,352 were observed in a 10 minute separation window leading to a peak capacity production rate of 105 peaks/min, nearly double the highest rates reported for on-line LC × LC. After accounting for the fraction of the separation space occupied by peaks, the adjusted 2D peak capacity was determined to be 776 demonstrating the potential for significant improvements in peak capacity with further optimization.

2.2 Introduction

Chromatography and electrophoresis separations have been powerful tools in the analysis of mixtures. Coupling a well resolved separation with a sensitive detection strategy provides unmatched selectivity and limits of detection. Unfortunately, increasingly complex mixtures are being encountered in modern biomedical and environmental research which often overwhelms the peak capacity achievable using traditional one-dimensional separations. The pairing of two separation techniques to generate a two-dimensional (2D) separation provides an attractive approach for handling these mixtures by substantially increasing peak capacity. As described by Giddings, the ideal peak capacity of a 2D separation ($n_{c,2D}$) is the product of the peak capacities from the first ($^{1}n_c$) and second ($^{2}n_c$) dimension separations (eq 1.1).[35]

2D gel electrophoresis is an example of a well-executed 2D separation and has been shown to be very powerful in the separations of protein mixtures.[1, 10] Online 2D separations, which capture fractions as they elute off of a first dimension and are then directly injected onto the second, have been developed to overcome some of the limitations of 2DGE such as analysis time and sample range.[13, 21] Often times these hyphenated methods do not satisfy the necessary criteria for achieving the ideal peak capacity. To achieve the ideal 2D peak capacity two criteria must be met: 1) the separation mechanisms of the two dimensions must be orthogonal and 2) no remixing or under sampling at the interface between the two separations occurs.[35] A modified equation accounting

for non-ideal orthogonality and under sampling was developed by Davis, Stoll, and Carr (see equation 1.6).[40]

The fractional coverage (*f)* accounts for losses in peak capacity due to the correlations in the separation modes chosen. In order to attain the maximum 2D peak capacity, the separation mechanisms must be completely orthogonal and make the entire separation space accessible to be occupied by an analyte peak.[112] Giddings proposed $n_{c,2D}$ could range from the maximum ideal case to a minimum of ${}^{1}n_{c}$, where the second dimension elution time is fully correlated to the first dimension elution time.[35] Fraction coverage and orthogonality have been calculated using a number of methods.[50, 53] Rutan *et al.* have shown the merits of the minimum convex hull method for estimating (*f)* due to its simplicity and ease of calculation.[53]

While losses in peak capacity due to orthogonality can be addressed with the appropriate choice of separation conditions, under sampling has remained a major limitation to the potential separation power of 2D separations. In many cases the second dimension separation is unable to sample the first dimension peaks fast enough, giving rise to substantial losses (>20%) of peak capacity at the interface. Davis *et al.* were able to quantify this loss in peak capacity due to under sampling (eq 1.4 and 1.5).[40]

Micro free flow electrophoresis (μFFE) offers a unique solution to the under sampling limitations found in current 2D separations. FFE is a separation technique where samples are introduced as a continuous stream at the entrance of a planar separation chamber. As the analytes are carried in a pressure driven

flow through the channel, an electric field is applied laterally, deflecting analyte streams according to their electrophoretic mobilities. Since devices were first miniaturized by Raymond *et al*.[66] µFFE devices have been fabricated in a variety materials such as polydimethylsiloxane[68-71] (PDMS), poly(methyl methacrylate) (PMMA)[72], biaxially-oriented polyethylene terephthalate (Mylar™)[73], and glass[74-80] for the separations of fluorescent dyes[71, 75], amino acids[66, 69, 71], proteins[67, 72, 76, 98, 100, 101], organelles[70, 77, 102], and whole cells[70]

To date, FFE, on either a preparative or micro scale, has only been used in 2D separations as a first dimension pre-fractionation tool.[106, 107] Although peak capacities greater than 5,000 were observed, excessively large analysis times were required due to the off-line analysis of FFE fractions collected. The reduced sample requirements and continuous nature of µFFE suggests an alternative approach: direct coupling to µFFE as a second dimension separation. Because µFFE performs a continuous separation of the incoming sample stream, the sampling time becomes the time required to collect an image for detection. Exposure times of 100-250 msec are typical for previously reported µFFE assays.[75, 81, 103] Cycle times of this low magnitude would allow significant reductions in the analysis time of 2D separations without incurring the under sampling limitations of previous liquid phase 2D platforms (Figure 1.6).

2.3 Experimental

2.3.1 Chemicals and Reagents

All solutions were made using deionized water (18.3 MΩ, Milli-Q; Millipore, Bedford, MA) and filtered with a 0.22 μm nitrocellulose membrane filter (Fisher Scientific, Fairlawn, NJ) unless otherwise described. μFFE separation buffer contained 300 μM Triton X-100, 8M Urea, and 50 mM MES hydrate, all of which were purchased from Sigma-Aldrich (St. Louis, MO). The pH of the solution was adjusted to 5.56. Poly(ethylene oxide) (PEO) was dissolved in water to 0.2% by mass with 0.1 M HCl at 95 ˚C for 2 h while stirring. Eluents for nLC were prepared using LC-MS grade water and LC-MS grade ACN, both purchased from J.T. Baker (Phillipsburg, NJ). Trifluoroacetic acid (TFA) was purchased from Sigma-Aldrich. Stock solutions of rhodamine 123 (Sigma-Aldrich) and rhodamine 110 chloride (Sigma-Aldrich) were prepared at concentrations of 1.5 mg/mL and 1.6 mg/mL, respectively, in 190 proof ethanol (Fisher Scientific). A 10 mM $NaHCO_3$ solution (Mallinkrodt, Paris, KY) in water and 10 mg/mL Chromeo™ P503 (Active Motif, Carlsbad, CA) solution in DMSO (Sigma-Aldrich) were used to label 1 nmol of a MassPREP™ BSA digestion standard purchased from Waters Corp. (Milford, MA). To perform this labeling reaction, 490 μL of $NaHCO_3$ buffer was added to the BSA standard and vortexed for 5 minutes. Next, 10 μL of the Chromeo™ P503 dye solution was added and vortexed for another 10 minutes. The vial was allowed to incubate at 25 ˚C for 3 hours before any separations were performed. The labeled BSA digest and Chromeo™ P503 solutions were stored at 0 ˚C when not in use. Piranha solution (2:1 H_2SO_4:H_2O_2)

(Ashland Chemical, Dublin, OH) was used to clean glass wafers and etch Ti. GE-6 (Acton Technologies, Inc., Pittston, PA) was used to etch Au. Concentrated HF (49%) (Ashland Chemical) was used to etch glass wafers. Silver conductive epoxy (MG Chemicals, Surrey, BC, Canada) was used to make electrical connections to the μFFE device. Crystalbond™ 509 (SPI Supplies, West Chester, PA) was used to fix fused silica capillaries in the etched capillary channel.

2.3.2 Device Design and Fabrication

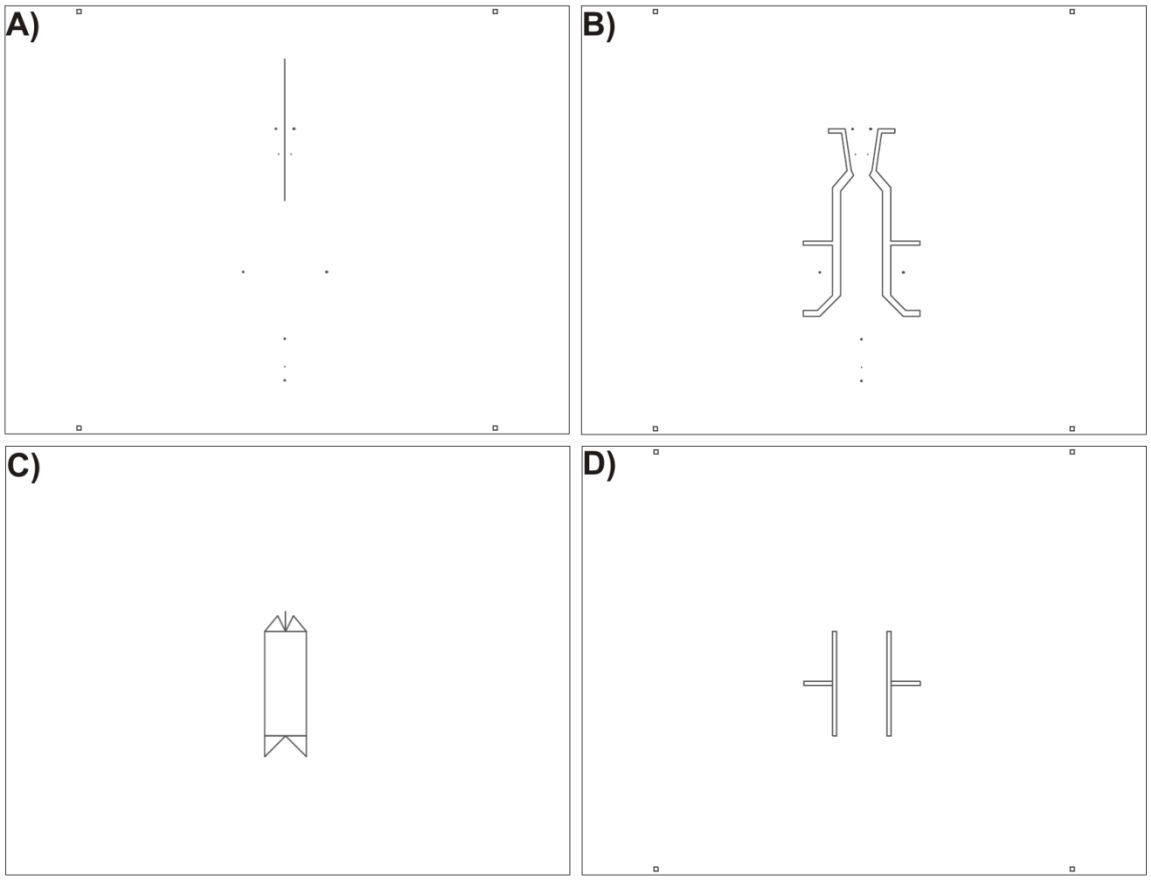

Figure 2.1: CAD drawings for the masks used to make μFFE devices. A) capillary channel B) electrode channels C) separation channel D) electrodes.

Figure 2.1 shows the masks used to fabricate the μFFE device used to interface with nLC. μFFE fabrication followed a similar procedure to those previously reported.[75, 81, 83, 108] Briefly, an 85 μm capillary channel was etched into two 1.1mm borofloat® glass wafers (Precision Glass & Optics, Santa Ana, CA) using standard photolithography techniques. A second photolithography step was performed, etching 30 μm deep electrode channels. Finally, a third photolithography step etched the remaining features to 10 μm. The end result was two mirror image wafers with a 125 μm deep capillary channel (~250 μm wide), 40 μm deep electrode channels, and a 10 μm deep × 1 cm wide × 2.5 cm long separation channel. To one of the wafers, a 150 nm thick layer of Ti was deposited using a Temescal electron beam evaporator, followed by a 150 nm thick layer of Au. A photolithography step was performed to remove unwanted Ti and Au to pattern the electrodes. Access holes (1 mm) were drilled into the other wafer and a ~90 nm thick layer of amorphous silicon (aSi) was deposited. The two wafers were then aligned and anodically bonded (900 V, 3 h, 450 ˚C, 5 μbar) using a Karl Suss SB-6 wafer bonder (Munich, Germany). The bonded device was diced to expose the capillary channel at the University of Minnesota Electrical Engineering/Computer Science Machine Shop. NanoPorts™ (Upchurch Scientific, Oak Harbor, WA) were aligned over the access holes and attached using epoxy rings. Silver conductive epoxy was used to connect lead wires to the electrodes. The device was then heated on a hot plate to ~150 ˚C while under vacuum. A 20 μm i.d. × 150 μm o.d. fused silica capillary (Polymicro Technologies, Phoenix, AZ) was inserted into the capillary channel and bonded

into place by pulling Crystalbond™ 509 through the remaining space between the capillary and the channel. The µFFE device was then perfused with a 1M NaOH solution to remove aSi from the channels.

2.3.3 Liquid Chromatography Conditions

A Thermo-Dionex UltiMate3000 RSLC nano pump with RS autosampler (Sunnyvale, CA) was used for LC separations. The analytical column (Thermo-Dionex part number 164562) was 75 µm i.d. × 15 cm long packed with 2 µm Acclaim® PepMap C18 particles. For interface broadening experiments mobile phase A was H_2O with 0.1% TFA and mobile phase B was 90:10 ACN:H_2O with 0.1% TFA. A gradient was applied from 10-80% B in 15 minutes, using 0.1 µL injection, and 300 nL/min flow rate. For 1D and 2D separations of Chromeo™ P503 labeled BSA tryptic digest, mobile phase A was H_2O with 0.05% TFA and mobile phase B was 90:10 ACN:H_2O with 0.05% TFA. A gradient from 30-95% B was applied in 10 minutes after holding at 10% B for 3 minutes. The injection volume was 1.0 µL and the flow rate was 300 nL/min.

2.3.4 µFFE Conditions

The µFFE separation channel was coated with PEO following a previously described method to suppress electroosmotic flow (EOF) and minimize analyte adsorption.[108] For 2D separations a syringe pump (Harvard Apparatus, Holliston, MA) was used to pump separation buffer through the µFFE device at a total flow rate of 0.5 mL/min (~0.15 cm/sec in the separation channel). Even though PEO has been shown to prevent the adsorption of proteins[113], adsorption was

observed for the more hydrophobic peptides. As a result, 8 M urea was added to the μFFE separation buffer to denature larger peptides and reduce surface adsorption. Triton-X 100 was added to the buffer to improve stream stability.[83] During analysis a 150 V separation potential was applied to the left electrode while the right electrode was held at ground.

2.3.5 Data Collection and Processing

An AZ100 stereomicroscope (Nikon Corp., Tokyo, Japan) mounted with a Cascade 512B CCD camera (Photometrics, Tucson, AZ) was used for fluorescence imaging. For the separation of rhodamine dyes the microscope was equipped with a GFP bandpass emission filter cube (Nikon Corp) containing two bandpass filters (450-490 and 500-550 nm) and a dichroic mirror (495 nm cutoff). For the Chromeo™ dye labeled digest a custom filter cube was used (Nikon Corp) containing two bandpass filters (470-500 nm and 570-640 nm) and a dichroic mirror (500 nm cutoff). Laser induced fluorescence (LIF) detection was performed using the 488 nm emission line of a 150 mW, argon-ion laser (Melles Griot, Carlsbad CA) expanded into a ~2.5 cm × ~150 μm line. The entire instrument setup was enclosed in a black, rubberized fabric (Thorlabs, Newton, NJ). For on-capillary detection a window was burned 70 cm down a 100 cm long piece of 20 μm i.d. × 280 μm o.d. fused silica capillary (Thermo-Dionex) which was attached to the end of the analytical column using a PTFE sleeve. The laser line was focused across the window and imaged using MetaVue software (Downington, PA). For 2D separations a separate piece of 20 μm i.d. × 280 μm capillary was connected to the capillary positioned in the μFFE separation

channel using a ZDV union (Upchurch Scientific). The total length from the column exit to the end of the capillary in the µFFE separation channel was 70 cm. Acquisition rates for on-capillary and on-chip detection were 4 Hz and 2 Hz, respectively, both with 4× gain. The nLC pump was controlled using Chromeleon v6.8 (Thermo-Dionex). Once logged, all data was then processed using in-house Matlab programs. Cutter v5.0[114] and an open source program (Peak Finder, available at http://omics.pnl.gov/software) were used to process line scans and chromatograms, as well as determine peak capacities. For 2D separations the background was corrected using an orthogonal background correction as described by Filgueira *et al,* with a correction window of 50.[115]

2.4 Results and Discussion

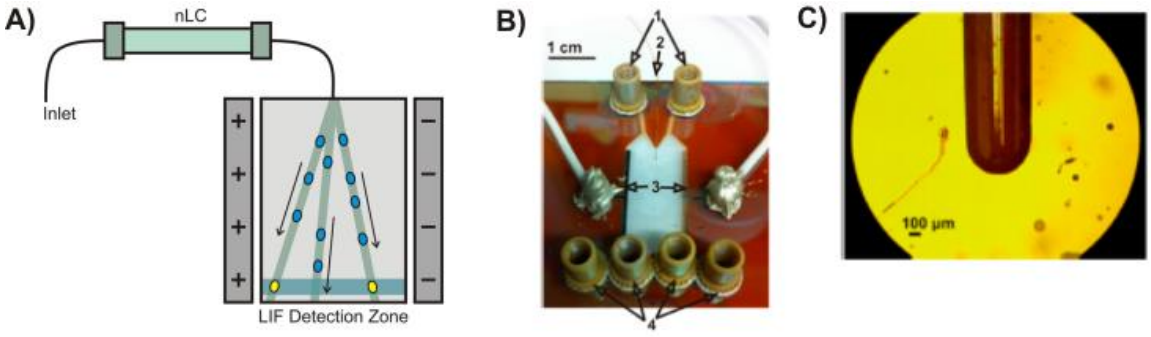

Figure 2.2: A) Schematic of the nLC × µFFE system. B) Image of a completed µFFE device. (1) buffer inlets (2) sample inlet capillary (3) electrodes (4) buffer outlets. C) Image of the nLC × µFFE interface.

Figure 2.2a shows a schematic demonstrating the principle of 2D nLC × µFFE separations. The exit of the nLC is coupled directly into the µFFE separation. Since µFFE performs a continuous separation, no complicated

injection or modulation mechanism is required to couple the two separations. Analyte peaks stream directly into the μFFE device as they elute off the nLC column where they are separated by a second mechanism. Analytes are detected as they cross the LIF detection zone in the separation channel.

The time it takes to reach the detection zone is determined by the first dimension nLC separation while the position where an analyte crosses the detection zone is determined by the second dimension μFFE separation. The sampling time of the μFFE separation is determined by the cycle time of the CCD camera recording fluorescence across the detection zone. In the current experiments cycle times ranged from 250 – 500 msec but significantly faster cycle times could easily be employed.

2.4.1 Comparison of Interface Broadening

In order to retain the peak capacity generated in the first dimension, remixing of the analytes must be minimized at the nLC × μFFE interface. If significant dead volume is present in the interface broadening will occur and peak capacity will be lost. Previously reported μFFE designs used a NanoPort™ to introduce the sample into the separation channel through an access hole drilled into the face of the device.[75, 83, 104] However, the access holes were much larger than the inner diameter of the capillaries used, introducing an unacceptably large dead volume. (Figure 1.11) An alternative design to minimize dead volume at the interface was explored. Sample was introduced through a capillary inserted through the side into a channel etched in the device (Figures 2.2b. & 2.2c.). This

arrangement allowed the capillary to extend into the separation channel. Capillary with an inner diameter of 20 µm was used to match the depth of the separation channel.

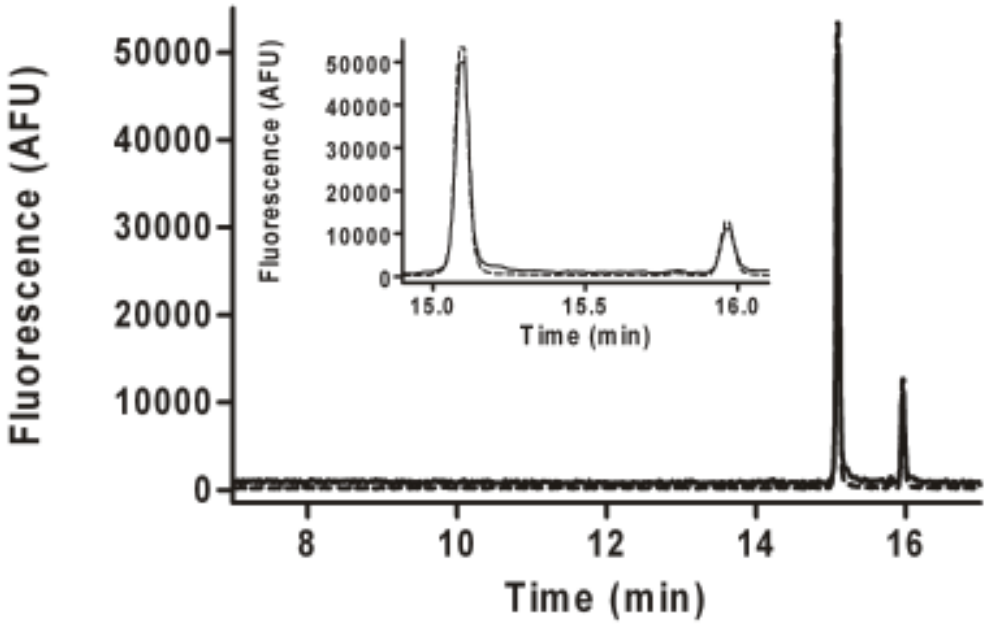

Figure 2.3: nLC separation of 30 nM rhodamine 110 and 40 nM rhodamine 123 comparing peak shape measured prior to (dashed line) and immediately after (solid line) the nLC × µFFE interface. Chromatograms were aligned to emphasize comparison in peak shape.

A nLC separation of rhodamine 110 and rhodamine 123 was used to determine the extent of broadening that would occur at this side-on interface. Figure 2.3 compares the peak shapes for rhodamine 110 and rhodamine 123 when detection is performed on-capillary to those recorded immediately after the interface inside of the µFFE separation channel. The peak shapes observed are

essentially identical, indicating that broadening introduced at the interface is minimal. The width at half height of the rhodamine 110 peak was 2.8 seconds on capillary and 2.9 seconds immediately after the interface. Similarly, the width at half height of the rhodamine 123 peak was 3.0 seconds on capillary and 3.2 seconds after the interface. Overall, the side-on interface provides a simple means to interface a nLC column with a μFFE device with neglible contribution to band broadening.

2.4.2 1D Liquid Chromatography of Peptides

A tryptic digest of BSA was chosen as a complex mixture of peptides suitable for challenging the peak capacity of the nLC and nLC × μFFE separations. Peptides in the digest were fluorescently labelled using the fluorogenic Chromeo™ P503 reagent.[116] Chromeo™ P503 reacts with amines resulting in the incorporation of a cationic fluorophore. This is an important characteristic since replacing positively charged amines with cationic fluorophores helps retain chemical diversity in the peptide mixture through the labelling reaction.

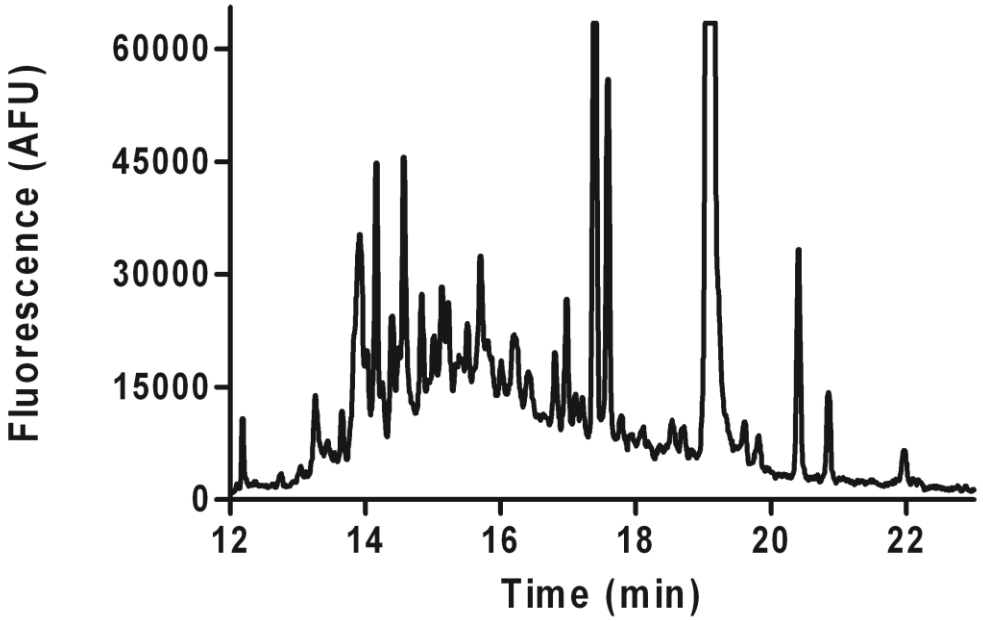

Figure 2.4: 1D nLC chromatogram of the Chromeo™ P503 labeled BSA tryptic digest.

Figure 2.4 shows a nLC separation of the fluorescently labelled BSA digest. Clearly, the complexity of this peptide mixture overwhelms the peak capacity of the 1D separation with numerous unresolved peaks observed across the 10 minute separation window. Over 30 distinguishable peaks were observed, however only 5 were baseline resolved. 17 peaks were selected and the integration method in Peak Finder was used to estimate a 1D nLC peak capacity of 101. The last three well resolved peaks had an observed average efficiency of 96,000 theoretical plates.

2.4.3 2D nLC × µFFE Performance

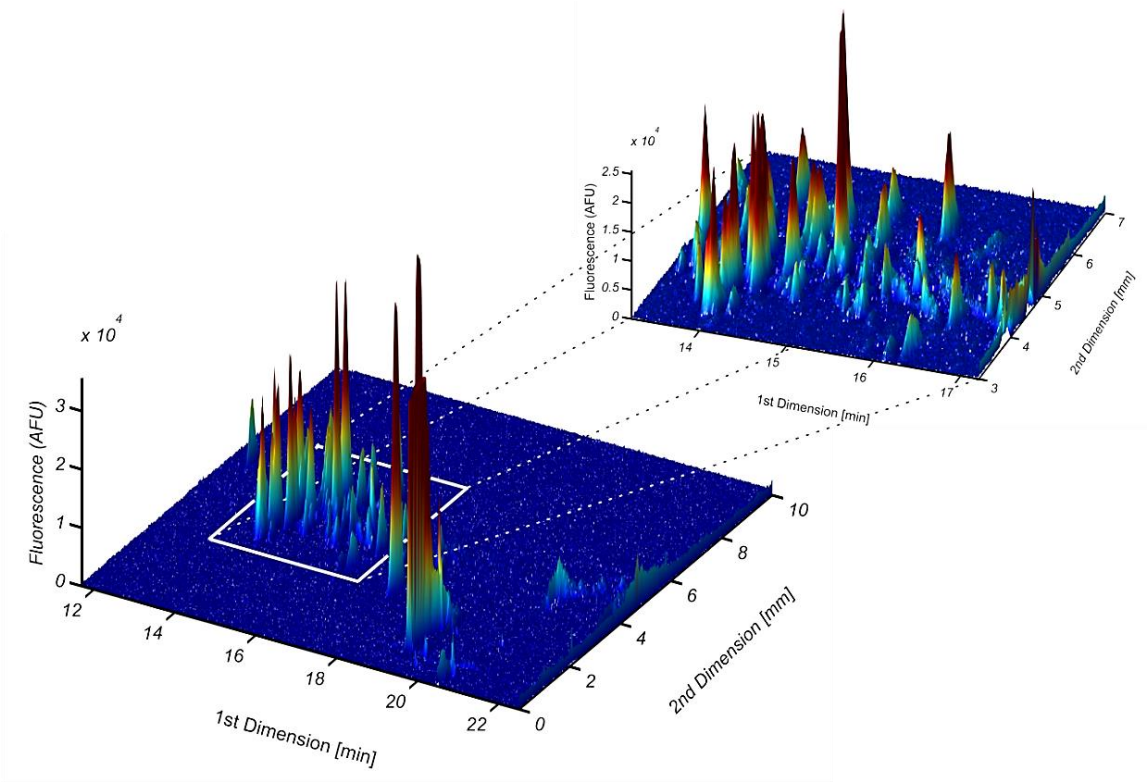

Figure 2.5: 2D nLC × µFFE separation of the Chromeo™ P503 labeled BSA tryptic digest.

Figures 2.5 and 2.6 demonstrate different views of a 2D nLC × µFFE separation of the same fluorescently labelled BSA digest analyzed using 1D nLC in Figure 2.4. It is important to note that the nLC gradient and separation time did not need to be adjusted to accommodate the 2D separation and are identical to those used to generate the 1D chromatogram shown in Figure 2.4. Clearly, the 2D separation is able to generate significantly higher peak capacity than the 1D nLC separation. With minimal optimization >65 resolved peaks could be distinguished in the 10 minute separation window, agreeing well with the

predicted 74 tryptic peptides of BSA. Figure 2.6b shows an expanded view of a high peak density region of the chromatogram. Over 40 peaks are observed with what appears to be a random distribution across this 4 minute window. Figures 2.6c and 2.6d show 1D nLC chromatograms and µFFE line scans extracted from the full 2D separation, respectively. These extracted chromatograms clearly demonstrate that the resolving power of each dimension was retained when nLC and µFFE were combined into a 2D separation.

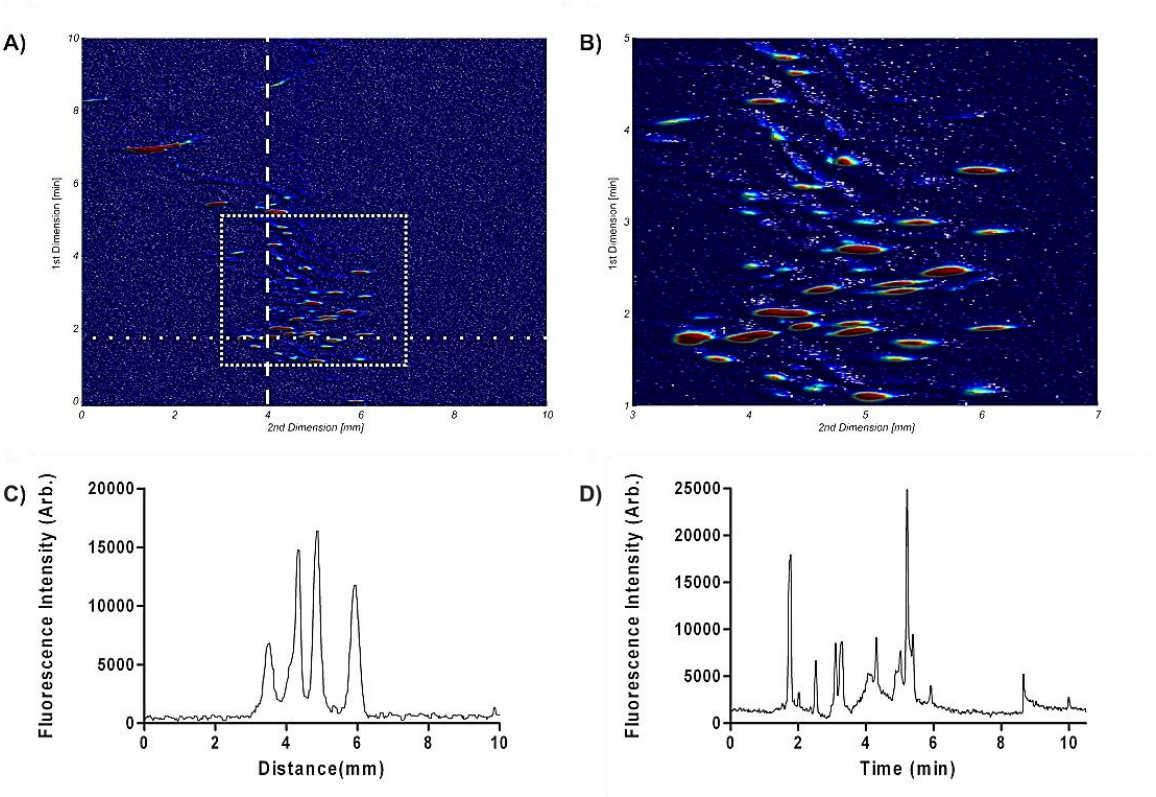

Figure 2.6: 2D nLC × µFFE separation of the Chromeo™ P503 labeled BSA tryptic digest. A) Top view B) Expanded view of the region enclosed in the dotted box in A) (i.e. 13.2 to 17.2 minutes in the first dimension and 3 to 7 mm in the second dimension) C) Extracted chromatogram from the first dimension measured at 4 mm on the µFFE device (shown as the vertical dashed line in A) D) Line scan across the second dimension taken at 14.0 minutes in the first dimension (shown as the horizontal dotted line in A)

To determine the observed peak capacity of the 2D separation 29 peaks were chosen for further analysis using the integration method in Peak Finder. The observed peak capacity in the nLC dimension (^1n_c) was determined to be 98, essentially identical to the results obtained for the 1D nLC separation shown in Figure 2.4. This peak capacity agrees well with the high efficiency peaks observed in the extracted chromatogram shown in Figure 2.6c. Considering the 500 msec sampling rate of the CCD camera, >12 measurements were taken across the 6.1 sec. average baseline width of a nLC peak. Based on these values, eq. 1.5 predicts that 99% of the nLC peak capacity is retained through the interface, eliminating under sampling as a factor limiting the observed 2D peak capacity. It should be noted that the CCD camera could easily be operated at much faster sampling rates to accommodate narrower peaks or faster separations in the first dimension.

Figure 2.6d shows a µFFE linescan extracted from the full 2D separation. The average baseline width for peaks in the µFFE dimension was estimated to be 0.41 mm using the same 29 peaks used to determine the nLC dimension peak capacity. Considering the 10 mm width of the separation channel the µFFE separation is able to generate a peak capacity of 24 (^2n_c). Combining the nLC (^1n_c) and µFFE (^2n_c) peak capacities according to eq. 1.1 gives rise to a 2D nLC × µFFE peak capacity ($n_{c,2D}$) of 2,352 in a 10 minute separation window. For comparison, Mellors *et al.* recently reported a peak capacity of 1,400 in a 40 minute separation window using UPLC coupled with microchip CE using a gated interface.[97] The 2D nLC × µFFE separations reported here yield a peak capacity

production rate of 105 peaks/min, nearly double the previously reported rate using on-line LC×LC.[14, 33]

As described in eq. 1.6, the fractional coverage of separation space should also be taken into account to determine a more representative measure of the useable peak capacity. Peaks are well distributed across the high density peak region shown in Figure 2.6b, suggesting that excellent orthogonality is achieved between the nLC and µFFE separations in this region. Examining the full 2D separation window demonstrates that there are significant areas that are void of peaks, suggesting that peak capacity in these regions is inaccessible for the current combination of separation modes and sample. For example, as shown Figure 2.6a, no analytes were deflected by more than 1 mm towards the cathode, while analytes were observed that were deflected almost 5 mm towards the anode. Using a minimum convex hull[53], the fraction of separation space where peaks were observed (f) was determined to be 33%, resulting in a realized 2D peak capacity of 776. Optimization of µFFE conditions to make better use of the full separation channel would dramatically improve f and consequently the realized 2D peak capacity. Similarly, further exploration of combinations of nLC and µFFE to maximize orthogonality is expected to improve f and realized 2D peak capacity and will be discussed in greater detail in Chapter 5. The use of Chromeo™ P503 is important for both of these approaches since it allows the native charge and isoelectric point of the peptides to be maintained through the labelling protocol, retaining the chemical diversity of the sample.[117]

2.5 Conclusions

The continuous nature of μFFE separations facilitates a unique solution to the under sampling limitation of existing liquid phase 2D separations. Coupling nLC with μFFE provided a 24-fold improvement in peak capacity with no increase in analysis time or restrictions on the nLC separation conditions. Peak capacities as high as 2,352 were observed in a 10 minute separation window. The CCD used for fluorescence measurements in the μFFE separation recorded an image of the detection zone every 500 msec. Much faster CCD sampling rates are possible though suggesting that faster 2D separations are also feasible using this approach. The described interface is simple with no complicated valving or timing required. The μFFE device was coupled with commercially available nLC instrumentation suggesting widespread compatibility of the approach. It should also be recognized that many combinations of nLC stationary phases and μFFE separation modes are available, suggesting that 2D nLC × μFFE could be successfully applied to a wide range of analyte mixtures. With the high performance of nLC × μFFE demonstrated, the following chapters will look in-depth into two factors that can affect the peak capacity achievable with this system: 1) surface adsorption of analytes and its effect on broadening in each dimension and 2) the impact of label and sample on orthogonality and peak capacity.

Chapter 3

Effect of Surface Adsorption on Temporal and Spatial Broadening in Micro Free Flow Electrophoresis

Geiger, M., Harstad, R., and Bowser, M.T. *Anal. Chem.*, **2015**, *87 (23),* 11682-11690

3.1 Summary

The adsorption of analytes onto surfaces presents a challenge for many separations, often becoming a significant source of peak broadening and asymmetry. This broadening can have a significant impact on the performance of a variety of applications of separations including the determination of dissociation constants and peak capacity of multidimensional separations. We have shown, however, that surface adsorption has no effect on peak position or spatial broadening in micro free flow (μFFE) separations. Surface adsorption still does affect the time it takes an analyte to travel through the μFFE separation channel and therefore contributes to temporal broadening. These results were confirmed using μFFE separations of fluorescein, rhodamine 110, and rhodamine 123 in a low ionic strength buffer to promote adsorption onto the surface of an all glass microfluidic device. Peak widths and asymmetries were measured in both temporal and spatial dimensions to assess the effect of adsorption. Under these conditions, rhodamine 123 exhibited significant interactions with the separation channel surface, causing increased peak broadening and asymmetry in the temporal dimension. Broadening or asymmetry in the spatial dimension was not significantly different than that of fluorescein, which was predicted to not interact with the capillary surface. The effect of strong surface interactions was demonstrated using μFFE separations of Chromeo™ P503 labeled myoglobin and cytochrome c. The proteins were well resolved and gave rise to symmetrical peaks in the dimension even though permanent adsorption onto the separation channel surface occurred.

3.2 Introduction

Capillary electrophoresis (CE) has become a powerful tool in protein and peptide separations due to its high resolution, speed, and sensitivity.[118] One limiting factor to the performance of CE, however, is the potential for protein-wall interactions which arise due to the ionization of the silica capillary surface above pH 3.[119] These interactions introduce a resistance to mass transfer between the capillary wall and the bulk flow which results in band broadening and peak asymmetry.[120, 121] The degree to which broadening and asymmetry occur is dependent on the type of interactions present between the molecule and the surface, as well as the rate of diffusion from the wall back into the bulk flow.[122] A number of studies have been performed characterizing the effect of surface adsorption on peak broadening, elution time delays, and electroosmotic flow.[123-125] Numerous methods have been implemented to mediate the effect of wall adsorption, with the most common being the use of buffer modifications, using polymers to coat the capillary surface, or combinations of both.[126-131] Without addressing wall adsorption as a major source of band broadening, CE becomes impractical for the analysis of larger biomolecules seen in the omics fields, especially when used for the study of protein-ligand affinity.[120, 123, 132] Surface interactions with ionized silica also impacts other time based separations, such as liquid chromatography (LC). The silica surface of stationary phase supports commonly used in LC are often inhomogeneous, containing unevenly distributed silanol groups which can have interactions with both the mobile phase and solute.[133-135] These interactions result in poor peak shape and

lowered separation performance, often requiring the addition of ion pairing agents to overcome these effects.[136]

Micro free flow electrophoresis (μFFE) is a separation technique where analytes are introduced as a continuous stream into a planar separation channel. Unlike traditional CE where the electric field is applied parallel to the direction of flow, the field in μFFE is applied perpendicularly causing analytes to deflect laterally based on their mobilities (Figure 1.8). As mentioned in previous chapters devices have been fabricated in a variety materials such as polydimethylsiloxane[68-71] (PDMS), poly(methyl methacrylate) (PMMA)[72], biaxially-oriented polyethylene terephthalate (Mylar™)[73], and glass[74-80] for the separations of fluorescent dyes[71, 75], amino acids[66, 69, 71], proteins[67, 72, 76, 98, 100, 101], organelles[70, 77, 102], and whole cells.[70] Continuous analysis has allowed μFFE to be used in a number of unique applications including: measuring the electrophoretic mobility of mitochondria[102], quantifying the dissociation constants of aptamer-protein complexes[104], isolating aptamers by SELEX[105], and rapid optimization of buffer conditions for CE separations.[103] Chapter 2 described the coupling of μFFE with nano LC (nLC) to perform high peak capacity multidimensional separations of peptides.[85] Understanding how surface adsorption affects μFFE separations is important for further development of these applications.

Raymond *et al.* were the first to demonstrate μFFE in 1994.[66] By analogy to mechanisms observed in CE and preparative FFE, they proposed potential sources of band broadening in μFFE:

$$\sigma_{total}^2 = \sigma_{inj}^2 + \sigma_D^2 + \sigma_{HD}^2 + \sigma_{ADS}^2 + \sigma_{JH}^2 \quad (3.1)$$

where the observed total variance of an analyte band (σ_{total}^2) is determined by the sum of the variances from individual broadening sources including initial stream width (σ_{inj}^2), diffusion (σ_D^2), hydrodynamic broadening (σ_{HD}^2), adsorption (σ_{ADS}^2), and Joule heating (σ_{JH}^2).[67] As highlighted in Chapter 1, Fonslow and Bowser experimentally verified the parameters that contribute to injection (σ_{inj}^2), diffusion (σ_D^2) and hydrodynamic broadening (σ_{HD}^2) in µFFE[108]:

$$\sigma_{total}^2 = \sigma_{inj}^2 + \sigma_D^2 + \sigma_{HD}^2 = \frac{w_{inj}^2}{12} + \frac{2DL}{v} + \frac{h^2 d^2 v}{105DL} \quad (3.2)$$

where (w_{inj}) is the width of the sample stream at the inlet, D is the analyte diffusion coefficient, L is the vertical distance between the sample inlet and the detection zone, v is the linear velocity of the buffer, h is the height of the separation channel and d is the lateral deflection distance of the analyte. It was determined that diffusion governed broadening at low flow rates, while hydrodynamic broadening dominated for analytes with significant deflection distances, especially at high combinations of buffer velocity and electric field. It should be noted that in this study conditions were chosen to minimize the potential effects of surface adsorption and Joule heating. This chapter will provide a detailed description of the effect surface adsorption has on band broadening in µFFE.

3.3 Experimental

3.3.1 Chemicals and Reagents

All solutions were made using deionized water (18.3 MΩ, Milli-Q; Millipore, Bedford, MA) and filtered through a 0.22 µm nitrocellulose membrane filter (Fisher Scientific, Fairlawn, NJ) unless otherwise stated. The µFFE and CE separation buffer for all experiments contained 300 µM Triton X-100 and 25 mM HEPES (Sigma-Aldrich, St. Louis, MO), adjusted to pH=7.00 using 1 M NaOH (Macron Chemicals, Center Valley, PA). Eluents for nLC were prepared using LC-MS grade water, acetonitrile, and methanol (J.T. Baker, Phillipsburg, NJ). Trifluoroacetic acid (TFA) was purchased from Sigma-Aldrich. Stock solutions of rhodamine 123, rhodamine 110, and fluorescein (Sigma-Aldrich) were prepared in 190 proof ethanol (Fisher Scientific) at concentrations of 1.2 mg/mL, 1.2 mg/mL, and 1.5 mg/mL, respectively. Stock solutions of myoglobin (equine skeletal muscle, Sigma-Aldrich) and cytochrome c (bovine heart, Sigma-Aldrich) were prepared in 10 mM $NaHCO_3$ (Mallinkrodt, Paris, KY) in water at concentrations of 1.1 mg/mL and 1.2 mg/mL, respectively. A 10 mg/mL Chromeo™ P503 (Active Motif, Carlsbad, CA) solution in DMSO (Sigma-Aldrich) was prepared to label the proteins. To perform the labeling, 10 µL of the Chromeo™ P503 dye solution was added to 490 µL of each protein solution and vortexed for 10 minutes. The vials were allowed to incubate at room temperature for 24 hours before any separations were performed. The labeled proteins were stored at 0 ˚C when not in use. Piranha solution (4:1 H_2SO_4:H_2O_2) (Ashland Chemical, Dublin, OH) was used to clean glass wafers and etch Ti. GE-6 (Acton

Technologies, Inc., Pittston, PA) was used to etch Au. Concentrated HF (49%) (Ashland Chemical) was used to etch glass wafers. Silver conductive epoxy (MG Chemicals, Surrey, BC, Canada) was used to make electrical connections to the μFFE device. Fused silica capillaries (Polymicro Technologies, Phoenix, AZ) were fixed into the devices using Crystalbond™ 509 (SPI Supplies, West Chester, PA).

3.3.2 Device Fabrication

Fabrication followed the procedure previously described by Geiger *et. al.*[85] in Chapter 1. Briefly, an 85 μm channel was etched into two 1.1 mm borofloat® glass wafers (Precision Glass & Optics, Santa Ana, CA) using standard photolithography to allow for the capillary connection. A second photolithography step was performed to pattern and etch 30 μm deep electrode channels. Finally, a third photolithography step etched the separation channel to 10 μm. These etching steps resulted in two wafers having a 125 μm capillary channel (~250 μm wide), 40 μm electrode channels, and a 10 μm deep × 1 cm wide × 2.5 cm long separation channel. (See Figure 2.1 in Section 2.3.2 for CAD files of the masks) A Temescal electron beam evaporator was used to deposit 150 nm thick layers of Ti and Au to one of the wafers. A photolithography step was performed to pattern the electrodes by removing unwanted Ti and Au. The other wafer had 1 mm diameter holes drilled for inlets, outlets, and over the electrodes. A ~90 nm thick layer of amorphous silicon was deposited. The two wafers were aligned under a microscope and anodically bonded (900 V, 3h, 450 ˚C, 5 μbar) using a Karl Suss SB-6 wafer bonder (Munich, Germany). The bonded device was cut to

expose the capillary channel at the University of Minnesota Electrical Engineering/Computer Science Machine Shop. NanoPorts™ (Upchurch Scientific, Oak Harbor, WA) were aligned over the access holes and attached using epoxy rings (IDEX Lake Forest, Il). Silver conductive epoxy was used to connect lead wires to the electrodes. The device was then heated on a hot plate to ~120 ˚C while under vacuum. A 20 μm i.d. x 150 μm o.d. fused silica capillary was inserted into the capillary channel and Crystalbond™ 509 was pulled through the remaining space between the capillary and channel to bond it in place. The chip was then perfused with 1M NaOH solution to remove the residual amorphous silica from the channels.

3.3.3 Capillary Electrophoresis Conditions

CE was performed using a P/ACE MDQ system (Beckman Coulter, Fullterton, CA equipped with a LIF detector (λ_{ex} = 488 nm; λ_{em} = 520 nm) and a 10 mW, 488 nm diode pumped solid state laser (Sapphire, Coherent, Santa Clara, CA). The separation capillary was 40 cm in total length, 50 um i.d. and the detector was 33 cm from the inlet. For protein separations, the capillary was rinsed at 20 psi with 0.1 M NaOH for 5 min, H_2O for 2 min, and separation buffer for 2 min at 20 psi between each run. Sample injections were performed at 0.1 psi for 2 seconds. The voltage applied was 30 kV. For dye separations, the capillary was rinsed at 20 psi with 0.1 M NaOH for 1 min, H_2O for 1 min, and separation buffer for 10 min between each run. Sample injections were performed at 0.1 psi for 2 seconds. The voltage applied was 30 kV for 20 min.

3.3.4 Liquid Chromatography Conditions

A Thermo-Dionex UltiMate3000 RSLC nano pump with WPS autosampler (Sunnyvale, CA) was used for LC separations. The analytical column (Thermo-Dionex Part number 164562) was 75 µm i.d. × 15 cm long packed with 2 µm Acclaim® PepMap C18 particles. For the fluorescent dye separations mobile phase A was 100% H_2O and mobile phase B was 90:10 MeOH:H_2O. An isocratic composition of 85:15 B:A was chosen, using 0.1 µL injection and a 300 nL/min flow rate. For protein adsorption experiments mobile phase A was H_2O with 0.1% TFA and mobile phase B was 90:10 ACN:H_2O with 0.1% TFA. An isocratic composition of 60:40 B:A was chosen, using 0.1 µL injection and a 300 nL/min flow rate.

3.3.5 µFFE Conditions

For fluorescent dye separations a syringe pump (Harvard Apparatus, Holliston, MA) was used to pump separation buffer through the µFFE device at a flow rate of 0.5 mL/min (~0.15 cm/sec in the separation channel). Upon injection, +50 V was applied to the right electrode while the left was held at ground. The same buffer flow rate was used for protein separations, and +150 V was applied across the device. For continuous, direct injection separations +75 V was applied.

3.3.6 Data Collection and Processing

An AZ100 stereomicroscope (Nikon Corp., Tokyo, Japan) mounted with a Cascade 512B CCD camera (Photometrics, Tucson, AZ) was used for µFFE LIF

detection and fluorescence imaging. For fluorescent dyes the microscope was equipped with a GFP bandpass emission filter cube (Nikon Corp) containing two bandpass filters (450-490 and 500-550 nm) and a dichroic mirror (495 nm cutoff). For the Chromeo™ dye labeled proteins a custom filter cube was used (Nikon Corp) containing two bandpass filters (470-500 nm and 570-640 nm) and a dichroic mirror (500 nm cutoff). Laser induced fluorescence (LIF) detection was performed using a 150 mW, diode pumped solid state laser (Coherent) expanded into a ~2.5 cm × ~150 μm line. For fluorescent dyes the line was positioned at various distances down the chip to measure broadening effects. For proteins the line was positioned 12.50 mm down the separation channel. The entire instrument was enclosed in a light-tight box (Newport, Irvine, CA). For on-capillary detection a window was burned 70 cm down a 100 cm long piece of 20 μm i.d. x 280 μm o.d. fused silica capillary (Thermo-Dionex) which was attached to the end of the nLC column using a PTFE sleeve. For all adsorption experiments a separate piece of 20 μm i.d. × 280 μm capillary was connected to the capillary placed in the chip using a ZDV union (Upchurch Scientific). The total length from the column to the end of the capillary in the μFFE device was 70 cm. Acquisition rates for on-capillary and on-chip detection were 4 Hz, with a 1× gain. The nLC pump was controlled using Chromeleon v6.8 software (Thermo-Dionex). Once logged, all data was processed using in-house Matlab programs. Cutter v5.0[114] was used to process line scans and chromatograms. Asymmetry values were calculated by fitting peaks to a 3rd degree Gaussian function using

the CurvFit application in Matlab. Peaks were assessed at 1/10 the max height to determine asymmetry.

3.4 Results and Discussion

In CE analyte surface adsorption results in distorted peak shapes. These distortions can manifest as band broadening and changes in peak symmetry[120, 121, 137] depending on the interactions between the analyte and the wall.[122]

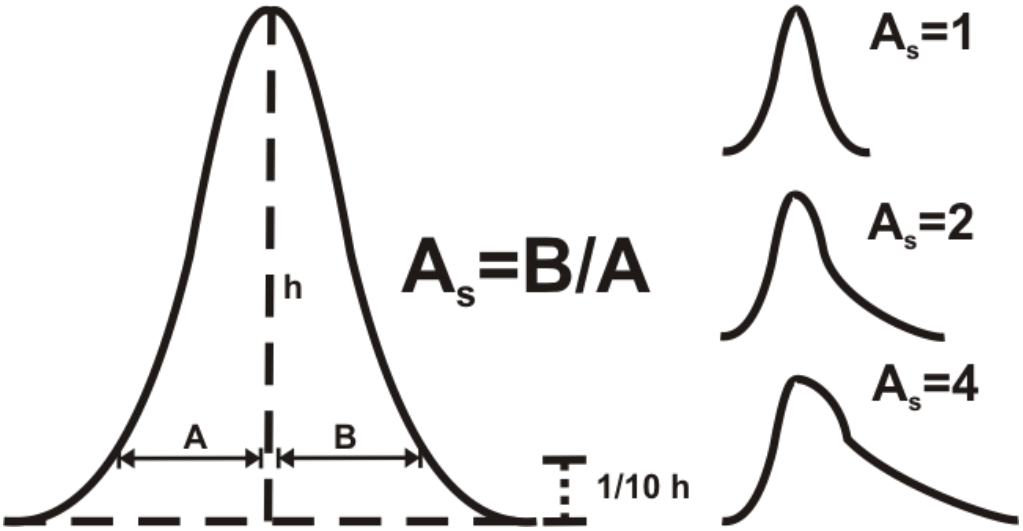

Figure 3.1: Calculation of peak asymmetry. Asymmetry (A_s) is the ratio of the peak tail (B) to peak front (A) taken at 10% of the peak height (h). Peak shapes for A_s values of 1,2, and 4 are also given.

Specifically, peak asymmetry can be incurred since the analyte will desorb over time, leading to peak tailing. The asymmetry of a peak is defined as the ratio of the width of the peak tail to the width of the peak front, taken at 1/10 the of the peak height. Peaks with ratios greater than 2 are often regarded as asymmetric. (Figure 3.1)

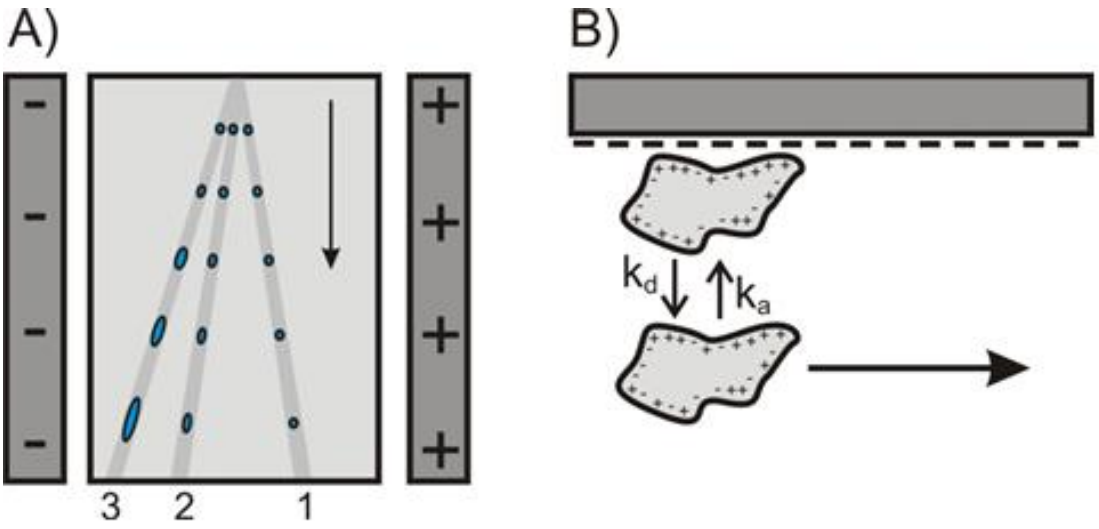

Figure 3.2: A) Schematic illustrating three hypothetical flow paths through a µFFE separation channel. Analyte 1 does not interact with the separation channel surface. Analytes 2 and 3 interact with the surface with increasing affinity giving rise to temporal broadening. B) Illustration of the adsorption/desorption equilibrium of an anlyte interacting with the glass surface of the separation channel. Note that the analyte is immobilized while adsorbed onto the surface.

The effect of surface adsorption on peak shape in µFFE is less clear. Figure 3.2A illustrates three hypothetical flow paths through a µFFE separation chamber. Analyte #1 does not interact with the surface as it travels through the device, giving rise to a well-defined peak with a width determined by the broadening terms listed in eq. 3.2. Analytes 2 and 3 do interact with the surface of the flow chamber according to the equilibrium shown in Figure 3.2B. While in solution they travel on a trajectory determined by their mobility and the linear velocity of the buffer. When the analytes adsorb onto the surface they remain fixed in place with no motion in either the lateral (mobility) or vertical (pressure driven flow) directions. When an analyte desorbs back into solution it resumes

its original trajectory as determined by the electric field and pressure driven flow. Since analytes do not move while adsorbed and the surface interactions do not affect their trajectory while in solution, the extent of an analyte's interaction with the surface does not affect the position where it crosses the detection zone. Therefore, wall interactions cannot contribute to broadening in the spatial dimension as an analyte moves through the μFFE separation chamber. In contrast, the time it takes an analyte to move through the separation chamber is clearly affected by the time that an analyte spends adsorbed onto the surface. If a discrete bolus of analyte (i.e. peak) is introduced into the μFFE separation chamber (as shown in Figure 3.2A), increased surface interaction will contribute to broadening in the time dimension as it travels through the device. Therefore to fully assess the effect of surface adsorption on μFFE separations both spatial and temporal broadening must be considered.

3.4.1 Surface Adsorption of Fluorescent Dyes

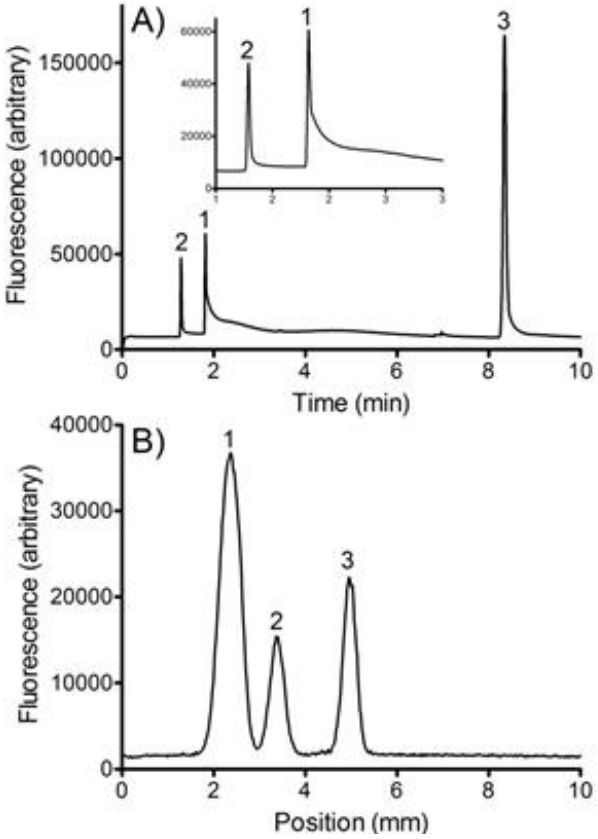

Figure 3.3: A) CE electropherogram and B) µFFE separation of (1) rhodamine 123, (2) rhodamine 110 and (3) fluorescein using a 25 mM, 300 µM Triton X-100, pH = 7.00 separation buffer.

Figure 3.3A shows a CE electropherogram of three fluorescent dyes (fluorescein, rhodamine 110 and rhodamine 123) commonly used to assess separation performance. The separation is performed in a HEPES/Triton X-100 buffer commonly used in µFFE separations to minimize current in the separation channel.[138] In this low ionic strength buffer even weak ionic interactions with the silica surface cause pronounced effects on peak shape. Fluorescein bears a -2 charge at pH 7 and is therefore not expected to interact with the silica surface.

Conversely, rhodamine 123 bears a +1 charge and interactions with the negative surface are expected. Rhodamine 110 is zwitterionic and predicted to exhibit a weak interaction. The peak shapes in the electropherogram shown in Figure 3.3A confirm the predicted trend. Fluorescein and rhodamine 110 both give rise to well defined peaks, with asymmetry values of 1.2 and 2.3, respectively. Distortion of the rhodamine 123 peak is consistent with surface adsorption. Significant tailing over a period of several minutes is observed, giving rise to a peak asymmetry value of 17.1. Wall interactions are severe enough to even reverse the expected migration order of rhodamine 110 and rhodamine 123.

Figure 3.3B shows a µFFE linescan of the same three fluorescent dyes separated in the same low ionic strength HEPES/Triton X-100 buffer. While the efficiency of the separation is clearly lower than that of CE, the peak shapes are strikingly symmetric. Asymmetry values for the rhodamine 123, rhodamine 110, and fluorescein peaks were 0.9, 1.0, and 1.1, respectively. The borofloat® glass surface of the µFFE flow chamber is not significantly different than that of the fused silica surface of the CE capillary. Rhodamine 123 still adsorbs onto the surface, but as predicted this interaction has no effect on spatial broadening in the µFFE separation. It should be noted that the order of the peaks in the µFFE separation follow the expected trend based on analyte charge, further reinforcing the premise that wall interactions do not affect the position where analytes cross the detection zone.

While the data presented in Figure 3.3 supports the hypothesis that wall interactions do not affect spatial broadening in µFFE, it does not address the

effect on temporal broadening. It would also be better to directly demonstrate that adsorption is indeed occurring in the μFFE device rather than rely on comparisons with CE data. To assess temporal broadening we must introduce a discrete bolus of analyte into the μFFE device. To accomplish this we used instrumentation previously developed to perform two-dimensional nLC × μFFE separations.[85] Analytes were injected onto an nLC column and then immediately eluted off the column and into the μFFE device as a discrete bolus.

Figure 3.4 shows 2D nLC × μFFE separations of fluorescein, rhodamine 110 and rhodamine 123 recorded at different positions along the length of the μFFE channel. The first dimension is the time required to reach the detector (i.e. nLC retention time) while the second dimension is the position that the analyte crossed the detection zone (i.e. μFFE deflection distance). Although the intent was to inject a discrete analyte bolus into the μFFE device, some nLC retention is observed as evidenced by differences in observed elution times. Resolution in the μFFE dimension increased as analytes moved through the separation channel due to increased time in the electric field. Chromatograms for fluorescein, rhodamine 110 and rhodamine 123 were extracted from the 2D separations shown in Figure 3.4 to more clearly illustrate the extent of temporal broadening as analytes travelled through the μFFE channel (see Figure 3.5). Individual chromatograms are generated since each analyte crosses the μFFE detection zone at a different spatial position. Near the entrance of the μFFE separation chamber, all three analytes gave rise to relatively well formed peaks as determined by their elution off the nLC column.

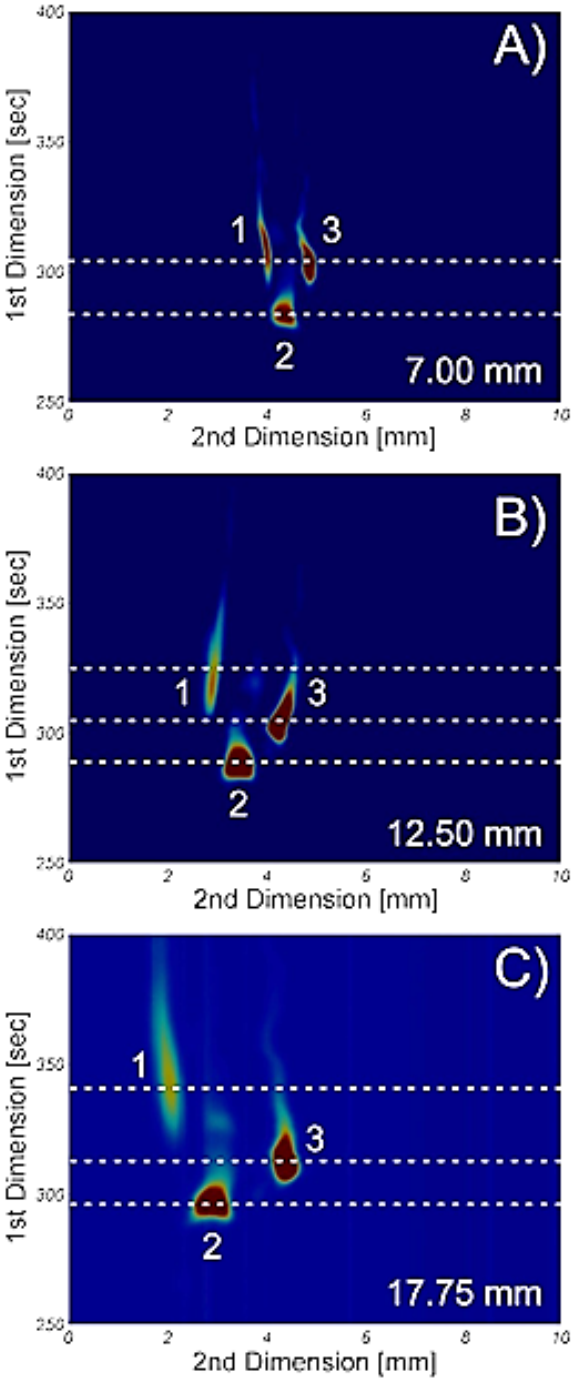

Figure 3.4: 2D nLC × µFFE separations of (1) rhodamine 123, (2) rhodamine 110, and (3) fluorescein recorded in the µFFE separation channel (A) 7.00 mm, (B) 12.50 mm, and (C) 17.75 mm from the sample inlet. The first dimension is the nLC elution time and the second dimension is the µFFE deflection distance. Dashed lines indicate the time points used to generate the µFFE linescans shown in Figure 3.5B.

As analytes progressed through the flow chamber, distinct differences are observed. The peaks for fluorescein and rhodamine 110 were relatively unchanged suggesting that temporal broadening introduced during the µFFE separation is minimal. Conversely, the rhodamine 123 peak broadened dramatically, consistent with the temporal broadening expected from surface adsorption. Surface adsorption was strong enough to induce a shift in elution time as rhodamine 123 flows through the µFFE flow chamber. Figure 3.5C illustrates these trends more clearly. No significant change in peak width in the temporal dimension was observed as fluorescein moves through the µFFE flow chamber. The peak width of rhodamine 123 increases from 9.3 to 49.7 seconds, suggesting that significant surface adsorption occurs in the µFFE separation chamber, which in turn contributes to temporal broadening.

Figure 3.5B shows µFFE linescans extracted from the 2D separations shown in Figure 3.4. The time points used to generate the extracted linescans are indicated by the dashed lines in Figure 3.4 and the color coded lines in Figure 3.5A. Again, detection was performed at different positions along the length of the flow channel to determine how peak shapes changed as analytes progressed through the µFFE separation. As expected, separation of fluorescein, rhodamine 110 and rhodamine 123 increased as the analytes travelled further through the separation channel. Broadening also occurred according to the diffusion and hydrodynamic terms described in equation 3.2. It is important to note that no significant difference in spatial broadening was observed between fluorescein and rhodamine 123. This is shown clearly in Figure 3.5D where the

peak widths of fluorescein and rhodamine 123 both increase linearly as they progress through the separation channel as would be expected for spatial broadening determined by diffusion and hydrodynamic sources.

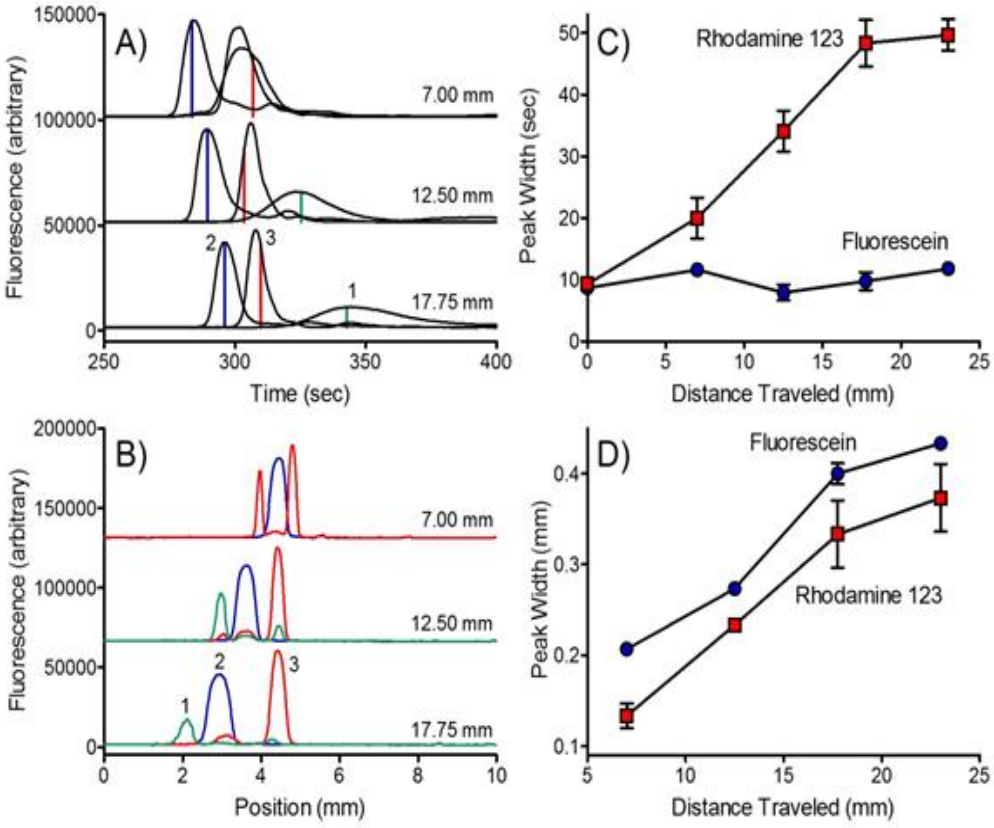

Figure 3.5: A) Extracted chromatograms of (1) rhodamine 123, (2) rhodamine 110, and (3) fluorescein measured in the µFFE separation channel 7.00 mm, 12.50 mm, and 17.75 mm from the sample inlet. B) Extracted µFFE linescans taken at various separation times (indicated by vertical lines of the corresponding color in (A) as (1) rhodamine 123, (2) rhodamine 110, and (3) fluorescein move from 7.00 mm to 17.75 mm from the inlet in the separation channel. Linescans were taken at 283.5 sec (blue) and 306.75 sec (red) at 7.00 mm, 289.25 sec (blue), 303.5 sec (red), and 325.25 sec (green) at 12.50 mm, and 296.0 sec (blue), 309.75 sec (red) , and 342.75 sec (green) at 17.75 mm. C) Temporal peak widths at helf height for fluorescein (blue circles) and rhodmaine 123 (red squares) at increasing distance from the sample inlet in the separation channel. D) spatial peak widths at half height for fluorescein (blue circles) and rhodamine 123 (red squares) at increasing distance from the sample inlet in the separation channel. Error bars are the standard error of the mean (n=3). Rhodamine 100 co-migrates with the nLC solvent through the µFFE separation channel, introducing an artifact that affected its peak shape. Rhodamine 110 was omitted from C) and D) for this reason.

The combined trends confirm our hypothesis that while analyte surface interactions contribute to broadening in the temporal dimension, no effect is observed in the spatial dimension.

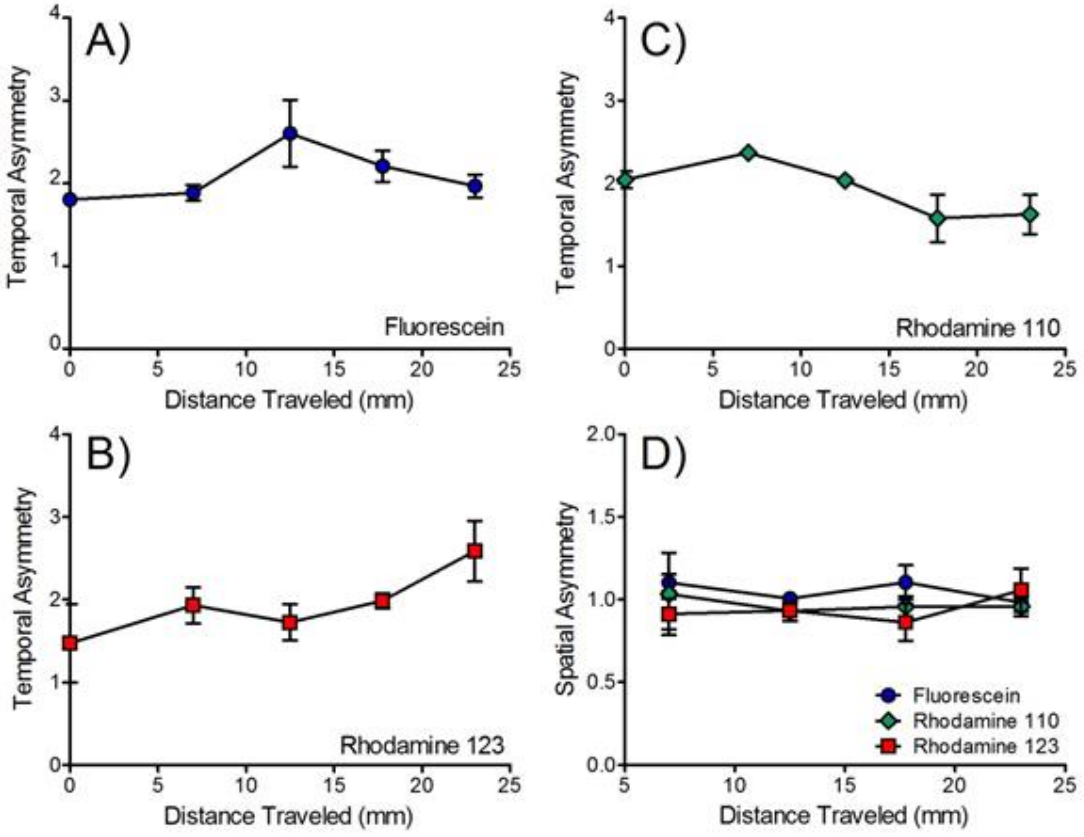

Figure 3.6: Plots of peak asymmetry in the temporal (A-C) and spatial (D) dimensions vs. distance traveled through the separation channel for fluorescein (blue circles), rhodamine 123 (red squares) and rhodamine 110 (green diamonds). Error bars are the standard error of the mean (n=3).

Figure 3.6 shows the asymmetry, in both the temporal (A-C) and spatial (D) dimensions, of the fluorescein, rhodamine 110 and rhodamine 123 peaks as they move through the μFFE separation channel. The asymmetry of the fluorescein and rhodamine 110 peaks did not change significantly as they moved

through the separation chamber. The initial asymmetry generated during their fast elution off the nLC column was maintained through the µFFE separation. Asymmetry in the temporal dimension increased for rhodamine 123 as expected due to its interaction with the separation channel surface. In contrast, µFFE peak shapes in the spatial dimension were nearly perfectly symmetrical in all cases, reinforcing the premise that surface interactions do not affect peak shape in the spatial dimension. It should also be noted that the temporal asymmetry of the peaks entering the flow chamber did not translate into spatial asymmetry in the µFFE separation.

3.4.2 Impact on Protein Separations

The surface interactions exhibited by rhodamine 123 in the HEPES/Triton X-100 buffer system were relatively modest. Much stronger interactions and consequently more severe peak distortions are commonly observed during CE analyses of proteins. We used Chromeo™ P503 labeled myoglobin and cytochrome c as model analytes to determine the effect of strong surface interactions on temporal and spatial broadening in µFFE. Figure 8A shows CE electropherograms of Chromeo™ P503 labeled myoglobin and cytochrome c using our low ionic strength buffer in a bare fused silica capillary. As expected for these non-ideal conditions, significant surface adsorption occurs, giving rise to extensive peak tailing. The baseline never returns to zero after the initial protein peaks migrate through the capillary suggesting that permanent adsorption onto the surface has taken place.

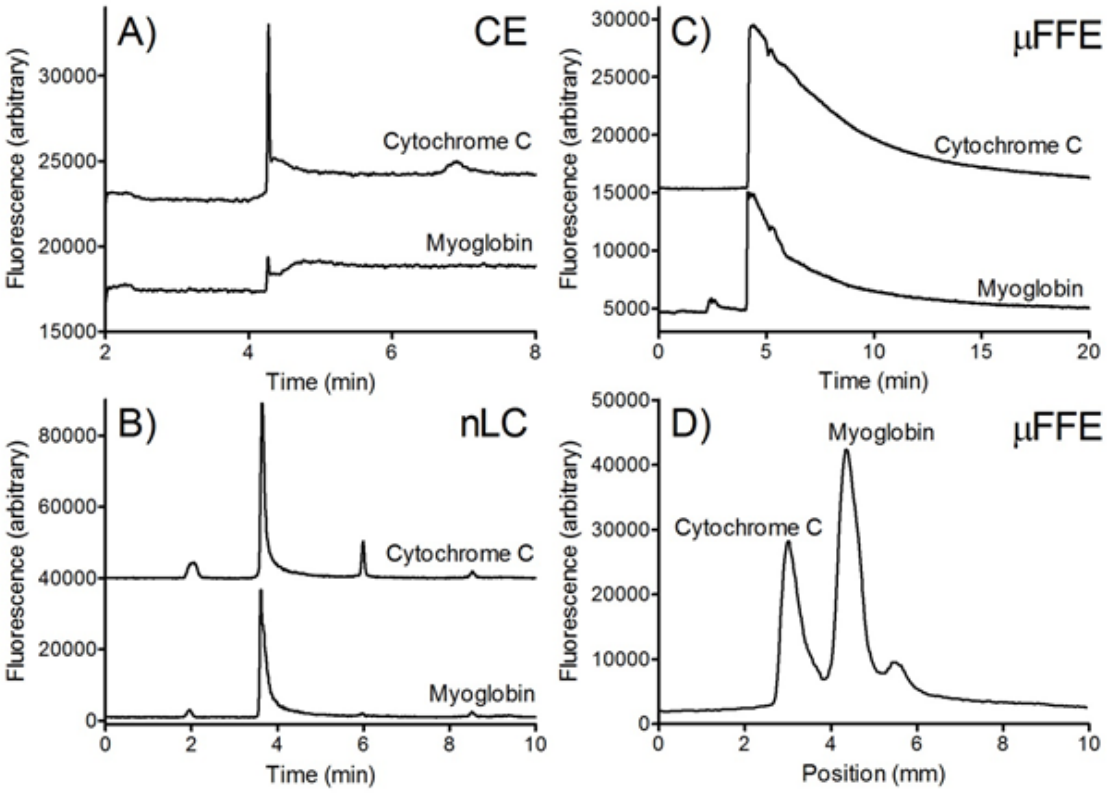

Figure 3.7: A) CE electropherogram of Chromeo™ P503 labeled cytochrome c and myoglobin. (B) nLC chromatograms measured on-column. (C) Extracted chromatograms recorded in the µFFE separation channel 12.5 mm from the sample inlet. (D) Extracted µFFE linescan recorded at 4.2 minutes.

Figure 3.7B shows individual 1D nLC chromatograms for Chromeo™ P503 labeled myoglobin and cytochrome c. TFA added to the mobile phase suppressed ionization of exposed silanol groups, minimizing surface interactions to generate good peak shapes. Initial peak widths were 97.5 and 95.0 seconds for myoglobin and cytochrome c, respectively. These well-defined peaks allowed us to inject discrete boluses of myoglobin and cytochrome c onto the µFFE device to assess spatial and temporal broadening. Figure 3.8 shows a 2D nLC × µFFE separation of myoglobin and cytochrome C. Extensive temporal

broadening is observed with peaks extending for >15 minutes after they initially reach the detector. Figure 3.7C shows extracted chromatograms for each protein after they travelled 12.5 mm through the μFFE separation chamber. Significant temporal broadening is observed due to protein adsorption onto the μFFE surface. The Chromeo™ P503 label preserves the native charge on the protein[117]. At a buffer pH of 7.00 myglobin (pI ~7) would be near neutral and cytochrome c (pI ~9.6) would be positively charged. Interactions at the wall can be attributed not only to net charge, but also local regions of positive charge or hydrophobic pockets.[139] Peak tailing was observed for >15 minutes after initial observation of the protein peaks. Proteins remained permanently adsorbed onto the glass surface requiring a NaOH rinse to regenerate the surface.

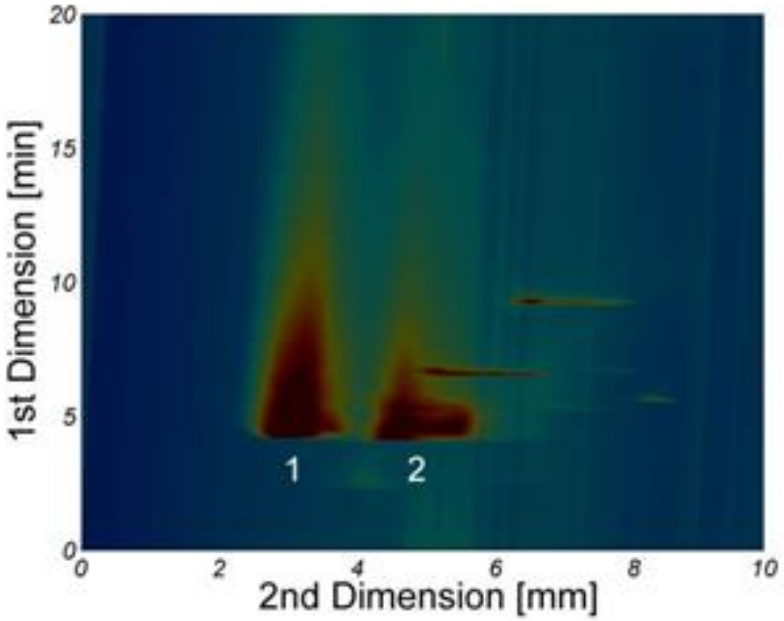

Figure 3.8: 2D nLC × μFFE separation of Chromeo™ P503 labeled (1) cytochrome c and (2) myoglobin. Detection was performed in the μFFE separation channel 12.50 mm from the sample inlet.

Figure 3.7D shows a μFFE linescan recorded at 4.2 minutes during the same Chromeo™ P503 labeled myoglobin and cytochrome c separation. Despite the dramatic surface adsorption that is evident in Figure 8C, spatial broadening in the μFFE separation remains unaffected. Only modest peak asymmetry is observed in the μFFE dimension, which can be attributed to heterogeneity in protein structure or labelling efficiency. The myoglobin and cytochrome c peaks are well resolved and symmetrical reinforcing that even severe surface adsorption does not contribute to spatial broadening in μFFE separations.

It should be noted that myoglobin and cytochrome c were chosen to present an extreme case of surface adsorption. The reversible adsorption shown in Figure 3.2B will be much more common. Irreversible adsorption to the separation channel will impact quantification. Signal intensity will decrease if analyte is adsorbed before reaching the detection zone. Conversely, irreversible adsorption of analytes in the detection zone may permit very long exposure times, potentially improving S/N.[140]

3.5 Conclusions

We have clearly demonstrated that surface adsorption does not contribute to spatial broadening in μFFE separations. μFFE may therefore be particularly well suited for performing separations of analytes that exhibit strong surface interactions. For example, the separations of many biomolecules, such as proteins and lipids, are challenging due to their propensity for interacting with a variety of surfaces. In contrast, surface adsorption does contribute to temporal

broadening in μFFE. It is therefore important to consider the effect of surface adsorption on the temporal response of a μFFE analysis when used to monitor changes in analyte concentration or composition over time.[141, 142] Surface interactions can be mediated using many of the same surface modifications previously developed for CE separations.[126-131] Eliminating surface interactions will be especially important for two-dimensional separations where temporal broadening in the μFFE separation will result in a loss of peak capacity generated by the first dimension separation.[85]

Chapter 4

Effect of Fluorescent Labels on Peptide and Amino Acid Sample Orthogonality in Two-Dimensional nLC × µFFE Separations

Geiger, M. and Bowser, M.T. *Anal. Chem.*, **2016,** *88 (4),* 2177-2187

4.1 Summary

As shown in Chapters 1 and 2, multidimensional separations present a unique opportunity for generating the high peak capacities necessary for the analysis of complex biological mixtures. In Chapter 2, the coupling of nano-liquid chromatography with micro free flow electrophoresis (2D nLC × μFFE) was shown to produce high peak capacity separations of fluorescently labelled peptide mixtures. Currently, μFFE largely relies on laser induced fluorescence (LIF) detection. We have demonstrated that the choice of fluorescent label significantly affects the orthogonality and peak capacity of 2D nLC × μFFE separations of peptides and amino acids.

Of the labeling reagents assessed. Chromeo™ P503 performed the best for 2D nLC × μFFE separations of peptides. A Chromeo™ P503 labeled BSA tryptic digest produced a 2D separation that made effective use of the available separation space (48%), generating a corrected peak capacity of 521 in a 5 minute separation window. 2D nLC × μFFE separations of NBD-F labeled peptides produced similar orthogonality and peak capacity but this reagent was able to react with multiple reaction sites, producing an unnecessarily complex analyte mixture. NBD-F performed the best for 2D nLC × μFFE separations of amino acids. NBD-F labeled amino acids produced 2D separations that covered 36% of the available separation space, generating a corrected peak capacity of 95 in a 75 second separation window. Chromeo™ P503 and Alexa Fluor® 488 labeled amino acids were not effectively separated in the μFFE dimension, giving 2D separations with poor orthogonality and peak capacity.

4.2 Introduction

Traditional chromatographic and electrophoretic separations have been powerful analytical tools in the analysis of mixtures.[118] However, the complexity of environmental and biomedical samples often exceeds the peak capacity of traditional one-dimensional (1D) separations (Chapter 1). Over the last several decades, multi-dimensional separations pairing two or more 1D separation techniques have been introduced as high peak capacity alternatives for complex samples. Online comprehensive separations using LC, GC, and CE in various combinations have all been demonstrated.[14, 16-20, 23-25, 143, 144] These 2D separations generate dramatically increased peak capacity when compared to 1D separations.[35] Total ideal peak capacities of over 1500 have been reported for on-line LCxLC in 15 minutes.[14] Giddings defined the ideal maximum peak capacity that a 2D separation could attain ($n_{c,2D}$) as the product of the peak capacities from the first (^1n_c) and second (^2n_c) dimension separations. [35]

To achieve the ideal 2D peak capacity described in eq. 1 there must be no remixing or under sampling at the interface between the two separations and the separation mechanisms must be orthogonal.[35, 40] These correction factors are represented by the fraction of the separation space occupied by peaks, f, and the under sampling of the first dimension, related to the ratio of the second dimension sampling time (t_s) and first dimension peak width ($^1\omega$), β (eq. 4.1).[40]

$$n_{c,2D} = {}^1n_c \, {}^2n_c \times \frac{1}{\beta} \times f \qquad (4.1)$$

In equation 4.1, $\frac{1}{\beta}$ defines the fraction of peak capacity lost due to under sampling. To avoid losses in peak capacity due to under sampling, the second dimension separation must operate much faster than the width of the peaks eluting off the first dimension separation. This has proven challenging especially in liquid phase separations, where 2D separation times of hours are not uncommon.[145] Under sampling of the first dimension in LC×LC can easily lead to 50% or greater loss in peak capacity before the second separation even occurs (Chapter 1).[40, 41]

In Chapter 2, it was demonstrated that under sampling could essentially be eliminated by using micro free-flow electrophoresis (μFFE) as the second dimension in a 2D separation.[85] Coupling nLC with μFFE generated peptide separations with a useable peak capacity of 776 in a 10 minute separation window. μFFE is a continuous separation technique where samples are introduced to the top of a planar separation channel and driven by pressure flow.[146] Unlike traditional capillary electrophoresis, where the electric field is applied along the flow direction, the field in μFFE is applied perpendicularly. Analyte's flow paths are deflected in the electric field and separate based on their electrophoretic mobilities. Since first demonstrated by Raymond et. al.[66] μFFE devices have been fabricated in a wide array of materials including silicon[66, 67], polydimethylsiloxane (PDMS)[68-71], and glass[74-80]. μFFE has been used to separate fluorescent dyes[71, 75], amino acids[66, 68, 69], peptides[85], proteins[67, 72, 76, 98, 100, 101], organelles[70, 77, 102], and whole cells[70]. Unique μFFE

applications include measurement of protein binding[142], aptamer selection[147] and optimization of electrophoretic separation conditions.[141]

Due to its high sensitivity and simplicity, laser induced fluorescence (LIF) has been the most commonly used detection method for μFFE to date.[148] While the sensitivity provided by LIF simplifies detection in microscale environments, this technique presents additional analytical challenges. In order to use LIF detection the sample must either be natively fluorescent or labeled with a fluorescent tag. Fluorescent labels have been developed for the analysis of a range of analytes including proteins, peptides, amino acids and nucleic acids.[149-151] These labels make high sensitivity LIF detection possible, but necessarily modify the sample. Labeling heterogeneity is possible for analytes with more than one reactive site.[116, 152] The chemical properties of the analytes are also changed. For example, labelling amine sites on a protein can dramatically affect a protein's isoelectric point.[117, 153]

Adding the same functional group to every molecule in a sample makes the analytes more similar to each other and, therefore, more difficult to separate. The chemical diversity of the analytes in a mixture can greatly impact orthogonality of a separation.[44] Orthogonality refers to how efficiently the separation space is used in a 2D separation. Giddings proposed several factors that determine orthogonality. The most commonly addressed is the separation dimensionality, which is the number of separation mechanisms employed in the system. For example, the number of columns linked together in multidimensional GC or LC separation. The second factor is the sample dimensionality, which is

the number of independent variables needed to identify the components of the sample. It follows that if the sample does not have enough complexity, a multidimensional separation would offer minimal to no gains in peak capacity.[44] The separation and sample dimensionality both contribute to the observed orthogonality of a separation. There are many methods for determining the orthogonality of a multidimensional separation including correlation coefficients[45, 46], fractal dimensionality[47], geometric approaches such as a fan area[48], peak counting[49], and modified forms of box counting[50-52]. Rutan *et. al.* have demonstrated the merits of the minimum convex hull method for estimating the fraction coverage (f).[53] The minimum convex hull defines the usable separation space by drawing the smallest convex polygon (i.e. all interior angles are ≤180°) around the outermost peaks of the 2D separation. It represents the area in which peaks could theoretically occupy in a separation, which agrees well with Giddings' original definition.[44]

It appears clear that labelling an analyte mixture with a fluorophore will impact its sample dimensionality and therefore, the orthogonality that will be observed in a 2D separation. Since 2D µFFE separations are, at this point, largely dependent on LIF detection, it is important to determine what extent different labels will limit the orthogonality of common separations. In the current chapter, the effect of three commonly used labeling reagents (Chromeo™ P503, NBD-F and Alexa Fluor® 488) on the observed peak capacity and orthogonality of 2D nLC × µFFE separations of peptide and amino acid mixtures are compared.

4.2 Experimental

4.2.1 Buffers and Solutions

All solutions were prepared using deionized water (18.3 MΩ, Milli-Q; Millipore, Bedford, MA) and filtered with a 0.22 µm nitrocellulose membrane filter (Fisher Scientific, Fairlawn, NJ) unless otherwise described. A buffer containing 300 µM Triton X-100, 1mM TEPA, and 25 mM MES hydrate (Sigma-Aldrich, St. Louis, MO) adjusted to pH = 5.50 in 95:5 H_2O:MeOH was used for µFFE separations of peptide mixtures. A buffer containing 300 µM Triton X-100 and 25 mM HEPES (Sigma) adjusted to pH=7.00 in H_2O was used for µFFE separations of amino acid mixtures. Poly(ethyleneoxide) (PEO) (Sigma) was dissolved in water to 0.2% by mass with 0.1 M HCl at 95 ˚C for 2 h while stirring. Eluents for nLC separations were prepared using LC-MS grade water and LC-MS grade ACN, both purchased from J.T. Baker (Phillipsburg, NJ). Trifluoroacetic acid (TFA) was purchased from Sigma-Aldrich. For labelling reactions a 10 mM $NaHCO_3$ solution (Mallinkrodt, Paris, KY) in water, 10 mg/mL Chromeo™ P503 (Active Motif, Carlsbad, CA) in DMSO (Sigma-Alrich), 4 mg/mL NBD-F (TCI, Portland, OR) in MeOH, and 10 mg/mL Alexa Fluor® 488 TFP ester (Thermo Scientific, Waltham, MA) in 10 mM $NaHCO_3$ buffer were prepared. All amino acid standards were purchased from Sigma-Aldrich. Piranha solution (2:1 H_2SO_4:H_2O_2) (Ashland Chemical, Dublin, OH) was used to clean glass wafers and etch Ti. *Caution: Piranha solution self-heats to ~70 ˚C and is extremely caustic*. GE-6 (Acton Technologies Inc., Pittston, PA) was used to etch Au. Concentrated HF (49%) (Ashland Chemical) was used to etch glass

wafers. Silver conductive epoxy (MG Chemicals, Surrey, BC, Canada) was used to make electrical connections to the μFFE device. Crystalbond™ 509 (SPI Supplies, West Chester, PA) was used to fix fused silica capillaries in the completed devices.

4.2.2 μFFE Device Fabrication

The μFFE device was fabricated following the procedure previously described by Geiger *et. al* in Chapter 2.[85] Briefly, three rounds of standard photolithography were performed to etch features into two 1.1 mm borofloat® glass wafers (Precision Glass & Optics, Santa Ana, CA). First, an 85 μm channel was etched for the capillary connection. A second etch was performed to etch 30 μm deep electrode channels. Finally, a third step etched the 1 cm wide × 2.5 cm long separation channel to 10 μm in depth. The final capillary and electrode channel depths were 125 μm (~250 μm wide) and 40 μm, respectively. The CAD files used to produce the photolithography masks are shown in Chapter 2, Figure 2.1. 150 nm Layers of Ti and Au (150 nm) were deposited to one of the wafers using a Temescal electron beam evaporator. A photolithography step was then performed to pattern the electrodes and remove unwanted Ti and Au. 1 mm diameter access holes were drilled in the second wafer for inlet, outlet, and electrode connections. A ~90 nm thick layer of amorphous silicon was deposited over this wafer. The two wafers were aligned under a microscope and anodically bonded (900 V, 3h, 450 ˚C, 5 μbar) using a Karl Suss SB-6 wafer bonder (Munich, Germany). The bonded device was cut by the University of Minnesota Electrical Engineering/Computer Science Machine Shop to expose the capillary

channel. NanoPorts™ (Upchurch Scientific, Oak Harbor, WA) were aligned over the access holes and bonded in place using epoxy rings (IDEX, Lake Forest, IL). Silver conductive epoxy was used to connect lead wires to the electrodes. The device was then heated on a hot plate at ~120ºC while under vacuum. A 20 µm i.d. × 150 µm o.d. fused silica capillary (Polymicro Technologies, Phoenix, AZ) was inserted into the sample channel and Crystalbond™ 509 was pulled through the remaining space between the capillary and channel to bond it in place. The chip was then perfused with 1M NaOH solution to remove residual amorphous silica in the channels.

4.2.3 Peptide and Amino Acid Labeling

Chromeo™ P503 labeling was performed by dissolving 1 nmol of BSA digestion standard (Waters Corp., Milford, MA) in 490 µL of $NaHCO_3$ buffer and vortexing for 5 minutes. 10 µL of the Chromeo™ P503 dye solution was added and the reaction mixture was vortexed for a further 10 minutes. The vial was allowed to incubate at room temperature overnight. Alexa Fluor® 488 labelling was performed by adding 100 µL of $NaHCO_3$ buffer to a 1 nmol of BSA digestion standard and vortexing for 5 minutes. The dissolved digest was then added to a vial containing 100 µg of Alexa Fluor® 488 TFP ester and incubated at room temperature for 2.5 hours. The final solution was diluted by a factor of 500 prior to analysis. For NBD-F labeling 1 nmol of BSA digestion standard was dissolved in 466 µL of $NaHCO_3$ buffer. After vortexing 5 minutes, 34 µL of 4 mg/mL NBD-F solution in methanol was added and the reaction was incubated at 80ºC for 10 minutes. Samples for each labeled mixture were filtered using 0.45 µm cellulose

acetate syringe filters (Sterlitech, Kent, WA). Amino acid labeling followed similar protocols as the protein digests. Briefly, 25 mM solutions of each amino acid were prepared and reacted at ratios of dye to amino acid of 4:1, 5:1, and 3:1 for Chromeo™ P503, Alexa Fluor® 488, and NBD-F, respectively.

4.2.4 nano-Liquid Chromatography (nLC) Conditions

A Thermo-Dionex UltiMate3000 RSLC nano pump with WPS autosampler (Sunnyvale, CA) was used for LC separations. The analytical column (Thermo-Dionex Part number 164562) was 75 µm i.d. × 15 cm long and packed with 2µm Acclaim® PepMap C_{18} particles. For all separations mobile phase A was 100% H_2O with 0.1% TFA and mobile phase B was 90:10 ACN:H_2O with 0.1% TFA. A gradient of 35-55% B over 5 minutes was used to separate peptides labeled with Chromeo™ P503 and NBD-F. A gradient of 10-35% B over 5 minutes was used to separate Alexa Fluor® 488 labeled peptides. A gradient of 5-85% B was applied over 2 minutes to separate Chromeo™ P503 and NBD-F labelled amino acids. A gradient of 5-75% B over 2 minutes was used to separate Alexa Fluor® 488 labelled amino acids. Injection volumes were 0.5 µL for all samples, and the flow rate was 300 nL/min.

4.2.5 Micro Free Flow Electrophoresis (µFFE) Conditions

Prior to separations the electroosmotic flow was suppressed by coating the µFFE device with PEO following a previously described method.[81] For 2D separations a syringe pump (Harvard Apparatus, Hollison, MA) was used to pump buffer through the separation channel at a total flow rate of 0.5 mL/min

(~0.15 cm/sec in the separation channel). 1 mM TEPA (Sigma) was added to the separation buffer to further reduce surface adsorption of peptides,.[154] Triton X-100 and 5 % MeOH were added to the buffer to improve stream stability.[83] For peptide samples +175 V was applied to the right electrode while the left electrode was held at ground. For amino acid separations +165 V was applied to the right electrode.

4.2.5 Data Collection and Processing

An AZ100 stereomicroscope (Nikon Corp., Tokyo, Japan) mounted with a Cascade 512B CCD camera (Photometrics, Tucson, AZ) was used for fluorescence imaging. For NBD-F and Alexa Fluor® 488 labelled samples the microscope was equipped with a GFP bandpass emission filter cube (Nikon Corp) containing two bandpass filters (450-490 nm and 500-550 nm) and a dichroic mirror (495 nm cutoff). For the Chromeo™ P503 labelled samples a custom filter cube was used (Nikon Corp) containing two bandpass filters (470-500 nm and 570-640 nm) and a dichroic mirror (500 nm cutoff). Laser induced fluorescence (LIF) detection was performed using a 150 mW, diode pumped solid state laser (Coherent) set to 100 mW and expanded into a ~2.5 cm × ~150 µm line positioned across the separation channel 2 cm from the sample inlet. The entire optical setup was enclosed in a light-tight box (Newport, Irvine, CA). For on-capillary detection of 1D separations a window was burned 70 cm down a 100 cm long piece of 20 µm i.d. × 280 µm o.d. fused silica capillary (Thermo-Dionex) which was attached to the end of the nLC column using a PTFE sleeve. For 2D separations a separate piece of 20 µm i.d. × 280 µm

capillary was connected to the capillary in the chip using a ZDV union (Upchurch Scientific). The total length from the column to the end of the capillary in the µFFE device was 70 cm. The acquisition rate for all separations was 4 Hz using a 1× gain for 1D separations and 4× gain for 2D separations. The nLC pump was controlled using Chromeleon v6.8 (Thermo-Dionex). Once logged, all data was processed using in-house Matlab programs. Cutter v5.0[114] and an open source program (Peak Finder, available at http://omics.pnl.gov/software) were used to process line scans and chromatograms, as well as determine peak capacities. For 2D separations the background was corrected using an orthogonal background correction as described by Filgueira *et. al.*, with a correction window of 50.[115]

4.3 Results and Discussion

Figure 4.1 shows the reactions for three commonly used, fluorescent labeling reagents for amines. Chromeo™ P503 is a fluorogenic chameleon dye which targets the amine side chains of lysine and arginine on peptides and proteins. The conjugated dye has a positive charge, thus retaining the native charge of the labeled molecule.[116, 117, 152] NBD-F is a fluorogenic reagent that

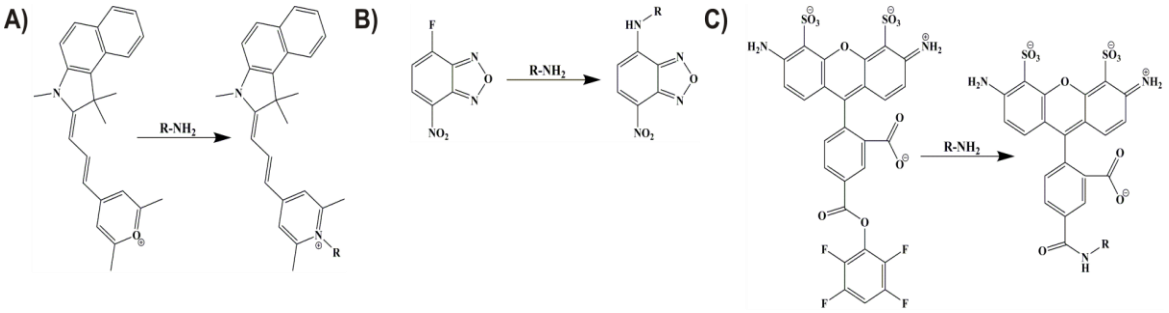

Figure 4.1: Labeling reactions for primary amines with the fluorophores A) Chromeo™ P503, B) NBD-F and C) Alexa Fluor® 488.

reacts with primary and secondary amines producing a neutral product.[151, 155] Alexa Fluor® 488 is a sulfonated rhodamine 110 dye with a net -2 charge across a typical pH range.[156, 157] On closer examination, these reactions clearly have the potential to impact sample orthogonality. Eliminating or even reversing positive charges on peptide or amino acid analytes will certainly decrease chemical diversity in the mixture. The size of the labeling reagents is also an issue. Labeling reagents will have little effect on overall size or structure when conjugated to a large protein. When conjugated to a smaller peptide or amino acid the relative size of the labeling reagent becomes significant. The labeling reagent may make a larger contribution to the chemical structure and properties of the resulting product than the analyte itself, making compounds in the mixture much more similar and consequently more difficult to separate.

Figures 4.2 A-C show 1D nLC chromatograms for BSA tryptic digests labelled with Chromeo™ P503, NBD-F or Alexa Fluor® 488. Differences in the chemical properties of the labeling reagents required modification of the mobile phase for each separation. For all dyes the mobile phase gradient was adjusted to elute all peaks in a ~5 minute window. The complexity of the tryptic digest has exceeded the peak capacity of the 1D separation with few, if any, baseline resolved peaks observed. The average baseline widths of peaks observed across the 5 minute separation window were estimated to be 10.0 sec, 9.38 sec, and 14.3 sec for the Chromeo™ P503, NBD-F, and Alexa Fluor® 488 labeled digests, respectively. Peak capacities for the 1D nLC separations were therefore

determined to be 30, 32, and 21 for Chromeo™ P503, NBD-F, and Alexa Fluor® 488 labeled peptides, respectively (see Table 4.1). These peak capacities are insufficient for a mixture of this complexity considering that a tryptic digest of BSA is predicted to produce 74 peptides. Multiple peptide labelling sites makes an even more complex sample possible.

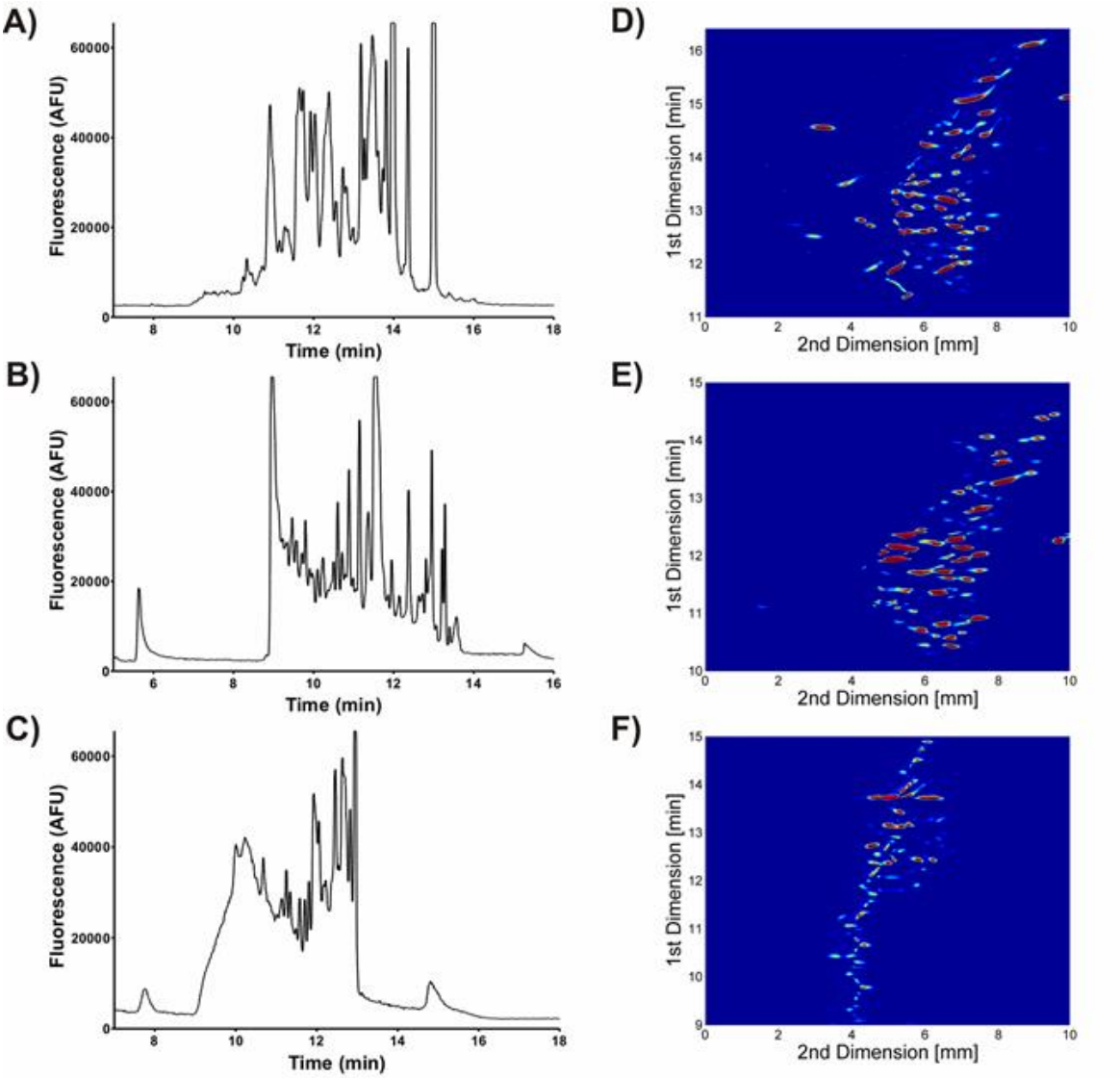

Figure 4.2: 1D nLC chromatograms of A) Chromeo™ P503, B) NBD-F and C) Alexa Fluor® 488 labeled BSA tryptic peptides. 2D nLC × µFFE separations of D) Chromeo™ P503, E) NBD-F and F) Alexa Fluor® 488 labeled BSA tryptic peptides.

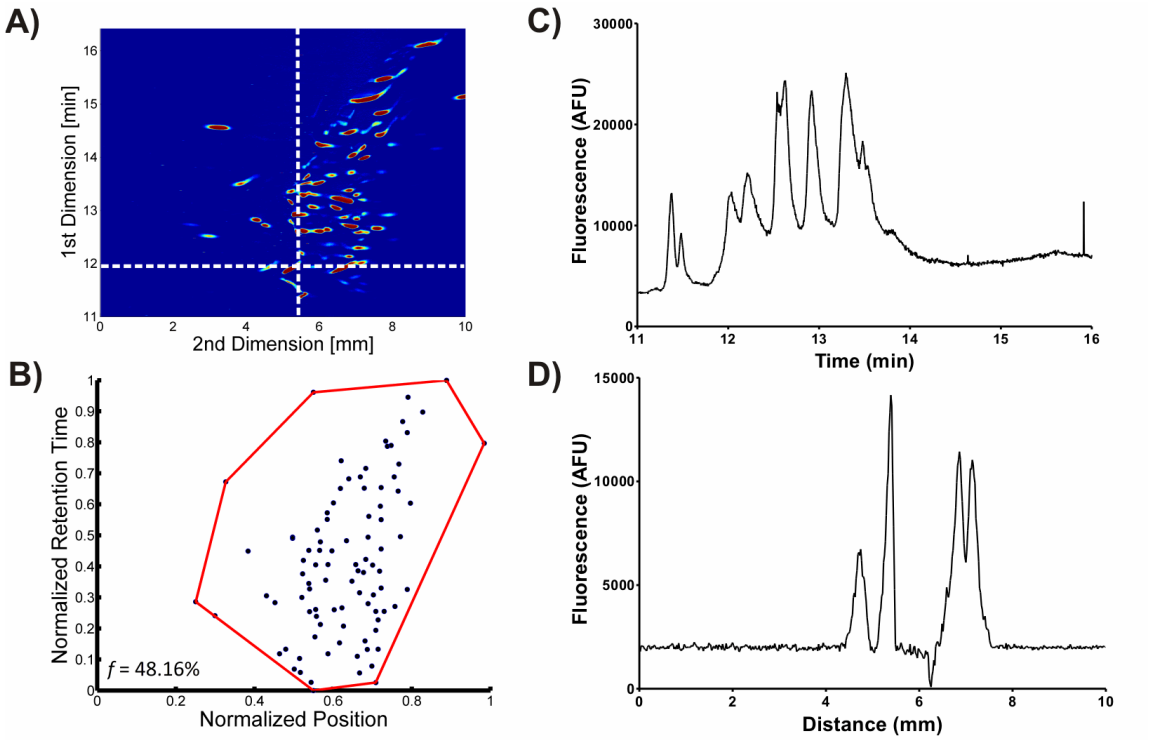

Figure 4.3: A) 2D nLC × µFFE separation of Chromeo™ P503 labeled BSA tryptic digest. B) Plot showing the calculation of the minimum convex hull to determine the fraction of separation space where peaks elute. Points are the elution position of the peaks shown in A). The red line is the boundary of the minimum convex hull that includes all observed peaks. C) Chromatogram extracted from the 2D separation shown in A) at 5.50 mm (illustrated by the vertical dashed line). D) µFFE linescan extracted line scan from the 2D separation shown in A) at 12.0 min (illustrated by the horizontal dashed line).

2D nLC × µFFE chromatograms for the same Chromeo™ P503, NBD-F and Alexa Fluor® 488 labeled BSA tryptic digests are shown in Figures 4.2 D-F. The additional peak capacity provided by coupling with µFFE results in separations that better demonstrate the complexity of the mixture with many baseline resolved peaks. Figures 4.3-4.5 present the 2D nLC × µFFE chromatograms for each labeled digest in more detail. Figures 4.3-4.5B show the minimum convex hull that encloses all of the peaks observed in the 2D separations. The minimum convex hull is a simple, yet powerful method for

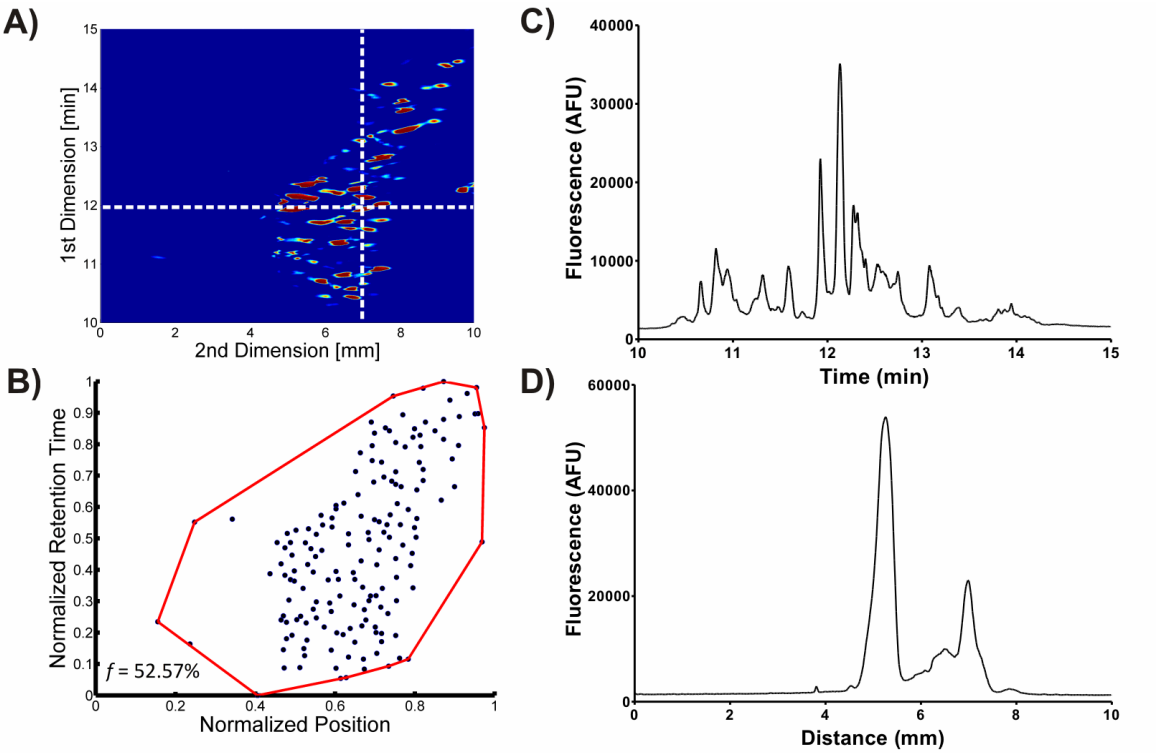

Figure 4.4: A) 2D nLC × µFFE separation of NBD-F labeled BSA tryptic digest. B) Plot showing the calculation of the minimum convex hull to determine the fraction of separation space where peaks elute. Points are the elution position of the peaks shown in A). The red line is the boundary of the minimum convex hull that includes all observed peaks. C) Chromatogram extracted from the 2D separation shown in A) at 7.06 mm (illustrated by the vertical dashed line). D) µFFE linescan extracted line scan from the 2D separation shown in A) at 11.9 min (illustrated by the horizontal dashed line).

estimating the fraction of separation space where peaks could reasonably be expected to elute.[53] These plots show clear differences in the observed orthogonality of each 2D separation. The minimum convex hull for the Chromeo™ P503, NBD-F, and Alexa Fluor® 488 labelled peptides covered 48.2%, 52.6%, and 14.6% of the available separation space, respectively. Labeling with Chromeo™ P503 and NBD-F effectively retained the sample diversity while labeling with Alexa Fluor® 488 negatively impacted the observed

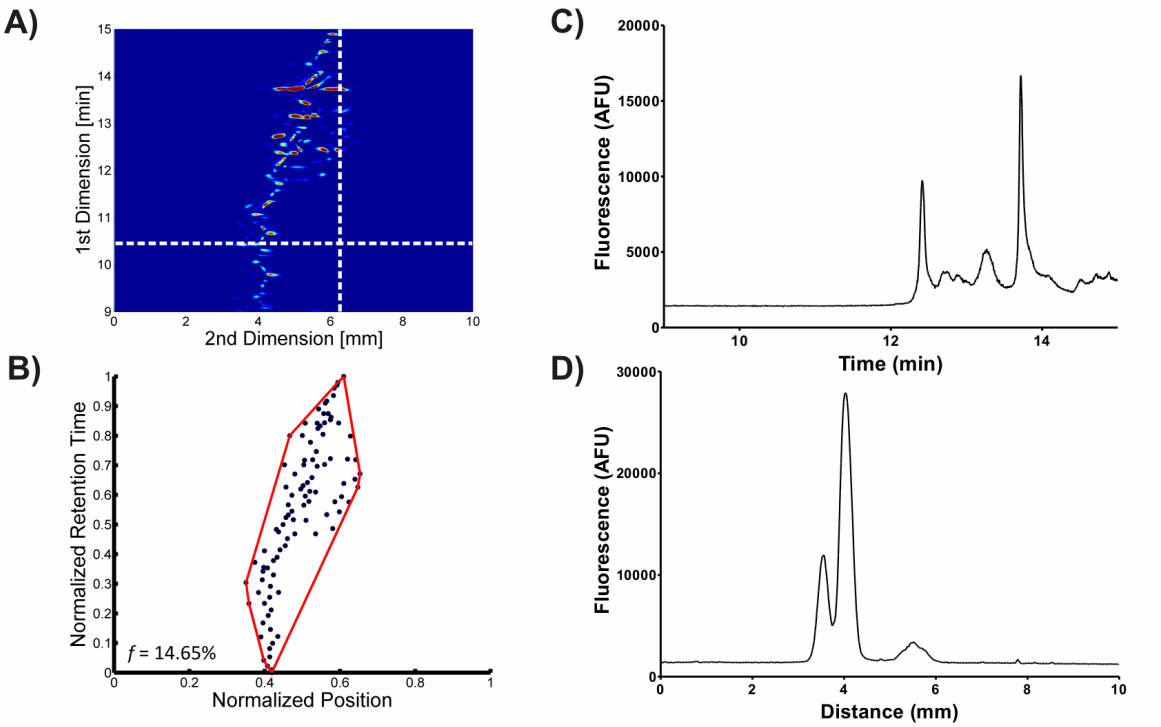

Figure 4.5: A) 2D nLC × µFFE separation of Alexa Fluor® 488 labeled BSA tryptic digest. B) Plot showing the calculation of the minimum convex hull to determine the fraction of separation space where peaks elute. Points are the elution position of the peaks shown in A). The red line is the boundary of the minimum convex hull that includes all observed peaks. C) Chromatogram extracted from the 2D separation shown in A) at 6.30 mm (illustrated by the vertical dashed line). D) µFFE linescan extracted line scan from the 2D separation shown in A) at 10.4 min (illustrated by the horizontal dashed line).

orthogonality. These results are not unexpected considering the reactions shown in Figure 4.1.

Labeling with Chromeo™ P503 dye retains the positive charge at the lysine and argenine reaction sites, leaving the pI of the peptides unchanged and retaining the chemical diversity of the analyte mixture.[117] Peptides with both positive and negatively net charges remain after labeling (at pH = 5.5) allowing analytes to deflect in both directions in the second dimension µFFE separation.

NBD-F reacts with primary and secondary amines, eliminating cationic sites on the peptides (see Figure 4.1). As a consequence, most analyte peaks deflect towards the anode in the µFFE separation indicating that they bear a net negative charge (see Figure 5A&B). Regardless of the inefficient use of µFFE separation, peaks still cover 52.6% of the available separation area. This high observed orthogonality may be due to the relatively small size of the NBD label, which may have less impact on the chemical properties of the final reaction product.

Alexa Fluor® 488 reacts with primary amines, replacing a cationic site with a double negative charge (see Figure 4.1). As shown in Figure 4.5 A&B, the Alexa Fluor® 488 labeled peptides all move towards the anode with little separation in the µFFE dimension. This is not surprising, since the labeling reaction effectively makes every peptide in the sample anionic, dramatically decreasing chemical diversity in the sample. Alexa Fluor® 488 is also the largest of the labels, which further masks differences in the derivatized analytes. Together, the replacement of anionic sites with cationic functional groups and the overall size of the Alexa Fluor® 488 label results in a significantly lower observed orthogonality than that observed for the Chromeo™ P503 or NBD-F labeled digests.

Figures 4.3-4.5C show examples of chromatograms extracted from each of the 2D separations. These chromatograms were used to estimate the first dimension peak capacity in the 2D separations. The average observed first dimension peak widths were 8.3, 6.8, and 8.8 seconds for the Chromeo™ P503,

NBD-F, and Alexa Fluor® 488 labelled peptides, respectively. The observed first dimension peak widths were actually lower than those observed in the 1D nLC separations (see Table 4.1) indicating that no peak broadening occurred in the nLC to µFFE interface.[85] The narrower nLC peaks widths observed in the 2D separation may be a consequence of the improved separation. Estimates of peak width are much more reliable when analytes are fully resolved. LIF measurements were collected with a sampling frequency of 4 Hz in the µFFE separation channel. At this acquisition rate, 27-35 data points were recorded across each peak, generating the smooth chromatograms observed in Figure 4.3-4.5C and more than enough to eliminate any peak capacity loss due to under sampling. The measured first dimension peak capacity for the Chromeo™ P503, NBD-F, and Alexa Fluor® 488 labelled peptides, was 36, 44 and 34, respectively. The NBD-F labeled peptides exhibited better performance on the nLC resulting in narrower peaks and a higher observed first dimension peak capacity.

Table 4.1: Comparison of peak capacity metrics for Chromeo™ P503, NBD-F, and Alexa Fluor® 488 labeled tryptic digests of BSA.

	Chromeo™ P503	**NBD-F**	**Alexa Fluor® 488**
1D nLC Peak Capacity	30	32	21
1D nLC Observed Peaks	24	33	18
2D nLC Peak Capacity	36	44	34
2D µFFE Peak Capacity	30	30	36
Ideal 2D Peak Capacity	1080	1320	1224
Fraction Coverage	48.2%	52.6%	14.6%
Adjusted 2D Peak Capacity	521	694	179
2D nLC×µFFE Observed Peaks	79	164	98

Figures 4.3-4.5D show examples of extracted µFFE linescans used to estimate the second dimension peak capacity. Based on average peak widths the second dimension peak capacities for the Chromeo™ P503, NBD-F, and Alexa Fluor® 488 labelled peptides were 30, 30, and 36, respectively. The higher observed peak capacity for the Alexa Fluor® 488 labelled peptides is a result of the lower µFFE deflection distances observed in this separation. Hydrodynamic broadening, a major source of band broadening in µFFE, scales with the deflection distance squared.[108] Reducing hydrodynamic broadening, albeit through a relatively poor use of µFFE separation space, resulted in narrower peaks and a higher peak capacity estimate.

The ideal 2D peak capacities (i.e. $n_{c,2d} = {}^{1}n_c \times {}^{2}n_c$) for the Chromeo™ P503, NBD-F, and Alexa Fluor® 488 labelled peptides were estimated to be 1080, 1320, and 1224, respectively. These ideal peak capacities compare well with previously reported peak capacities for LC × LC (793 in 15 minutes)[14] and UPLC × CE (1400 in 40 minutes)[97] that were calculated in a similar manner. The ideal peak capacities of the nLC × µFFE separations are even more impressive considering that they were generated in a 5 minute separation window. Our nLC × µFFE separations generated 216 – 264 peaks/minute, >4-fold greater than previously reported LC × LC separations.

The ideal peak capacities estimated for the Chromeo™ P503, NBD-F, and Alexa Fluor® 488 labeled peptides show the pitfalls of reporting ideal values that do not consider losses due to under sampling or non-ideal orthogonality. Based on ideal peak capacity alone, it would be predicted that the Alexa Fluor® 488

labeled peptides would yield the best separation (see Table 4.1). The 2D separations shown in Figure 4.2 clearly show that this is not the case. Poor orthogonality limits the fraction of separation space utilized in the Alexa Fluor® 488 labeled peptide separations (see Figure 4.5B). Accounting for orthogonality, the corrected 2D peak capacities (see eq. 4.1) of the Chromeo™ P503, NBD-F, and Alexa Fluor® 488 labeled peptides were 521, 694, and 179, respectively. These values give a more accurate representation of the resolving power of the 2D nLC × μFFE separations shown in Figures 4.2-4.5. Even after the correction, the Chromeo™ P503 and NBD-F labeled peptides separations still produce peaks at an impressive rate of 104 and 139 peaks/minute, respectively.

Although the 2D nLC × μFFE separation of NBD-F labeled peptides produced the highest peak capacity and fractional coverage of the tested labels, the high resolving power of the separation reveals a significant drawback associated with this reagent. The total number of peaks observed in the 2D nLC × μFFE separations of Chromeo™ P503, NBD-F, and Alexa Fluor® 488 labeled peptides were 79, 164, and 98, respectively. The impressive peak capacity generated by the 2D separation of NBD-F labeled peptides is able to resolve a large number of peaks. Unfortunately, a tryptic digest of BSA is only predicted to produce 74 peptide fragments. NBD-F is able to react efficiently with both the terminal peptide amine as well as arginine/lysine residues, introducing the opportunity for heterogeneous labeling at multiple reaction sites. This heterogeneous labeling produces a mixture that is even more complex than the original. Chromeo™ P503 labeling produced a separation with 79 peaks, which

closely matches the predicted number of BSA tryptic peptides. Due steric restrictions, Chromeo™ P503 only reacts efficiently with lysine and arginine residues, not terminal amines.[117, 158, 159] Most tryptic peptides only contain a single arginine or lysine residue, limiting the opportunity for multiple labeling reactions.

Figures 4.6 A-C show 1D nLC separations of a group of 25 amino acids that have been labeled by Chromeo™ P503, NBD-F or Alexa Fluor® 488. As shown in Figure 4.1, each of the fluorescent labels is significantly larger than the amino acid analytes. We anticipated that the label would therefore have an increased effect on the chemical diversity of the mixture and the resulting separation. As shown in Figures 4.6 A-C, the complexity of the mixture overwhelms the peak capacity of the 1D nLC separations. It should be noted that fast nLC gradients were employed to elute all peaks in a 1.5-2.0 minute separation window.

Figures 4.6 D-F show 2D nLC × µFFE separations of the same 25 amino acid mixture labeled with Chromeo™ P503, NBD-F or Alexa Fluor® 488. No separation of the Chromeo™ P503 labeled amino acids was observed in the µFFE dimension, giving rise to a very low separation orthogonality (see Figure 4.6D). Most of the amino acids are neutral at pH = 7.0. Chromeo™ P503 retains the positive charge on the amine, resulting in a reaction product that is also neutral and therefore does not migrate in the µFFE electric field. Another issue was the labeling efficiency of Chromeo™ P503. Due to steric factors Chromeo™ P503 does not react efficiently with peptide terminal amines. Similarly, reaction

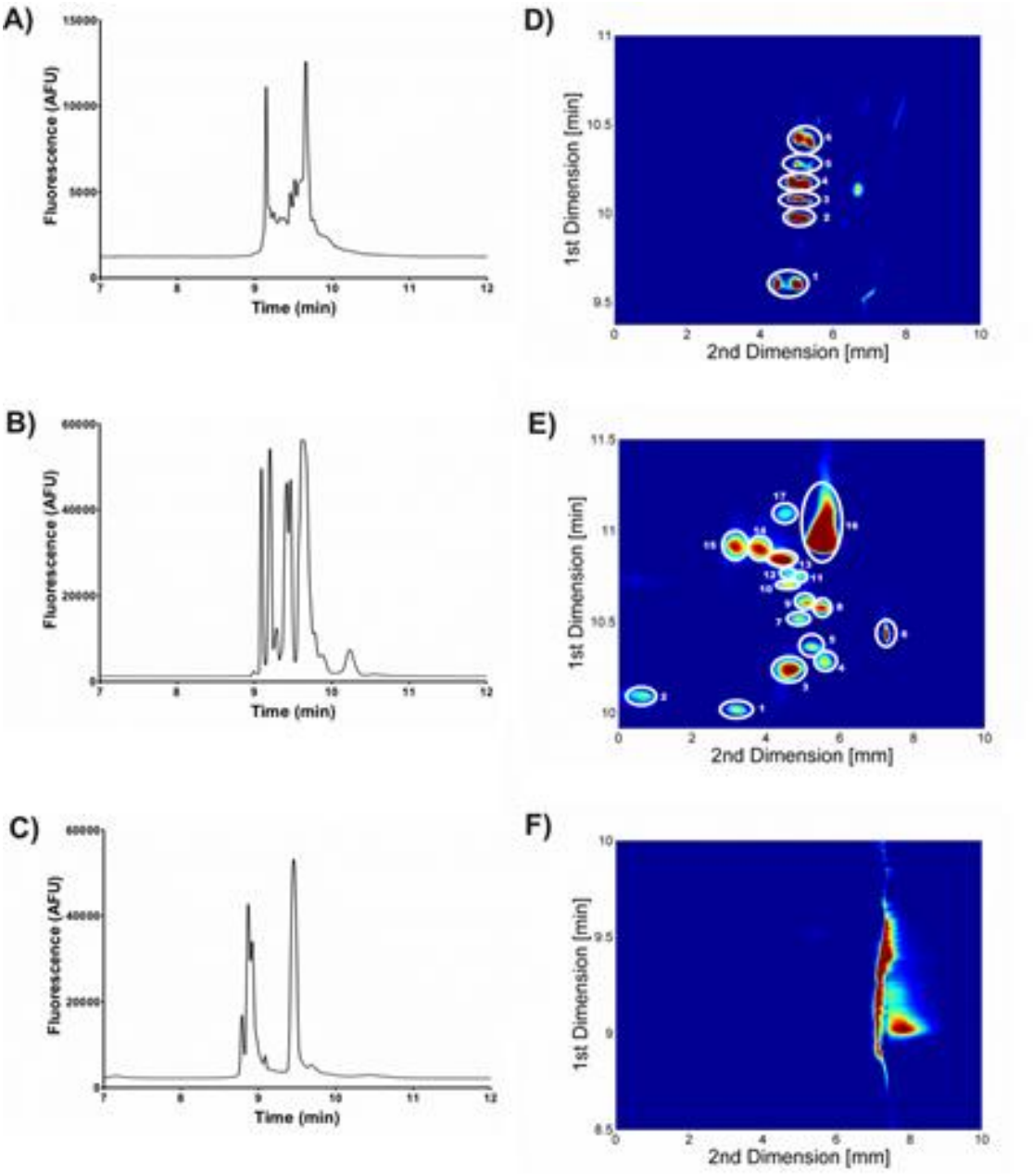

Figure 4.6: 1D nLC chromatograms of A) Chromeo™ P503, B) NBD-F and C) Alexa Fluor® 488 labeled amino acids. 2D nLC × µFFE separations of D) Chromeo™ P503, E) NBD-F and F) Alexa Fluor® 488 labeled amino acids. Peaks identified in D) include: (1) Histidine, (2) Leucine/ Lysine/ Asparagine, (3) Phenylalanine/Methionine/Taurine/Isoleucine/ β-ABA/ Arginine/Serine/Valine/Threonine, (4) Glycine/Alanine, (5) β-Alanine and (6) γ-ABA/Cysteine. Peaks identified in E) include: (1) Histidine, (2) Arginine/Lysine, (3) β-Alanine/Alanine/Glutamine/Asparagine, (4) Taurine, (5) α-ABA, (6) Glutamic Acid/Aspartic Acid, (7) α-ABA, (8) Glycine, (9) Phenylalanine, (10) γ-ABA, (11) Methionine, (12) β-ABA, (13) NBD-OH, (14) Proline/Cysteine/Tryptophan, (15) Valine, (16) NBD-OH, and (17) Threonine/Tyrosine.

with certain amino acids was challenging with only 18 of the 25 amino acids producing fluorescent products. Of these 18 labeled amino acids most eluted at the same time. Surprisingly, resolution was higher in the 2D nLC × µFFE separation than the 1D nLC separation, even though almost no orthogonality was observed. The apparent increase in resolution could be due to a difference in quantum yield between the nLC mobile phase and the µFFE buffer or surface adsorption in the µFFE separation channel which could selectively increase the retention time of certain analytes.

The Alexa Fluor® 488 labeled amino acids did not separate well using nLC × µFFE (see Figure 4.6F). Alexa Fluor® 488 is not a fluorogenic reagent, giving rise to a large reactant peak that dominated the separation. Alexa Fluor® 488 is a relatively large label that imparts a -2 charge at the amine reaction site, effectively making all analytes in the mixture highly negative with an overall size/structure not that different from the unreacted label. This is observed in Figure 4.6F where all analytes are pulled strongly to the anode and are not resolved from the excess Alexa Fluor® 488 reagent.

As shown in Figure 4.6, only NBD-F labeled amino acids were effectively separated using 2D nLC × µFFE. The addition of second dimension µFFE separation increased the resolving power with 17 peaks observed. In this case reaction with the label actually increased the sample dimensionality. Prior to labelling, most of the amino acids bear a net neutral charge and would not be expected to separation in the µFFE dimension. Reaction with NBD-F removes the positive charge of the amine reaction site. After reaction with NBD-F, most of

the amino acid analytes bear a -1 charge, ideal for µFFE separation. NBD-F is also significantly smaller than Chromeo™ P503 or Alexa Fluor® 488 (see Figure 4.1), and therefore has less impact on the final structure of the labeled amino acids. With minimal optimization 10 of 25 amino acids were baseline resolved in a 75 second separation window. This narrow elution window is much faster than previously reported 1D HPLC amino acids separations [160, 161] and even approaches separation times achieved using high-speed CE.[162]

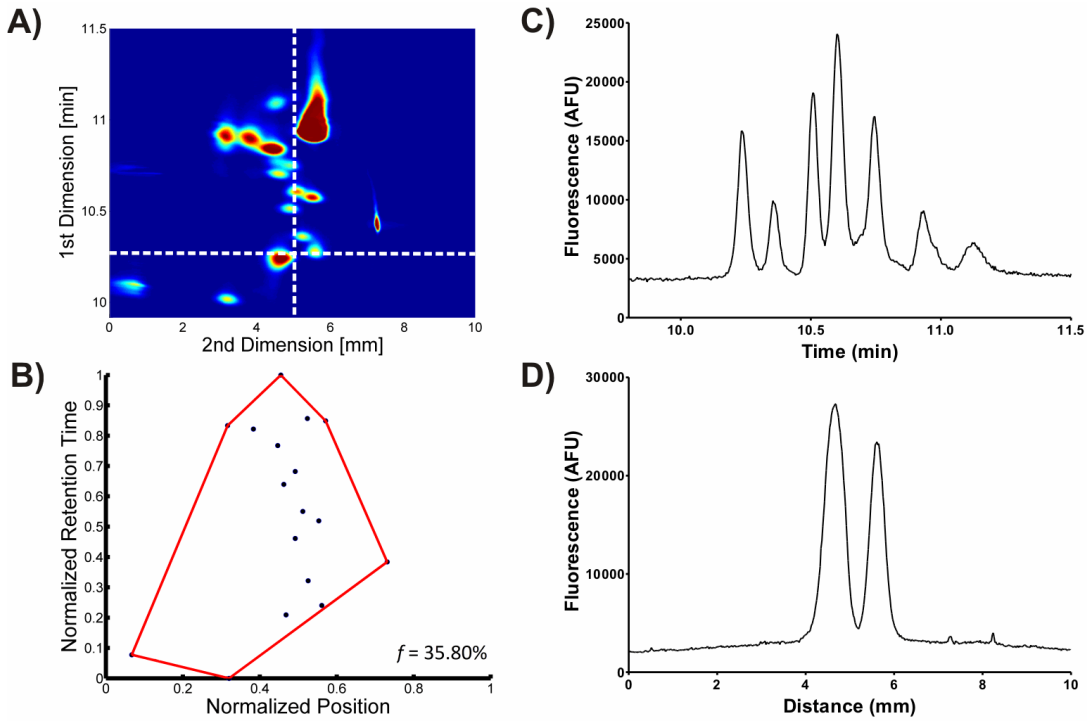

Figure 4.7: A) 2D nLC × µFFE separation of NBD-F labeled amino acids. B) Plot showing the calculation of the minimum convex hull to determine the fraction of separation space where peaks elute. Points are the elution position of the peaks shown in A). The red line is the boundary of the minimum convex hull that includes all observed peaks. C) Chromatogram extracted from the 2D separation shown in A) at 5.04 mm (illustrated by the vertical dashed line). D) µFFE linescan extracted line scan from the 2D separation shown in A) at 10.27 min (illustrated by the horizontal dashed line).

The 2D nLC × µFFE separation of NBD-F labeled amino acids is examined in more detail in Figure 4.7. As shown in Figure 4.7B, the nLC and µFFE dimensions are fairly orthogonal with peaks spread across ~36% of of the available the separation space. Improved orthogonality would be expected with further refinement of the nLC and µFFE separation modes. Figure 4.7C shows a chromatogram extracted from the 2D separation. The improved resolving power of the 2D separation makes clear identification of individual peaks (compare with Figure 4.6B). The average observed peak width in the nLC dimension was 6.50 sec, giving rise to a first dimension peak capacity of 12. Even with the 75 second elution time, 26 data points were recorded for each peak, reinforcing that µFFE effectively eliminates peak capacity losses due to under sampling. Figure 4.7D shows a µFFE linescan extracted from the 2D separation. The average observed peak width in the µFFE dimension was 0.45 mm, giving rise to a second dimension peak capacity of 22. Combining the observed first and second dimensions peak capacities give an ideal 2D peak capacity of 264, again in a 75 second elution window. Accounting for orthogonality (eq. 4.1), gives a corrected peak capacity of ~95, or 76 peaks/minute.

4.5 Conclusions

2D nLC × µFFE was used to generate high peak capacity separations of Chromeo™ P503, NBD-F or Alexa Fluor® 488 labeled peptides and amino acids. The choice of labeling reagent significantly affected the performance of the 2D separations. nLC × µFFE separations of Chromeo™ P503 or NBD-F labeled BSA tryptic digests achieved corrected peak capacities of 521 and 694,

respectively, in a 5 minute separation window. 2D separations of Chromeo™ P503 and NBD-F labeled BSA tryptic digests were highly orthogonal, with peaks covering nearly 50% of the available separation space. 2D nLC × μFFE separations of Alexa Fluor® 488 labeled peptides resulted in relatively poor orthogonality and observed peak capacity. Alexa Fluor® 488 reduced sample dimensionality by replacing the positively charged amine reaction site with a -2 charged fluorophore, effectively making all of the peptides anionic. Although nLC × μFFE separations of NBD-F labeled peptides showed the highest peak capacity, heterogeneous labeling at multiple labeling sites made the sample unnecessarily complex. Chromeo™ P503 was identified as the preferred labeling reagent for peptides due to the combination of high peak capacity and homogenous labeling efficiency.

Of the labels assessed, NBD-F performed the best for 2D nLC × μFFE separations of amino acids. A corrected 2D peak capacity of 90 was achieved in a 75 second elution window. Moderate orthogonality was observed with peaks covering 36% of the available separation space. Chromeo™ P503 labeled amino acids did not separate in the μFFE dimension since they remained neutral after reaction. Modification to a μFFE separation mode better suited for the separation of neutrals (e.g. MEKC) could address this issue. 2D nLC × μFFE separations of Alexa Fluor® 488 labeled amino acids performed particularly poorly. The high negative charge imparted on all analytes and the relatively large size of the Alexa Fluor® 488 significantly reduced the chemical diversity of the sample, making separation from the excess labeling reagent difficult.

Chapter 5

Summary and Future Outlook

5.1 Summary

Micro free flow electrophoresis (μFFE) is a separation technique which can be used for unique applications due to its continuous nature. Separations are performed in space, as opposed to time, as laminar flow drives analytes down the separation chamber. This continuous nature makes it an attractive option to be used as a second dimension in multidimensional separations. The major focus of this work was the development of a 2D separation platform coupling a commercial nano-liquid chromatography (nLC) instrument with an all glass μFFE device. Once the technique was demonstrated to be a powerful tool in separations of a complex sample, the subsequent chapters studied several factors which are important to consider if the technique is going to reach is maximum potential as a separation tool, specifically broadening in temporal and spatial dimensions and the effect of fluorescent labels on orthogonality.

In Chapter 2, a new μFFE device was designed and fabricated for coupling with nLC. A zero dead volume (ZDV) interface needed to be implemented to overcome the remixing of analytes seen using traditional fluidic connections. A narrow channel was fabricated down the center of the device to allow for a glass capillary to be inserted, resulting in a connection which was demonstrated to have no impact on peak broadening through the interface. The capillary could easily be removed and replaced in the event of clogging or breakages. Once the interface was in place, a Chromeo™ P503 labelled BSA digest was separated to test the resolving power of the technique. In a 10 minute separation window, a 2D peak capacity of 2,352 was observed. Peak capacity

generation over the entire analysis was found to be 105 peak/min, nearly double the maximum peak capacity production rate achieved using online LC × LC.[33, 34] During experiments, some peptides were observed to adsorb to the surface of the device. However, peak widths were only significantly impacted in the time dimension (nLC), not space (µFFE). Additionally, the Chromeo™ P503 label was carefully chosen to maintain the sample dimensionality to maximize orthogonality. Chapters 3 and 4 further addressed these factors.

The width of analyte peaks is the determining factor in achieving high peak capacities. The adsorption of analytes onto surfaces of columns, capillaries, and microfluidic devices often becomes a major source of peak broadening in separations of biological samples. In Chapter 3 the surface adsorption of 3 fluorescent dyes was measured in the temporal and spatial dimensions as they moved down the separation channel of the previously designed µFFE device. It was demonstrated that surface adsorption does not affect the peak position or spatial broadening in µFFE separations, even though broadening in the temporal dimension was still taking place. Using a low ionic strength buffer to promote adsorption, rhodamine 123 exhibited significant surface interactions, causing peak broadening and increased asymmetry in the temporal dimension. Broadening and symmetry in the spatial dimension, however, was not observed to be different from the other separated dyes. Strong surface interactions were further demonstrated by separating Chromeo™ P503 labelled myoglobin and cytochrome c. In the spatial dimension, the proteins were well resolved and had fairly symmetrical peaks despite permanently adsorbing onto the surface of the

separation channel. It is clear that in order to maximize peak capacity the adsorption in the temporal dimension must be addressed and minimized with the use of surface coatings or buffer additives. In Chapter 2, a PEO coating was used in addition to adding 8M urea to the buffer, while in Chapter 4, a PEO coating was used with the addition of 1 mM TEPA.

The high peak capacity capabilities of the nLC × µFFE platform were demonstrated in Chapter 2. Chapter 4 took a closer look at how fluorescent labels can affect the peak capacity and orthogonality of the separation of peptides and amino acids. To date, most of the work using µFFE has relied on laser induced fluorescence (LIF) as a detection scheme.[148] The use of LIF requires the sample either be natively fluorescent or labelled with a fluorescent dye. The choice of label was shown to greatly impact separation performance. Chromeo™ P503 was shown to perform best in the separations of peptides since it does not affect the pI of the peptides, preserving sample dimensionality, and is a more selective label compared to NBD-F or Alexa Fluor® 488, rediucing the likelihood that the sample would become more complex due to multiple labelling. As with the separation in Chapter 2, high peak capacities in this work were observed in all separations (>1000 in 5 minutes). Using the fraction of the separation space (48%) utilized by the separation a corrected peak capacity of 521 was observed for the Chromeo™ P503 labelled sample. Though this label worked well for peptides, poor labeling efficiency and the nature of the sample made it ineffective for separating amino acids. NBD-F was shown to provide adequate orthogonality and generated a corrected peak capacity of 95 in a 75

second separation window. The dependence on fluorescence is a current limitation for all µFFE applications. However, fluorescent labels can still be used effectively if they are chosen appropriately based on the sample of interest.

5.2 Future Applications

Micro free flow electrophoresis is a technique that can be applied for a wide variety of unique applications. The work presented in this thesis demonstrated its use a second dimension to provide high peak capacity separations of complex samples. In order to make it a more universal platform, there are several areas in which further research and development are needed. First, the demonstration of a range of separation modes to a variety of real samples would help establish protocols and methods to be applied for real world applications and find modes which are most orthogonal. Additionally the cost of the devices could be reduced through the recent advancements in 3D printing. The proper implementation of mass spectrometry detection is long overdue and could provide very powerful information for biological samples.

5.2.1 Combining Separation Modes

The appropriate choice of orthogonal separation modes in each dimension is critical for obtaining maximum separation performance since the entire separation space will be accessible to analytes.[44, 47] Combining liquid chromatography (LC) with µFFE provides a wide range of separation mode combinations which need to be explored and evaluated. Previous work with 2DLC separations revealed, somewhat surprisingly, that choosing two reversed-

phase (RP) columns and employing significantly different pH mobile phases achieved the highest effective peak capacity when testing various combinations of RP, SCX, SEC, and HILIC.[51]

As mentioned in Chapter 1, µFFE can be operated in several electrophoretic separation modes. Peak capacity for the µFFE second dimension separations shown were ~30 (Table 4.1). Implementing µFFIEF in the second dimension is predicted to have several advantages over the modes used in this work. FFIEF is a higher resolution technique and has been predicted to separate proteins and peptides differing by only ~0.2 pI units.[78] Peak capacities are

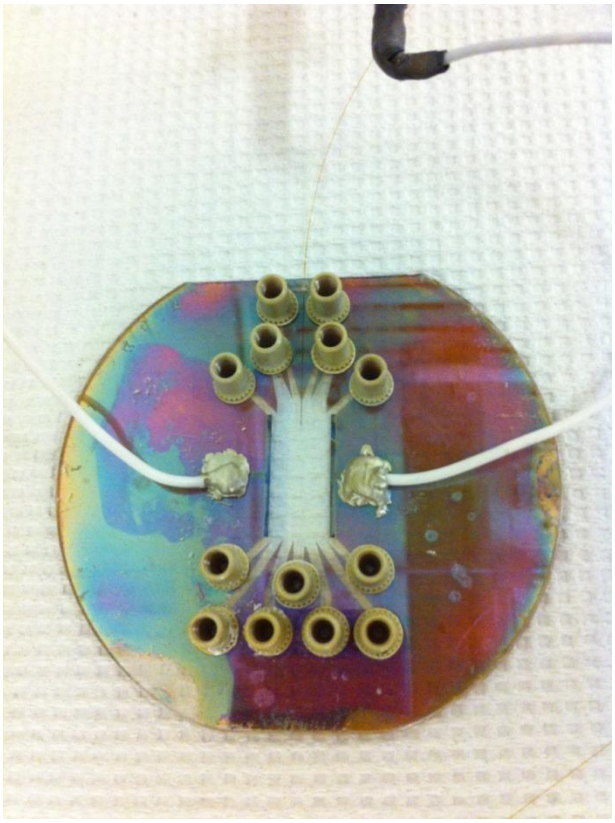

Figure 5.1: Completed µFFIEF device. Multiple inlets and outlets allow for presorted ampholytes to be introduced and multiple fractions to be collected.

estimated to be as high as 50, increasing total peak capacity by over 50%. Additionally, it is predicted, FFIEF will provide more orthogonal separations, possibly making better use of the separation space. FFIEF when combined with SEC, for example, would provide a comprehensive 2D separation which would be very similar to 2DGE since the first dimension would separate based on size, and the second on pI. µFFIEF devices have already been fabricated and tested.[71, 73, 78, 163] An example of a device for µFFIEF fabricated by similar methods to the device used in this work can be seen in Figure 5.1. A device such as this one could operate in any of the electrophoretic modes by simply changing buffer compositions. In the first dimension varying mobile phases could be used across an array of column types to see which combinations provide the greatest degree of orthogonality and effective peak capacity. Additionally, it would be ideal if these techniques could be applied to more real world samples. For example, the current nLC × µFFE method used for NBD-F labeled amino acids has been used to separate the amino acids released from 3T3-L1 cells (Figure 5.2). Application to protein samples would also advance the technique, though as seen in Chapter 3, adsorption would have to be addressed.

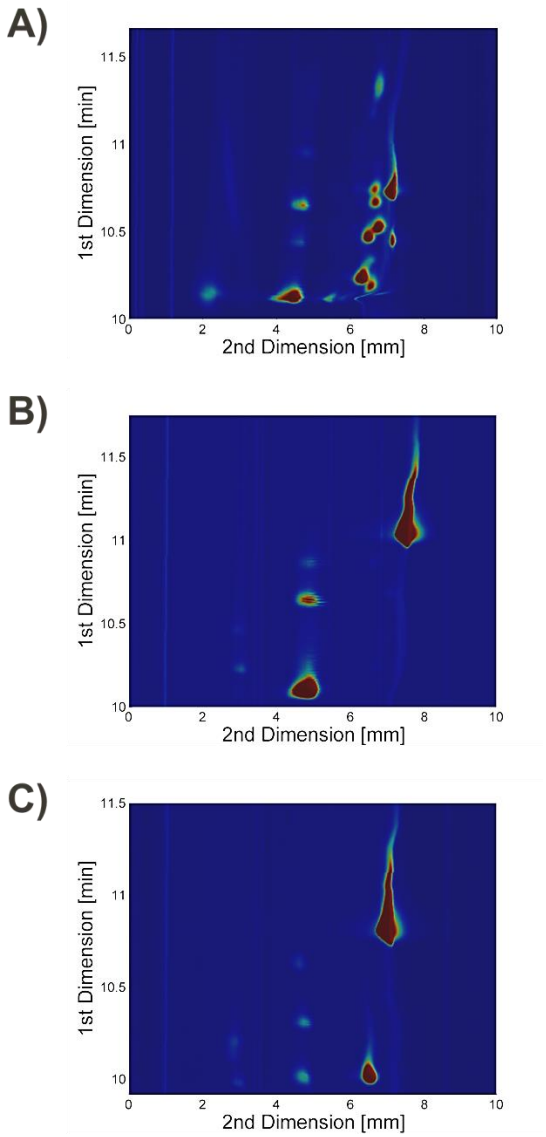

Figure 5.2: A) Separation of NBD-F labelled amino acids collected from 3T3-L1 cells.. Standards of ornithine (B) and citrulline (C) were labelled and separated for identification in (A).

5.2.2 Device Design and Fabrication

The fabrication of microfluidic devices is often a very labor intensive and expensive process. In order to produce the devices used in this work, many hours of access to a cleanroom facility was required, which many researchers do not have access to. Weeks of fabrication are often required to produce even one

functional µFFE device. Polymeric materials such as PDMS[69] and PMMA[72] have been implemented into devices, but the need for rapid prototyping and one-step manufacturing is still highly desired. 3D printing technology has come a long way since its original introduction in the mid 1980's.[164] Features of only a few microns in height can now be produced in a wide array of polymeric materials.[165] The ability to generate new designs for µFFE devices and have them fully printed in a single day for <$1 are now possible. With this rapid, low cost, production, µFFE could be much more accessible to researchers.

It has been stated many times throughout this thesis that LIF has been the primary detection method used in µFFE. Chapter 4 clearly demonstrated the impact fluorescent labelling can have on separation performance. Though LIF provides unmatched sensitivity, no identification information is provided without the use of spiked samples (Figure 5.2), and even then, identity can still be uncertain in the case of highly complex samples. Mass spectrometry has been the work horse for detection and anlysis of many proteomic samples and its integration with traditional 1D separation techniques has allowed for many advances. Recently MS detection was implemented in µFFE using nanospray MS.[80] This method proved useful for continuous separations, however to sample the entire separation space required varying the right:left inlet flow ratio over time to "scan" the separation region. This technique would not be applicable in multidimensional separations since it would not be able to adequately and efficiently sample first dimension peaks. A method more similar to how Anderson *et al.*[166] coupled CE with western blotting could be more effective. By designing

an open-edge µFFE device a membrane mounted to a translational stage could be moved across the edge during the separation, and further imaged using desorption electrospray ionization or matrix assisted laser desorption ionization imaging. 3D printing would be critical in allowing many designs to be rapidly fabricated and tested.

Micro free flow electrophoresis has found its way into many areas of research since it was first miniaturized. The types of devices, materials, designs, and applications have continued to grow. It is my belief that µFFE will soon become a commercially viable option to couple to LC instrumentation. Hopefully the groundwork for nLC × µFFE I was able to produce will inspire unique applications for the technique and someday lead to a method which can have the separation power of 2DGE in a matter of minutes.

Bibliography

1. J. Lopez, *Journal of Chromatography B-Analytical Technologies in the Biomedical and Life Sciences*, 2007, **849**, 190-202.
2. M. Fournier, J. Gilmore, S. Martin-Brown and M. Washburn, *Chemical Reviews*, 2007, **107**, 3654-3686.
3. D. Wishart, T. Jewison, A. Guo, M. Wilson, C. Knox, Y. Liu, Y. Djoumbou, R. Mandal, F. Aziat, E. Dong, S. Bouatra, I. Sinelnikov, D. Arndt, J. Xia, P. Liu, F. Yallou, T. Bjorndahl, R. Perez-Pineiro, R. Eisner, F. Allen, V. Neveu, R. Greiner and A. Scalbert, *Nucleic Acids Research*, 2013, **41**, D801-D807.
4. D. Wishart, C. Knox, A. Guo, R. Eisner, N. Young, B. Gautam, D. Hau, N. Psychogios, E. Dong, S. Bouatra, R. Mandal, I. Sinelnikov, J. Xia, L. Jia, J. Cruz, E. Lim, C. Sobsey, S. Shrivastava, P. Huang, P. Liu, L. Fang, J. Peng, R. Fradette, D. Cheng, D. Tzur, M. Clements, A. Lewis, A. De Souza, A. Zuniga, M. Dawe, Y. Xiong, D. Clive, R. Greiner, A. Nazyrova, R. Shaykhutdinov, L. Li, H. Vogel and I. Forsythe, *Nucleic Acids Research*, 2009, **37**, D603-D610.
5. S. Bouatra, F. Aziat, R. Mandal, A. Guo, M. Wilson, C. Knox, T. Bjorndahl, R. Krishnamurthy, F. Saleem, P. Liu, Z. Dame, J. Poelzer, J. Huynh, F. Yallou, N. Psychogios, E. Dong, R. Bogumil, C. Roehring and D. Wishart, *Plos One*, 2013, **8**.
6. T. Rabilloud, *Proteomics*, 2002, **2**, 3-10.
7. Y. Shen, S. Berger and R. Smith, *Journal of Chromatography a*, 2001, **914**, 257-264.
8. J. Busnel, B. Schoenmaker, R. Ramautar, A. Carrasco-Pancorbo, C. Ratnayake, J. Feitelson, J. Chapman, A. Deelder and O. Mayboroda, *Analytical Chemistry*, 2010, **82**, 9476-9483.
9. S. Chiou and S. Wu, *Analytica Chimica Acta*, 1999, **383**, 47-60.
10. P. O'Farrell, *Journal of Biological Chemistry*, 1975, **250**, 4007-4021.
11. G. Guiochon, N. Marchetti, K. Mriziq and R. Shalliker, *Journal of Chromatography a*, 2008, **1189**, 109-168.
12. F. Erni and R. Frei, *Journal of Chromatography*, 1978, **149**, 561-569.
13. M. Bushey and J. Jorgenson, *Analytical Chemistry*, 1990, **62**, 161-167.
14. M. Filgueira, Y. Huang, K. Witt, C. Castells and P. Carr, *Analytical Chemistry*, 2011, **83**, 9531-9539.
15. C. Evans and J. Jorgenson, *Analytical and Bioanalytical Chemistry*, 2004, **378**, 1952-1961.
16. H. Cortes, B. Winniford, J. Luong and M. Pursch, *Journal of Separation Science*, 2009, **32**, 883-904.
17. Z. LIU and J. PHILLIPS, *Journal of Chromatographic Science*, 1991, **29**, 227-231.
18. C. Venkatramani, J. Xu and J. Phillips, *Analytical Chemistry*, 1996, **68**, 1486-1492.

19. S. de Koning, H. Janssen and U. Brinkman, *Journal of Chromatography a*, 2004, **1058**, 217-221.
20. S. de Koning, H. Janssen, M. van Deursen and U. Brinkman, *Journal of Separation Science*, 2004, **27**, 397-409.
21. M. Bushey and J. Jorgenson, *Analytical Chemistry*, 1990, **62**, 978-984.
22. X. Yang, X. Zhang, A. Li, S. Zhu and Y. Huang, *Electrophoresis*, 2003, **24**, 1451-1457.
23. C. Zhu, X. He, J. Kraly, M. Jones, C. Whitmore, D. Gomez, M. Eggertson, W. Quigley, A. Boardman and N. Dovichi, *Analytical Chemistry*, 2007, **79**, 765-768.
24. X. Chen, M. Fazal and N. Dovichi, *Talanta*, 2007, **71**, 1981-1985.
25. J. Dickerson, L. Ramsay, O. Dada, N. Cermak and N. Dovichi, *Electrophoresis*, 2010, **31**, 2650-2654.
26. C. Wu, M. MacCoss, K. Howell and J. Yates, *Nature Biotechnology*, 2003, **21**, 532-538.
27. D. Wolters, M. Washburn and J. Yates, *Analytical Chemistry*, 2001, **73**, 5683-5690.
28. M. Washburn, R. Ulaszek, C. Deciu, D. Schieltz and J. Yates, *Analytical Chemistry*, 2002, **74**, 1650-1657.
29. M. Washburn, D. Wolters and J. Yates, *Nature Biotechnology*, 2001, **19**, 242-247.
30. A. Link, J. Eng, D. Schieltz, E. Carmack, G. Mize, D. Morris, B. Garvik and J. Yates, *Nature Biotechnology*, 1999, **17**, 676-682.
31. T. Hooker and J. Jorgenson, *Analytical Chemistry*, 1997, **69**, 4134-4142.
32. J. Ramsey, S. Jacobson, C. Culbertson and J. Ramsey, *Analytical Chemistry*, 2003, **75**, 3758-3764.
33. D. Stoll, J. Cohen and P. Carr, *Journal of Chromatography a*, 2006, **1122**, 123-137.
34. D. Stoll and P. Carr, *Journal of the American Chemical Society*, 2005, **127**, 5034-5035.
35. J. Giddings, *Analytical Chemistry*, 1984, **56**, 1258-&.
36. B. L. Karger, L. R. Snyder and C. Horvath, *An introduction to Separation Science*, Wiley & Sons, New York, 1973.
37. G. Guiochon, M. Gonnord, M. Zakaria, L. Beaver and A. Siouffi, *Chromatographia*, 1983, **17**, 121-124.
38. M. Martin, D. Herman and G. Guiochon, *Analytical Chemistry*, 1986, **58**, 2200-2207.
39. R. Murphy, M. Schure and J. Foley, *Analytical Chemistry*, 1998, **70**, 1585-1594.
40. J. Davis, D. Stoll and P. Carr, *Analytical Chemistry*, 2008, **80**, 461-473.
41. L. Potts, D. Stoll, X. Li and P. Carr, *Journal of Chromatography a*, 2010, **1217**, 5700-5709.
42. H. Gu, Y. Huang and P. Carr, *Journal of Chromatography a*, 2011, **1218**, 64-73.
43. K. Horie, H. Kimura, T. Ikegami, A. Iwatsuka, N. Saad, O. Fiehn and N. Tanaka, *Analytical Chemistry*, 2007, **79**, 3764-3770.

44. J. Giddings, *Journal of Chromatography a*, 1995, **703**, 3-15.
45. M. Dumarey, R. Put, E. Van Gyseghem and Y. Heyden, *Analytica Chimica Acta*, 2008, **609**, 223-234.
46. R. Al Bakain, I. Rivals, P. Sassiat, D. Thiebaut, M. Hennion, G. Euvrard and J. Vial, *Journal of Chromatography a*, 2011, **1218**, 2963-2975.
47. M. Schure, *Journal of Chromatography a*, 2011, **1218**, 293-302.
48. Z. Liu, D. Patterson and M. Lee, *Analytical Chemistry*, 1995, **67**, 3840-3845.
49. M. Dumarey, Y. Heyden and S. Rutan, *Analytical Chemistry*, 2010, **82**, 6056-6065.
50. M. Gilar, J. Fridrich, M. Schure and A. Jaworski, *Analytical Chemistry*, 2012, **84**, 8722-8732.
51. M. Gilar, P. Olivova, A. Daly and J. Gebler, *Analytical Chemistry*, 2005, **77**, 6426-6434.
52. J. Davis, D. Stoll and P. Carr, *Analytical Chemistry*, 2008, **80**, 8122-8134.
53. S. Rutan, J. Davis and P. Carr, *Journal of Chromatography a*, 2012, **1255**, 267-276.
54. M. Islinger, C. Eckerskorn and A. Volkl, *Electrophoresis*, 2010, **31**, 1754-1763.
55. V. J. Barrolier, E. Watzke and H. Gibian, *Naturforschung*, 1958, **13B**, 754
56. K. Hannig, *Anal. Chem.*, 1961, **181**, 244-254.
57. S. Hoffstetterkuhn and H. Wagner, *Electrophoresis*, 1990, **11**, 451-456.
58. R. Kuhn, S. Hoffstetterkuhn and H. Wagner, *Electrophoresis*, 1990, **11**, 942-947.
59. D. Burggraf, G. Weber and F. Lottspeich, *Electrophoresis*, 1995, **16**, 1010-1015.
60. S. Hoffstetterkuhn, R. Kuhn and H. Wagner, *Electrophoresis*, 1990, **11**, 304-309.
61. J. Caslavska and W. Thormann, *Journal of Chromatography*, 1992, **594**, 361-369.
62. J. Caslavska, P. Gebauer and W. Thormann, *Journal of Chromatography*, 1991, **585**, 145-152.
63. P. Hoffmann, H. Wagner, G. Weber, M. Lanz, J. Caslavska and W. Thormann, *Analytical Chemistry*, 1999, **71**, 1840-1850.
64. X. Yi, J. Eijkel and A. Manz, *Chinese Journal of Analytical Chemistry*, 2000, **28**, 1295-1299.
65. A. Manz and J. Eijkel, *Pure and Applied Chemistry*, 2001, **73**, 1555-1561.
66. D. E. Raymond, A. Manz and H. M. Widmer, *Analytical Chemistry*, 1994, **66**, 2858-2865.
67. D. E. Raymond, A. Manz and H. M. Widmer, *Anal Chem*, 1996, **68**, 2515-2522.
68. C. X. Zhang and A. Manz, *Analytical Chemistry*, 2003, **75**, 5759-5766.
69. S. Kohler, C. Weilbeer, S. Howitz, H. Becker, V. Beushausen and D. Belder, *Lab on a Chip*, 2011, **11**, 309-314.
70. J. W. Albrecht and K. F. Jensen, *Electrophoresis*, 2006, **27**, 4960-4969.

71. Y. Xu, C. X. Zhang, D. Janasek and A. Manz, *Lab on a Chip*, 2003, **3**, 224-227.
72. M. Mazereeuw, C. M. de Best, U. R. Tjaden, H. Irth and J. van der Greef, *Analytical Chemistry*, 2000, **72**, 3881-3886.
73. K. Macounova, C. Cabrera, M. Holl and P. Yager, *Analytical Chemistry*, 2000, **72**, 3745-3751.
74. S. Jezierski, D. Belder and S. Nagl, *Chemical Communications*, 2013, **49**, 904-906.
75. B. R. Fonslow and M. T. Bowser, *Analytical Chemistry*, 2005, **77**, 5706-5710.
76. P. Wang, L. Zhang, Y. Shan, Y. Cong, Y. Liang, B. Han, Z. Liang and Y. Zhang, *J Sep Sci*, **33**, 2039-2044.
77. H. Lu, S. Gaudet, M. A. Schmidt and K. F. Jensen, *Analytical Chemistry*, 2004, **76**, 5705-5712.
78. D. Kohlheyer, J. C. T. Eijkel, S. Schlautmann, A. van den Berg and R. B. M. Schasfoort, *Analytical Chemistry*, 2007, **79**, 8190-8198.
79. D. Kohlheyer, G. A. J. Besselink, S. Schlautmann and R. B. M. Schasfoort, *Lab on a Chip*, 2006, **6**, 374-380.
80. C. Benz, M. Boomhoff, J. Appun, C. Schneider and D. Belder, *Angewandte Chemie-International Edition*, 2015, **54**, 2766-2770.
81. B. R. Fonslow, V. H. Barocas and M. T. Bowser, *Analytical Chemistry*, 2006, **78**, 5369-5374.
82. D. Kohlheyer, J. C. T. Eijkel, S. Schlautmann, A. van den Berg and R. B. M. Schasfoort, *Analytical Chemistry*, 2008, **80**, 4111-4118.
83. N. Frost and M. Bowser, *Lab on a Chip*, 2010, **10**, 1231-1236.
84. H. Lee, C. Barber and A. Minerick, *Electrophoresis*, 2014, **35**, 1782-1789.
85. M. Geiger, N. W. Frost and M. T. Bowser, *Analytical Chemistry*, 2014, **86**, 5136-5142.
86. R. Jackman, T. Floyd, R. Ghodssi, M. Schmidt and K. Jensen, *Journal of Micromechanics and Microengineering*, 2001, **11**, 263-269.
87. H. Holman, R. Miles, Z. Hao, E. Wozei, L. Anderson and H. Yang, *Analytical Chemistry*, 2009, **81**, 8564-8570.
88. R. Herzig-Marx, K. Queeney, R. Jackman, M. Schmidt and K. Jensen, *Analytical Chemistry*, 2004, **76**, 6476-6483.
89. N. Abu-Hatab, J. John, J. Oran and M. Sepaniak, *Applied Spectroscopy*, 2007, **61**, 1116-1122.
90. J. Huang, Y. Zhang, H. Ding and H. Sun, *Advanced Optical Materials*, 2015, **3**, 618-633.
91. P. Kuban and P. Hauser, *Electrophoresis*, 2009, **30**, 3305-3314.
92. J. Fritz, E. Cooper, S. Gaudet, P. Sorger and S. Manalis, *Proceedings of the National Academy of Sciences of the United States of America*, 2002, **99**, 14142-14146.
93. H. Ayliffe, A. Frazier and R. Rabbitt, *Journal of Microelectromechanical Systems*, 1999, **8**, 50-57.
94. L. Nagels and I. Poels, *Trac-Trends in Analytical Chemistry*, 2000, **19**, 410-417.

95. S. Forry, J. Murray, M. Heien, L. Locascio and R. Wightman, *Analytical Chemistry*, 2004, **76**, 4945-4950.
96. S. Ahola, F. Casanova, J. Perlo, K. Munnemann, B. Blumich and S. Stapf, *Lab on a Chip*, 2006, **6**, 90-95.
97. J. Mellors, W. Black, A. Chambers, J. Starkey, N. Lacher and J. Ramsey, *Analytical Chemistry*, 2013, **85**, 4100-4106.
98. C. Herzog, E. Beckert and S. Nagl, *Analytical Chemistry*, 2014, **86**, 9533-9539.
99. D. Janasek, M. Schilling, A. Manz and J. Franzke, *Lab on a Chip*, 2006, **6**, 710-713.
100. B. Han, P. Wang, G. Zhu, L. Zhang, F. Qu, Y. Deng and Y. Zhang, *J Sep Sci*, 2009, **32**, 1211-1215.
101. J. Wen, E. W. Wilker, M. B. Yaffe and K. F. Jensen, *Analytical Chemistry*, 2010, **82**, 1253-1260.
102. V. Kostal, B. Fonslow, E. Arriaga and M. Bowser, *Analytical Chemistry*, 2009, **81**, 9267-9273.
103. B. Fonslow and M. Bowser, *Analytical Chemistry*, 2008, **80**, 3182-3189.
104. R. Turgeon, B. Fonslow, M. Jing and M. Bowser, *Analytical Chemistry*, 2010, **82**, 3636-3641.
105. M. Jing and M. Bowser, *Lab on a Chip*, 2011, **11**, 3703-3709.
106. R. Moritz, H. Ji, F. Schutz, L. Connolly, E. Kapp, T. Speed and R. Simpson, *Analytical Chemistry*, 2004, **76**, 4811-4824.
107. H. Xie, G. Onsongo, J. Popko, E. de Jong, J. Cao, J. Carlis, R. Griffin, N. Rhodus and T. Griffin, *Molecular & Cellular Proteomics*, 2008, **7**, 486-498.
108. B. R. Fonslow and M. T. Bowser, *Analytical Chemistry*, 2006, **78**, 8236-8244.
109. N. Bings, C. Wang, C. Skinner, C. Colyer, P. Thibault and D. Harrison, *Analytical Chemistry*, 1999, **71**, 3292-3296.
110. F. Mikkers, *Analytical Chemistry*, 1999, **71**, 522-533.
111. F. Mikkers, F. Everaerts and T. Verheggen, *Journal of Chromatography*, 1979, **169**, 11-20.
112. P. Dugo, F. Cacciola, T. Kumm, G. Dugo and L. Mondello, *Journal of Chromatography A*, 2008, **1184**, 353-368.
113. N. Iki and E. Yeung, *Journal of Chromatography a*, 1996, **731**, 273-282.
114. J. G. Shackman, C. J. Watson and R. T. Kennedy, *Journal of Chromatography A*, 2004, **1040**, 273-282.
115. M. Filgueira, C. Castells and P. Carr, *Analytical Chemistry*, 2012, **84**, 6747-6752.
116. E. Turner, J. Dickerson, L. Ramsay, K. Swearingen, R. Wojcik and N. Dovichi, *Journal of Chromatography a*, 2008, **1194**, 253-256.
117. D. B. Craig, B. K. Wetzl, A. Duerkop and O. S. Wolfbeis, *Electrophoresis*, 2005, **26**, 2208-2213.
118. M. Geiger, A. Hogerton and M. Bowser, *Analytical Chemistry*, 2012, **84**, 577-596.
119. B. Verzola, C. Gelfi and P. G. Righetti, *Journal of Chromatography A*, 2000, **868**, 85-99.

120. M. R. Schure and A. M. Lenhoff, *Analytical Chemistry*, 1993, **65**, 3024-3037.
121. M. Minarik, B. Gas, A. Rizzi and E. Kenndler, *Journal of Capillary Electrophoresis*, 1995, **2**, 89-96.
122. L. Castelletti, B. Verzola, C. Gelfi, A. Stoyanov and P. Righetti, *Journal of Chromatography a*, 2000, **894**, 281-289.
123. J. K. Towns and F. E. Regnier, *Analytical Chemistry*, 1992, **64**, 2473-2478.
124. S. Ghosal, *Analytical Chemistry*, 2002, **74**, 4198-4203.
125. S. Ghosal, *Analytical Chemistry*, 2002, **74**, 771-775.
126. S. Hjerten, *Chromatogr Rev*, 1967, **9**, 122-219.
127. R. M. McCormick, *Anal Chem*, 1988, **60**, 2322-2328.
128. H. H. Lauer and D. Mcmanigill, *Analytical Chemistry*, 1986, **58**, 166-170.
129. D. Corradini, *Journal of Chromatography B-Analytical Technologies in the Biomedical and Life Sciences*, 1997, **699**, 221-256.
130. B. Verzola, C. Gelfi and P. G. Righetti, *Journal of Chromatography A*, 2000, **874**, 293-303.
131. C. A. Lucy, A. M. MacDonald and M. D. Gulcev, *Journal of Chromatography A*, 2008, **1184**, 81-105.
132. B. Gas, M. Stedry and E. Kenndler, *Electrophoresis*, 1997, **18**, 2123-2133.
133. G. Schomburg, A. Deege, J. Kohler and U. Bienvogelsang, *Journal of Chromatography*, 1983, **282**, 27-39.
134. J. Kohler, D. Chase, R. Farlee, A. Vega and J. Kirkland, *Journal of Chromatography*, 1986, **352**, 275-305.
135. J. Kohler, A. Deege and G. Schomburg, *Chromatographia*, 1984, **18**, 119-124.
136. B. Bidlingmeyer, *Journal of Chromatographic Science*, 1980, **18**, 525-539.
137. L. Castelletti, B. Verzola, C. Gelfi, A. Stoyanov and P. G. Righetti, *Journal of Chromatography A*, 2000, **894**, 281-289.
138. N. W. Frost and M. T. Bowser, *Lab on a Chip*, 2010, **10**, 1231-1236.
139. M. Malmsten, *Journal of Colloid and Interface Science*, 1998, **207**, 186-199.
140. R. T. Turgeon and M. T. Bowser, *Electrophoresis*, 2009, **30**, 1342-1348.
141. B. R. Fonslow and M. T. Bowser, *Analytical Chemistry*, 2008, **80**, 3182-3189.
142. R. T. Turgeon, B. R. Fonslow, M. Jing and M. T. Bowser, *Anal. Chem.*, 2010, **82**, 3636-3641.
143. M. M. Bushey and J. W. Jorgenson, *Analytical Chemistry*, 1990, **62**, 161-167.
144. M. M. Bushey and J. W. Jorgenson, *Analytical Chemistry*, 1990, **62**, 978-984.
145. R. Vonk, A. Gargano, E. Davydova, H. Dekker, S. Eeltink, L. de Koning and P. Schoenmakers, *Analytical Chemistry*, 2015, **87**, 5387-5394.
146. R. T. Turgeon and M. T. Bowser, *Anal. Bioanal. Chem.*, 2009, **394**, 187-198.
147. M. Jing and M. T. Bowser, *Lab on a Chip*, 2011, **11**, 3703-3709.

148. R. Turgeon and M. Bowser, *Analytical and Bioanalytical Chemistry*, 2009, **394**, 187-198.
149. L. Kricka and P. Fortina, *Clinical Chemistry*, 2009, **55**, 670-683.
150. T. Terai and T. Nagano, *Pflugers Archiv-European Journal of Physiology*, 2013, **465**, 347-359.
151. Y. Watanabe and K. Imai, *Journal of Chromatography*, 1982, **239**, 723-732.
152. R. Wojcik, K. Swearingen, J. Dickerson, E. Turner, L. Ramsay and N. Dovichi, *Journal of Chromatography a*, 2008, **1194**, 243-248.
153. K. Slais, M. Horka, J. Novackova and Z. Friedl, *Electrophoresis*, 2002, **23**, 1682-1688.
154. B. Verzola, C. Gelfi and P. Righetti, *Journal of Chromatography a*, 2000, **868**, 85-99.
155. Y. Watanabe and K. Imai, *Analytical Chemistry*, 1983, **55**, 1786-1791.
156. D. Milanova, R. Chambers, S. Bahga and J. Santiago, *Electrophoresis*, 2011, **32**, 3286-3294.
157. A. Griebel, S. Rund, F. Schonfeld, W. Dorner, R. Konrad and S. Hardt, *Lab on a Chip*, 2004, **4**, 18-23.
158. B. Wetzl, S. Yarmoluk, D. Craig and O. Wolfbeis, *Angewandte Chemie-International Edition*, 2004, **43**, 5400-5402.
159. O. Kostenko, S. Dmitrieva, O. Tolmachev and S. Yarmoluk, *Journal of Fluorescence*, 2002, **12**, 173-175.
160. T. Teerlink, P. Vanleeuwen and A. Houdijk, *Clinical Chemistry*, 1994, **40**, 245-249.
161. M. Frank and R. Powers, *Journal of Chromatography B-Analytical Technologies in the Biomedical and Life Sciences*, 2007, **852**, 646-649.
162. C. Klinker and M. Bowser, *Analytical Chemistry*, 2007, **79**, 8747-8754.
163. K. Shimura, *Electrophoresis*, 2009, **30**, 11-28.
164. Y. Huang, M. Leu, J. Mazumder and A. Donmez, *Journal of Manufacturing Science and Engineering-Transactions of the Asme*, 2015, **137**.
165. J. Erkal, A. Selimovic, B. Gross, S. Lockwood, E. Walton, S. McNamara, R. Martin and D. Spence, *Lab on a Chip*, 2014, **14**, 2023-2032.
166. G. Anderson, C. Cipolla and R. Kennedy, *Analytical Chemistry*, 2011, **83**, 1350-1355.